University of Stavanger

FACULTY OF SCIENCE AND TECHNOLOGY

MASTER'S THESIS

Study programme/specialisation: **Biological chemistry**	Autumn/Spring semester, 2020/2021 Open access
Author: **Cyrell Ann S. Ruales**	
Program coordinator: Supervisor(s): **Marina Alexeeva / Svein Bjelland**	
Title of master's thesis: **Uracil-excising activity of hSMUG1 in bubble and R-loop DNA**	
Credits: **60 stp.**	
Keywords: **hSMUG1** **Uracil-DNA glycosylase** **DNA glycosylases** **Base excision repair** **Uracil-DNA incision** **Cytosine deamination**	Number of pages: …… 43 Date/year: **July 2021**

Acknowledgments

This thesis was performed from July 2020 to June 2021 at the Centre for Organelle Research (CORE) of the Department of Mathematics and Natural Sciences, Faculty of Science and Technology, University of Stavanger, Norway

I would like to express my gratitude to my supervisor, Professor Svein Bjelland, for giving me the opportunity to be part of their project, to work in the field of DNA damage and repair. Thank you for extending your help without any hesitations. For sharing your expertise and for the relevant lectures.

I would also like to express my heartfelt gratitude to my laboratory supervisor, Dr. Marina Alexeeva for her patience in teaching and guiding me all throughout this journey. Your way of working and guidance have shaped up my skills even more, for all of your good advices and for providing us with everything that we need in the lab, thank you.

Thank you especially to my colleagues at the CORE. To Celine lorentsen, Trond Bærheim and Shimaa Mehanna, thank you so much for helping me in so many ways. I will miss our late-lunch-chitchat every Friday, dancing sessions in the lab, sharing about our life's experiences and our future plan. Despite the difficulty of our project, all the uncertenties, hard time purifying and all the problems in between, you guys continued to be positive, I admire you all for that. I learned a lot from all of you. Studying in a foreign country was never easy, yet, with these beautiful people, it feels like home. I am forever grateful.

Lastly, Thank you so much to my support system: my family. I couldn't have done it without all of you. Thank you for the prayers. Indeed, God has been there for me every step of the way. Nahuman ra jud!

Abstract

Uracil arises in cellular DNA by hydrolytic cytosine (C) deamination and by erroneous replicative incorporation of deoxyuridine monophosphate opposite adenine. The former event is devastating by generation of C → thymine transition mutations, causing cancer, aging and neurodegenerative diseases, if uracil is not removed by uracil-DNA glycosylase (UDG) and replaced by cytosine through downstream base excision repair (BER) proteins before replication. The most important human UDG is hUNG, with hSMUG1 as back-up. During immunoglobulin gene diversification in activated B cells, targeted deamination by activation-induced cytidine deaminase (AID) followed by uracil excision by hUNG is important for class switch recombination (CSR) and somatic hypermutation (SHM) by providing DNA double strand breaks and mutagenesis, respectively. hSMUG1 may substitute for hUNG in CSR, but its role in CSR and SHM is largely unclear. The aim of this investigation was to determine hSMUG1 excision activity for uracil in R-loop DNA, the product of AID and formed during transcription, and compare it to that in bubble U-DNA, which is formed transiently in cellular processes as e.g. DNA replication. The results show that hSMUG1 excises uracil in bubble more efficient than in R-loop DNA, indicating a back-up UDG function rather than a specific function during CSR/SHM and/or transcription. hSMUG1 also function in ribosomal and telomerase RNA quality control by e.g. regulating the presence of base modifications, and binds the major pseudouridine synthase in mammals DKC1, where the (non-catalytic) Ser26 and Glu35 residues participate. The results show that hSMUG1 S26R/E35D mutant protein excises uracil in R-loop slightly more efficient than in DNA bubble, i.e., close to the opposite of wild type hSMUG1, suggesting altered enzyme function. hSMUG1 Pro240 is part of the His239–Lys249 intercalating loop being inserted into the damaged site in the DNA double helix. The hSMUG1 P240G protein excised uracil in R-loop much more efficient than in DNA bubble, demonstrating significantly altered enzyme function. Thus, while wild type hSMUG1 excised uracil in DNA bubble significantly more efficient than in R-loop, this was completely reversed regarding the hSMUG1 P240G mutant protein, indicating a role of Pro240 in stabilizing the hSMUG1–bubble U-DNA complex, or inhibiting the hSMUG1–R-loop U-DNA complex. When compared to results on hUNG from another research group member, hSMUG1 excises uracil in R-loop DNA more than two orders of magnitude less efficient than hUNG.

List of Figures

List of Tables

Abbreviations

A, adenine
AcTEV protease, tobacco etch virus protease
AID, activation-induced cytidine deaminase
AP, apurinic/apyrimidinic, abasic
APE, apurinic/apyrimidinic endonuclease
APOBEC, apolipoprotein B mRNA-editing enzyme, catalytic polypeptide
BER, base excision repair
βFU, 1-[2´-deoxy-2´-fluoro-β-D-arabinofuranosyl]-uracil
C, cytosine
CSR, class switch recombination
dRP, deoxyribose phosphate
dsDNA, double-stranded DNA
dUMP, deoxyuridine monophosphate
dTMP, thymidine monophosphate
fU, 5-formyluracil
FU, 5-fluorouracil
G, guanine
hmU, 5-hydroxymethyluracil
hSMUG, human single-strand-selective monofunctional uracil-DNA glycosylase
hUNG, human uracil-*N*-glycosylase
hmU, 5-hydroxymethyluracil
MBD4, methyl-CpG binding domain protein 4
m^5C, 5-methylcytosine
MMR, mismatch repair
PMSF, phenylmethylsulfonyl fluoride
RNP, ribonucleoprotein
RPA, replication protein A
Pol, DNA polymerase
ROS, reactive oxygen species
SHM, somatic hypermutation
ssDNA, single-stranded DNA
SSB, single strand breaks
T, thymine
TDG, thymine-DNA glycosylase
tRNA, transfer RNA
U, uracil
UDG, uracil-DNA glycosylase
UIP, uracil-DNA incision product
UPP, uracil-DNA processing product
UV, ultraviolet

Table of Contents

1 Introduction

Because the maintenance of genomic integrity is of utmost importance to all living organisms, they have developed different molecular mechanisms to repair damaged DNA. In mammals including humans, an inability to eliminate different kinds of DNA damage brings about a broad spectrum of pathologies, for example, neuronal deficits, immune-deficiencies, premature aging and cancer. The most abundant type of DNA damage is chemical base modifications including base removal by hydrolysis, which happens at the rate of several thousand base pairs per cell per day in humans. In addition to water, base damages are caused by endogenous metabolic and immune processes rather than environmental toxins, aside from the ultraviolet (UV) damage to the skin from sunlight and a multitude of different damages to lung and blood from cigarette smoke (1-3).

1.1 Hydrolytic DNA damages

1.1.1 The abundance and mutagenicity of uracil necessitate its removal from DNA

Uracil (U) arises spontaneously in cellular DNA by hydrolytic deamination of cytosine (C), and by misincorporation of deoxyuridine monophosphate (dUMP) rather than incorporation of thymidine monophosphate (dTMP) opposite adenine (A) during replication. Deamination of cytosine has been estimated to happen at a rate of 60–500 events per day in human cells (1). The non-blocking nature of uracil makes it highly mutagenic causing C → thymine (T) transition mutations if not repaired before replication. Misincorporated uracil is not miscoding, however, may alter binding of certain proteins to DNA (4). The consideration that cells must possess an ability to eliminate uracil from DNA, prompted the discovery of an enzyme capable of cleaving the uracil–deoxyribose bond; the uracil *N*-glycosidase (Ung) in *Escherichia coli* (5).

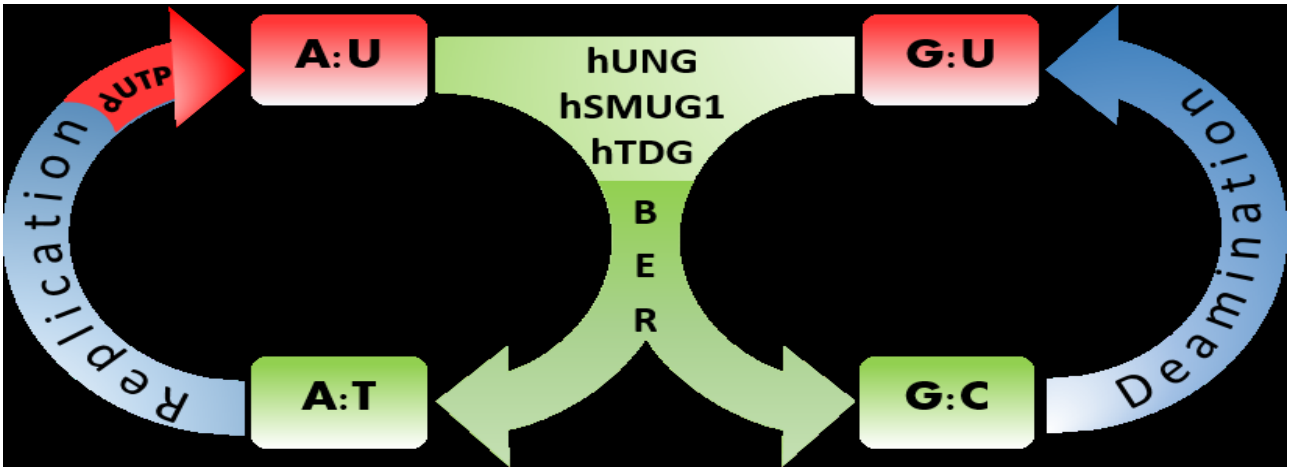

Figure 1. Introduction and fate of uracil in DNA. The left circle represents misincorporation of dUMP during replication resulting in the A:U pair. The right circle represents the spontaneous deamination of cytosine leading to formation of the G:U mispair. In both cases, human uracil-DNA glycosylases, i.e. hUNG, hSMUG1 and hTDG, recognize uracil and initiate the base excision repair (BER) pathway to restore the correct base. Reproduced from (6).

1.1.2 The deamination products uracil and thymine are corrected by repair enzymes.

The extracyclic amino group at cytosine C4 position is unstable to hydrolysis and lost slowly at physiological pH to form uracil. The proposed major chemical mechanisms for this involves protonation at the cytosine N3 position followed by direct nucleophilic attack by OH^- at the C4 position and the subsequent elimination of the amino group (7). In addition to cytosine, the other bases in DNA also deaminate losing their exocyclic amine and contribute to spontaneous mutagenesis in human cells. Thus, adenine, guanine (G) and 5-methylcytosine (m^5C) convert to hypoxanthine, xanthine and thymine, respectively. However, C and m^5C are the most frequently deaminated, where m^5C is deaminated 3–4 times more frequently than C. Importantly, deamination events happen at a much higher frequency in single-stranded DNA (ssDNA) than in double-stranded DNA (dsDNA), and are thus exacerbated in transient ssDNA regions during replication, transcription and recombination. While deaminated cytosine is rapidly removed from DNA by an uracil-DNA glycosylase (UDG; e.g., the highly efficient family 1 UDG, see below), the G:T mispair resulting from deamination of m^5C is a substrate for the thymine-DNA glycosylase (TDG) and the relatively slow mismatch repair (MMR) process. Therefore, the G:C → A:T transitions at the CpG sequences account for one-third of the single site mutations responsible for hereditary diseases in humans (8).

1.1.3 Enzymatic deamination

Enzymatic deamination of cytosine at the immunoglobulin gene loci by activation-induced cytidine deaminase (AID) starts the antigen-dependent antibody diversification processes by initiating class switch recombination (CSR) and somatic hypermutation (SHM) in B cells (9). Aberrant or elevated levels of AID in such cells may thus contribute to mutagenesis and cancer. An enzyme with similar activity, APOBEC1 (apolipoprotein B mRNA editing enzyme catalytic polypeptide 1), mediates host defense against retroviruses.

1.2 Oxidative damages

Reactive oxygen species (ROS) are the typical byproducts of the electron transport chain during respiration in aerobic organisms, and are also products of catabolic oxidases, anabolic processes and peroxisomal metabolism. At low levels, ROS perform important cellular functions such as serving as messengers in redox signaling reactions and effecting defense responses to invading pathogens as an important part of the immune system. However, ROS cause a total of 100 different oxidative base lesions and 2´-deoxyribose modifications. Usually, the deleterious consequences of ROS are reduced in cells by the restriction of respiration to the mitochondrial compartment, DNA complexed and protected by histones and the extinguishing of surplus ROS by the antioxidant enzymes superoxide dismutase, catalase, and peroxiredoxin (10). Despite this, an excess of ROS is related to the development of human diseases, such as cancer, Alzheimer's disease, Parkinson's disease, diabetes, and heart failure. The most conspicuous of the ROS are the superoxide radical, hydrogen peroxide (H_2O_2) and the hydroxyl radical (•OH), the latter produced by the Fenton reaction when Fe^{2+} reacts with H_2O_2 (11,12).

A major and biologically significant ROS-formed base from guanine is 7,8-dihydro-8-oxoguanine (Fig. 8C), which mispairs with adenine thereby adding to the overall mutational load. In addition, it oxidizes further to other deleterious secondary DNA lesions due to its low oxidation potential (13). As the most reactive ROS, •OH is damaging to most cellular constituents and adds to the double bonds of the DNA bases and abstracts hydrogen atoms from their methyl groups, as well as it attacks the sugar residue in their immediate vicinity (14). For example, thymine glycol (Fig. 8C) and several ring-opened and ring-fragmented products is generated from a •OH attack on the C5–C6 double bonds of thymine. Attack on its methyl group results in 5-hydroxymethyluracil (hmU) and 5-formyluracil (fU), both capable of mispairing causing mutations.

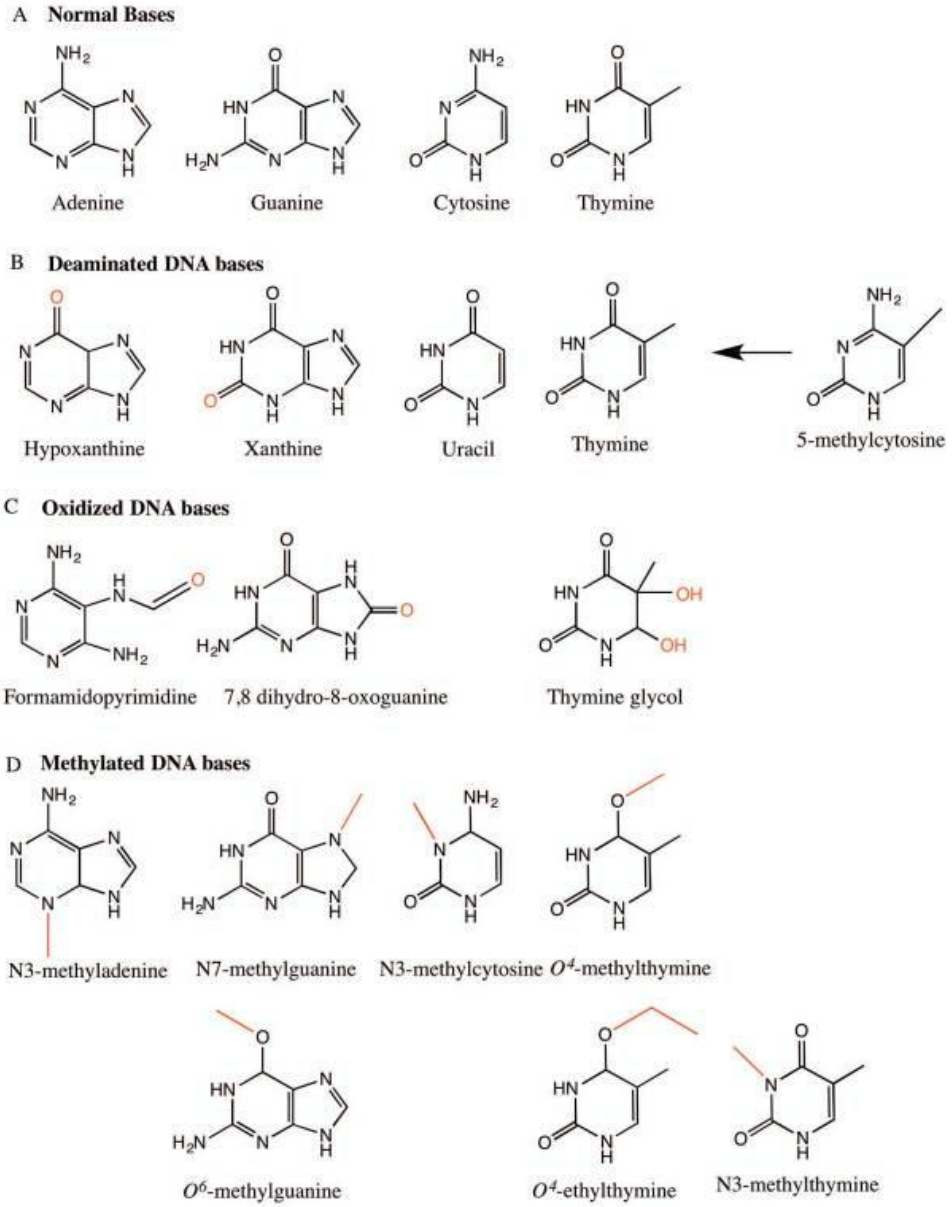

Figure 2. Common DNA base lesions. (A) Normal structures of DNA bases: adenine, guanine, cytosine and thymine. (B) Deaminated bases: hypoxanthine, xanthine, uracil and thymine arising from deamination of exocyclic bases of adenine, guanine, cytosine and 5-methylcytosine, respectively. (C) Oxidized DNA bases: formamidopyrimidine derivative of adenine, 7,8-dihydro-8-oxoguanine and thymine glycol. (D) Methylated DNA bases: N3-methyladenine, N7-methylguanine, *O*^{6}-methylguanine, N3-methylcytosine, *O*^{4}-methylthymine, *O*^{4}-ethylthymine and N3-methylthymine. Figures from (3).

Aside from attacking the DNA bases, ROS compromise the DNA backbone by causing single strand breaks (SSB) estimated to be 2300/cell/h in mammals. Breaks in the DNA backbone are repaired by the SSB repair or the double strand break repair pathways (15).

1.3 Bases damaged by alkylation

Several distinct alkylation repair pathways have developed to counteract both endogenous and exogenous alkylation, providing the cell with a diverse arsenal to protect its DNA from such damage. While the causes of endogenous alkylation damage are unknown, *S*-adenosylmethionine has been shown to methylate DNA (i.e., non-enzymatically) at a biologically important level and is consequently able to cause the simplest type of DNA alkylation damage: the addition of a single methyl group to a DNA base. Indeed, twelve different base lesions can be produced in DNA by methylating agents reacting with ring nitrogen or oxygen atoms. The most common methylation product is N^7-methylguanine (Figure 2), which accounts for about 75% of all methylated base lesions in DNA. While N^7-methylguanine is rather innocuous on its own, it is susceptible to depurination resulting in an apurinic/apyrimidinic (AP) site, which can be toxic and mutagenic. Many of the remaining lesions, such as N^3-methyladenine or N^1-methyladenine (Figure 2), are naturally cytotoxic because they inhibit replicative DNA polymerases (Pols). Three different repair pathways, at least, are involved in the repair of methylation damage: direct demethylation by O^6-methylguanine DNA methyltransferase, and oxidative demethylation by the AlkB enzyme family, as well as base excision repair (16).

1.4 Base excision repair

The base excision repair (BER) pathway corrects most DNA base damages before they reach causing mutagenicity or toxicity, and is consequently operating in both actively replicating and non-replicating cells. First enzymatic step in BER is typically excision of an aberrant or damaged base from dsDNA by a DNA glycosylase, which catalyzes the cleavage of the *N*-glycosidic bond between the base and the 2´-deoxyribose creating an AP site. To facilitate recognition, glycosylases appear to pinch gently while scanning the DNA, ultimately bending it at the position of the damaged base to create a widened and flattened minor groove. This localized DNA distortion promotes the damaged base to flip out of the double helix (base flipping) and enter the binding site of the enzyme for surveying and protein-substrate complex formation (17). DNA glycosylases are classified as mono-functional or bi-functional based on their inability or ability, respectively, to execute AP lyase strand cleavage activity. The mono-functional glycosylases utilize a water molecule as a nucleophile to attack the C´1 of deoxyribose to pro-

mote base release, generating an AP site product that is identical to that formed upon spontaneous DNA depurination or depyrimidination. This AP site is a substrate for an AP endonuclease, which breaks the phosphodiester bond of DNA. The bi-functional glycosylases utilize an active site amine moiety as a nucleophile to excise the damaged base and generate a covalent Schiff base protein-DNA intermediate during the catalytic process. The result may be incision of the DNA strand within the phosphodiester linkage 3´ to the AP site, either by β-elimination or by two consecutive (β,δ) elimination steps (enzymes performing this are also called tri-functional), creating a single-strand break (SSB) with a non-conventional 3´-terminus.

Normally, after base removal by a DNA glycosylase, an AP endonuclease incises the DNA backbone immediately 5´ to the AP site to generate a strand break with a priming 3´-OH group and a 5´-deoxyribose phosphate (dRP) remnant. The major AP endonuclease in mammals is APE1, which accounts for more than 95% of the total cellular AP site incision activity. APE1 catalyzes an acid-base hydrolytic reaction to incise the phosphodiester (P–O) bond of DNA, which is promoted by Mg^{2+}. Aside from its primary AP endonuclease activity, APE1 can catalyze the removal of 3´-blocking ends generated by bi-functional DNA glycosylases, ROS and other DNA damaging agents by its 3´-phosphodiesterase activity (18-21).

To replace the excised nucleotide, organisms utilize Pols to execute repair synthesis. A Pol requires a 3´-OH terminus on the primer strand, and ideally an unmodified template to incorporate the correct complementary deoxynucleotide(s). Many Pols also have 3´ to 5´ exonuclease (proofreading) activity that removes non-complementary or altered nucleotides immediately after phosphodiester bond formation and before the addition of another nucleotide. Polβ is the main human Pol that works on short nucleotide gaps, for example, those that emerge during short-patch BER/repair (SPR) which typically involves the incorporation of only a single nucleotide. In that case Polβ simultaneously removes the 5´-dRP by its lyase function and prepares for the final ligation step. In some instances, e.g. if the 5´-dRP is modified and resistant to being removed by Polβ, a replicative Pol is recruited to continue synthesis several nucleotides downstream. A displaced DNA strand (a flap) is generated, which is removed by the flap endonuclease 1 (FEN1), also preparing for ligation. This is called long-patch BER/repair (LPR). The final step in BER is catalyzed by the DNA ligase LIG1, which also is the main DNA ligase in chromosomal replication, and/or the LIG3α/XRCC1 complex, which is primarily involved in SPR; both are dependent on ATP as cosubstrate (Figure 3). However, the exact molecular basis for choosing SPR (or LPR) over the other is unclear. For example, the presence or absence of some

Pols and cofactors, the type of initiating lesion, different protein–protein interactions, the cell cycle stage, or whether the cell is terminally differentiated or actively dividing, all appear to have an impact on the final decision. The decision also seems to be influenced, at least in part, by the relative ATP concentration after 5´-dRP removal. If the ATP concentration is high, BER is likely to proceed immediately to ligation by LIG3α. Alternatively, LPR will occur more frequently at low ATP concentration where ligation is less favored (4,22-25).

1.4.1 Uracil-DNA glycosylases

Uracil and some uracil analogs formed by oxidation of cytosine and thymine are excised from the genome by UDGs. Mammalian cell nuclei contains at least four UDGs; UNG2 (uracil-*N*-glycosylase 2), SMUG1 (single-strand-specific monofunctional UDG), TDG and MBD4 (methyl-CpG binding domain protein 4). UNG2 and SMUG1 are the enzymes responsible for repair of spontaneously deaminated cytosine (26), while post-replicative excision of misincorporated dUMP (U:A) and excision of AID-generated uracil (U:G) are performed mainly by UNG2 alone (27). UNG is profoundly specific for processing uracil in DNA, yet also inefficiently excises 5-fluorouracil (FU), a common cancer chemotherapeutic agent (28). Interactions with the replication clamp PCNA (proliferating cell nuclear antigen) and the ssDNA- binding protein RPA (replication protein A) indicate recruitment of UNG2 to sites of DNA synthesis, where its primary function is to rapidly excise uracil incorporated opposite adenine (29). *E. coli* Ung (5) turned out to be the founding member of a large superfamily of UDGs (30), which currently includes six subfamilies, three of which are present in Eukarya. In addition to UNG itself (family 1/UNG family), these include the mismatch-specific UDG (family 2/Mug family; TDG in mammals) (31) and SMUG1 (family 3/SMUG family) (32). Despite a considerable amino acid sequence divergence, all UDGs share a common αβ-fold-structured catalytic domain (33). The family 2 UDGs emerged with the identification of TDG, an enzyme capable of excising thymine from G:T mismatches. Regardless, the family was named after the *E. coli* Mug protein (31) crediting that the G:U rather than the G:T mismatch is the most efficient substrate for the members of this subfamily. In contrast to UNG, the family 2 glycosylases have a spacious and rather non-discriminating active site pocket, accommodating a broad range of substrates including pyrimidine derivates like FU, 5-hydroxymethyluracil (hmU) and 3,*N*4-ethenocytosine (34). However, these substrates are excised at an extremely low turnover rate (35). Compared to *E. coli* Mug, which mainly comprises of the catalytic

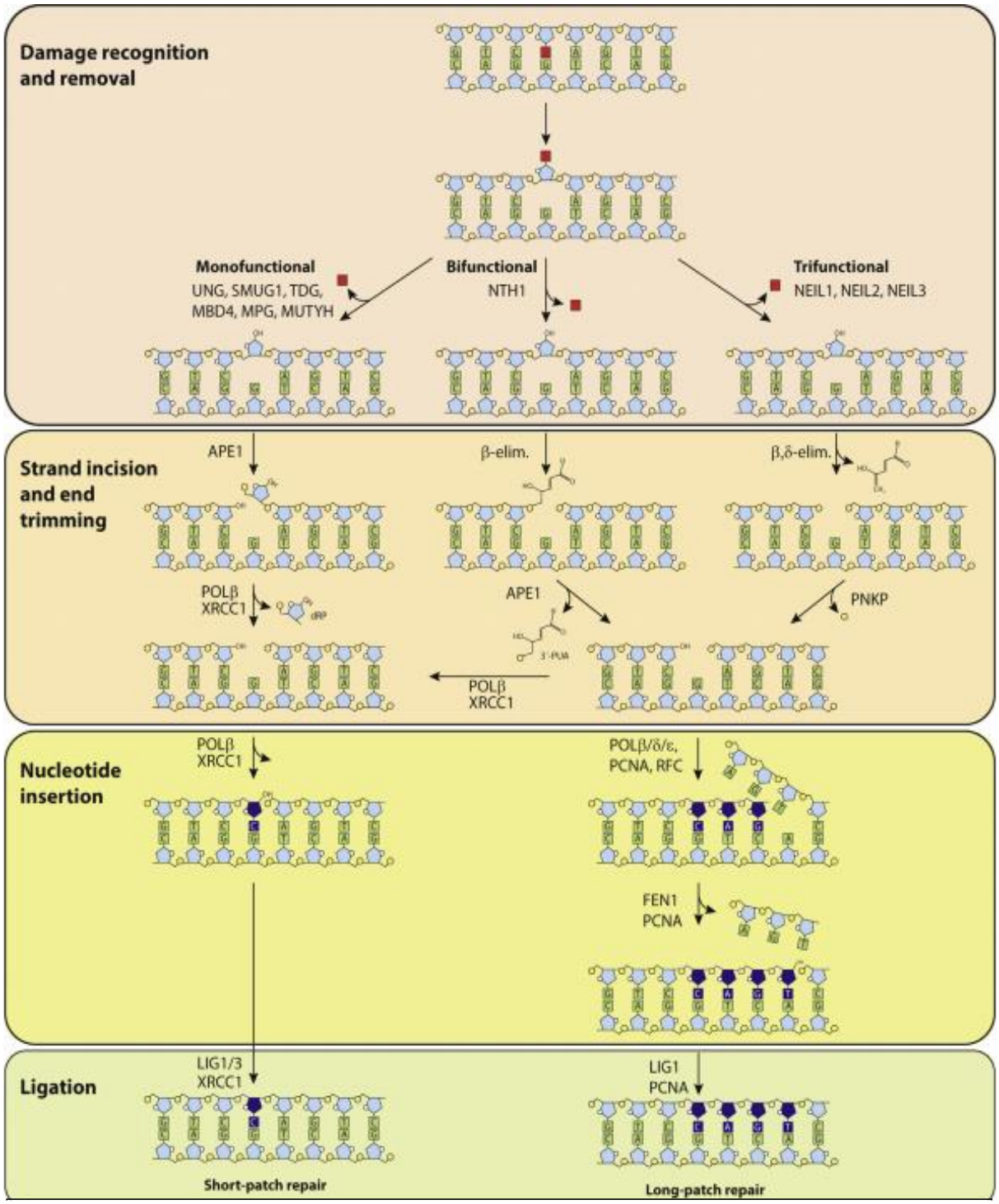

Figure 3. The mammalian base excision repair pathway. The four steps of BER is divided into; damage recognition and removal; strand incision and end trimming; nucleotide insertion; ligation. The continuation of BER is then either short-patch repair (SPR) or long-patch repair (LPR). The method is often chosen by what type of cell of BER is initiated in, where LPR is often located in proliferating cells and SPR is found in both proliferating and non-proliferating cells (4).

core only, TDG contains additional N-and C-terminal areas providing non-specific DNA interaction and regulatory functions (36). Additional subfamilies of UDGs appear to have evolved in archaeal and bacterial organisms thriving under extreme environmental conditions such as high temperature, favoring hydrolytic deamination of cytosine and m^5C.

1.4.2 SMUG1

The uracil-excising activity ascribed to the SMUG family was initially identified in *Xenopus laevis*, insect and human cells (32), and was thought to be present in vertebrates and insects only (37). Vertebrates contain both SMUG1 and UNG, yet their roles as UDGs are still not completely understood. At the beginning it was believed that SMUG1 mainly served as a back-up for UNG (38), but subsequent discoveries of other activities and interactions have prompted investigations into other biological functions. When first discovered in *X. laevis*, the xSMUG1 enzyme was characterized as "single-strand-selective" which indeed resulted in its name (32). Unfortunately, overlooking the strong feedback inhibition of the AP site in the initial characterization of xSMUG failed to show its actually higher activity for U:G and U:A than for U in ssDNA (38).

Like TDG, SMUG1 excises FU from DNA, which, in contrast to TDG, appears to protect cells from the cytotoxic effects of the drug, as shown by siRNA knockdown experiments (39). Interestingly, a hmU-DNA glycosylase activity originally discovered in calf thymus was later identified as SMUG1 (40). Since hmU is the deamination product of 5-hydroxymethylcytosine, which has been recognized both as an intermediate substrate in the m^5C demethylation pathway as well as an epigenetic marker itself, SMUG1 may be involved in epigenetic regulation. However, hmU is also a common ROS-induced DNA damage, and together with the activity for other abundant oxidized pyrimidines like 5-hydroxyuracil and fU demonstrated by SMUG1 (41) it is now believed to play a significant role in the repair of oxidized bases.

Recently, our research group demonstrated that hSMUG1 is able to incise the AP site after uracil removal, which results in a 3´-α,β-unsaturated aldehyde (designated uracil-DNA incision product, UIP) and a 5´-phosphate. UIP is removed from the 3´-end by hAPE1. hSMUG1 also incises DNA or processes UIP to a 3´-phosphate (designated uracil-DNA processing product, UPP) (Figure 4) (42). Further studies demonstrated that also hUNG is able to form UIP (43).

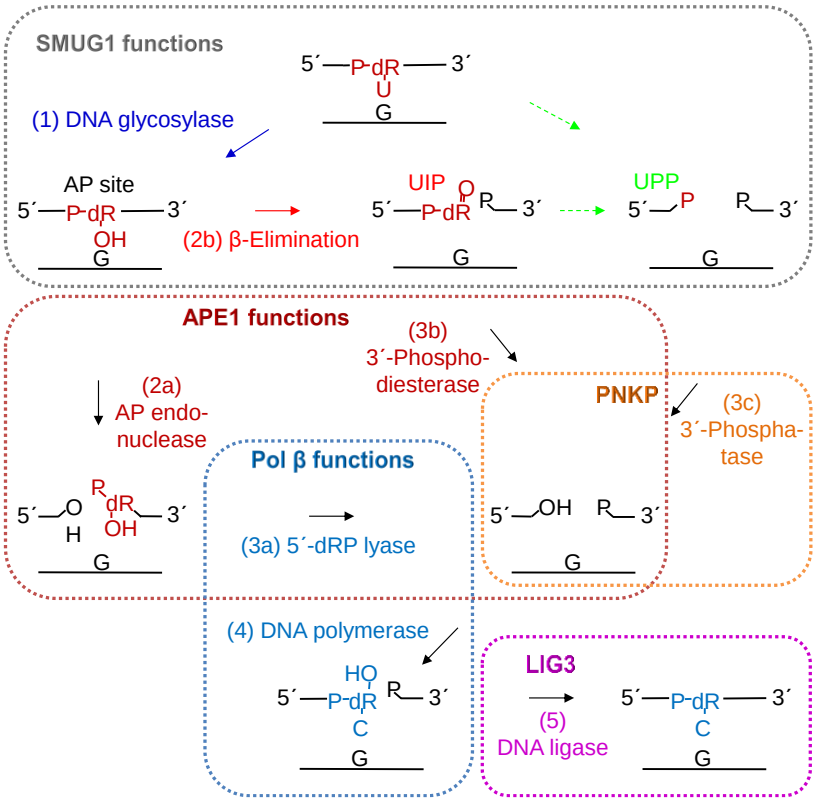

Figure 4. Proposed human BER pathway. After uracil has been removed by the DNA glycosylase activity of SMUG1 (step 1; blue), the latter is either replaced by APE1 (dark red) which incises the AP site (step 2a), or SMUG1 itself incises the AP site (step 2b; red) leaving behind a 3´-α,β-unsaturated aldehyde (UIP) which can be removed by APE1 (step 3b). Further processing of UIP (or maybe an alternative type of incision of the AP site; green broken arrows) results in a 3´-phosphate (UPP) which is a substrate for PNKP (orange). The cleaned one nucleotide gap in DNA is now ready for insertion of the correct dCMP (step 4) by the repair DNA polymerase β (Pol β; dark blue), which also exhibits the dRP lyase activity which removes the 5´-dRP remnant (step 3a) after APE1 incision. BER is concluded by nick-sealing (step 5) by DNA ligase III (LIG3; purple). The residues removed are indicated in dark red; those resulting from replacement in dark blue, respectively; dR, deoxyribose. From (42).

During immunoglobulin gene diversification in activated B cells, targeted cytosine deamination by AID followed by uracil excision by hUNG (4) is important for CSR and SHM by providing the substrate for DNA double strand breaks and mutagenesis, respectively (44), where SMUG1 also may be involved (27,45). However, considerable uncertainty remains regarding the mechanisms leading to DNA incision following uracil excision, but based on the general BER scheme an AP endonuclease (APE1 and/or APE2) is believed to be required for strand-break formation (Figure 5, right square). Although a substantial residual CSR level (~20%) has been demonstrated present in cells in the absence of both APE1 and APE2, suggesting that other enzymes may contribute DNA nicking activity (46). The finding in our research group that hSMUG1 (42), and now also hUNG (43), is able to incise the AP site fol

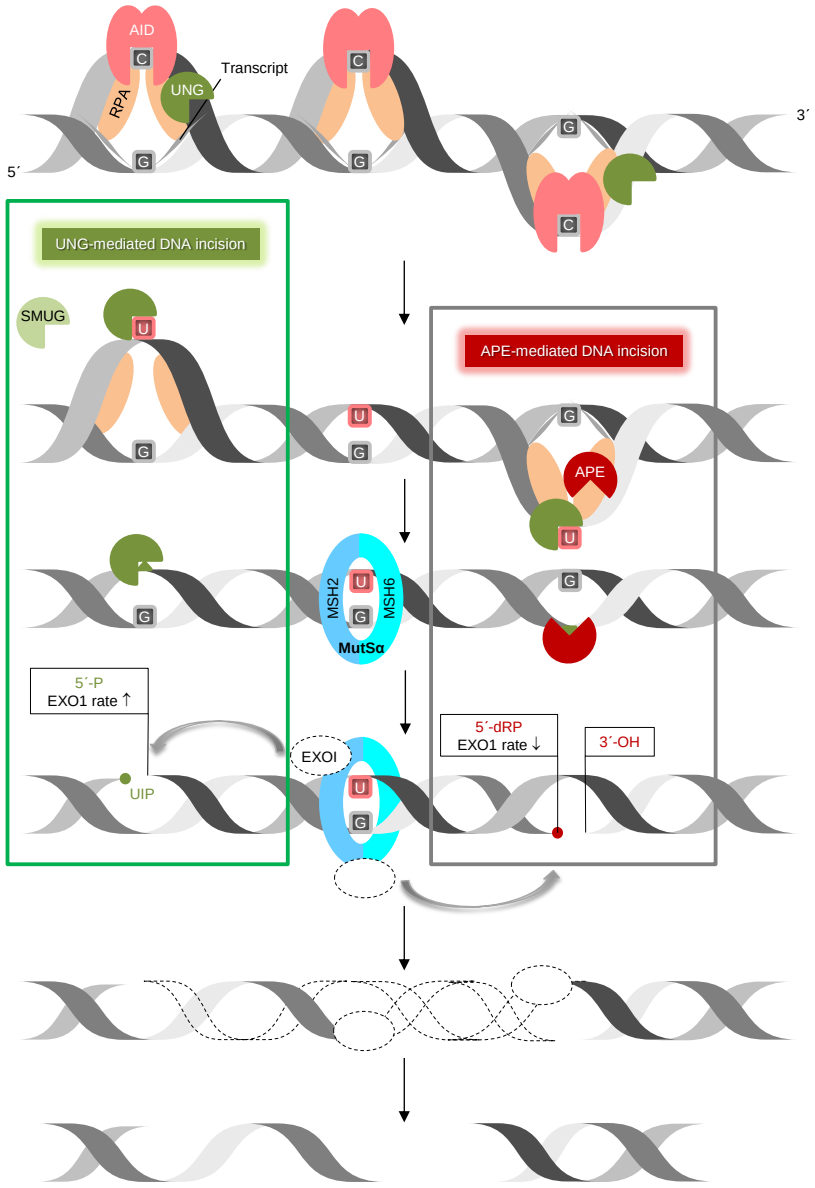

Figure 5. UNG-mediated DNA incision in CSR. This working model suggests how removal of AID-generated uracil followed by incision of the AP site by UNG and nick processing by exonuclease 1 (EXO1) form double-stranded breaks in immunoglobulin switch regions. Transcription of the targeted immunoglobulin gene region forms bubbles in DNA, so granting AID access to ssDNA (stabilized by RPA) to deaminate C to U. This results in UNG recruitment (by RPA) and uracil excision. According to our results (left square), UNG (with SMUG1 as a backup) is able to incise the AP site, leaving behind a 5´-phosphate which is a better substrate for exonuclease 1 (EXO1) 5´→ 3´ digestion than the 5´-deoxyribose phosphate left behind by APE1 incision (right square). This model relies on the MMR component MutSα (MSH2/6), which recognizes an U:G mismatch and recruits EXO1. This also applies to ssDNA patch generation by EXO1 in SHM. ↑, increased. From reference (43).

lowing uracil excision, may obviate the need of involving AP endonucleases in explaining the molecular mechanism of UNG and SMUG1 in CSR, and opens up a possibility that SMUG1 act as a back-up UDG for UNG in CSR and SHM (Figure 5, left square). This may partially

explain the reported dispensability of APE enzymes in SHM through providing MMR complex accessibility at an earlier stage.

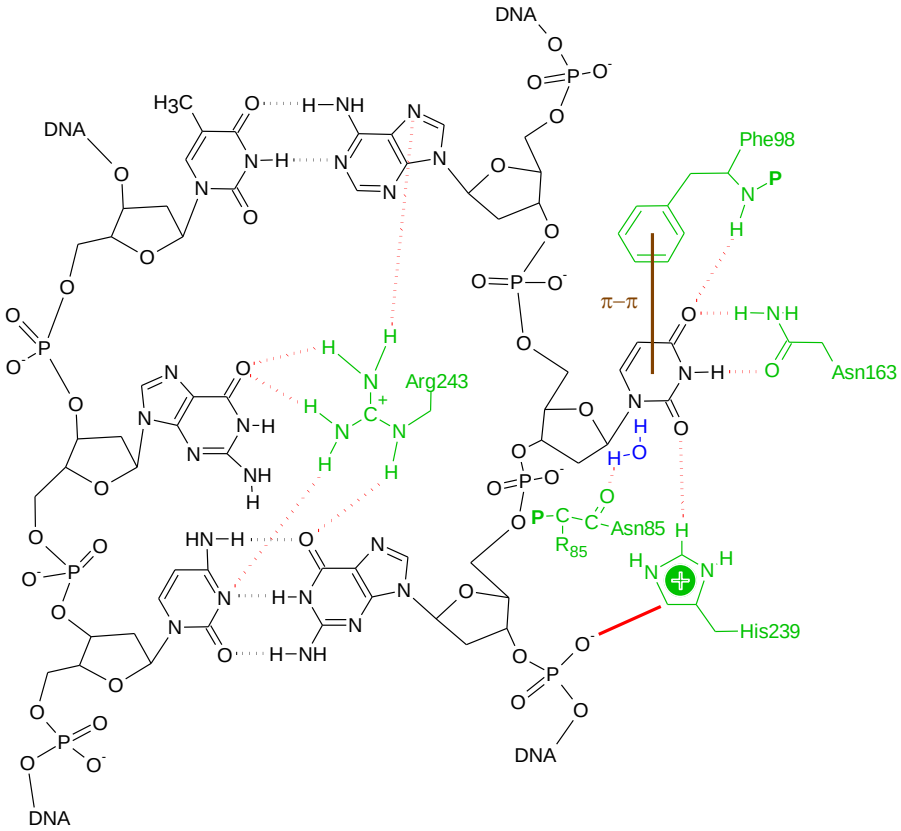

Figure 6. hSMUG1 active site interactions. DNA structure in black; protein amino acid residues in green; catalytic water in blue; **P**, protein; R, amino acid residue. Red unbroken line, ionic interaction; red dotted line, hydrogen bond; black dotted line, H bond between cognate bases; brown unbroken line, van der Waals interaction. Courtesy of Svein Bjelland.

1.4.2.1 Structure of hSMUG1 explains its base recognition

The SMUG family exhibits only limited amino-acid sequence similarity with members of the other UDG subfamilies and the conservation seems restricted to catalytic site residues, showing mosaic features of the UNG and MUG enzymes. Crystallographic analysis of xSMUG1 recognized a pyrimidine-binding pocket topologically similar to those of other UDGs, and implicated a water displacement/replacement mechanism to account for its preference for uracil over thymine. In the crystal structure of xSMUG1 in complex with uracil-containing dsDNA, the enzyme detached from the AP site product and rebound to the DNA ends. Such behavior was also observed with the substrate analog 1-[2´-deoxy-2´-fluoro-β-D-arabinofuranosyl]-uracil (βFU). At the 5´-end of the damage-containing strand, a cytosine has an extrahelical conformation and

points towards the pyrimidine specificity pocket of the xSMUG1. Upon replacing the 5´-end cytosine base with βFU, a mixed population of extrahelical cleaved AP sites and βFU in a productive orientation in the active site was observed. Two motifs, the minor groove intercalation loop (xSMUG1 251-PSPRN-225) and the short α helix unique to the SMUG1 family (xSMUG1 256-PQANK-260), are inserted as a wedge into the DNA duplex, flipping the scissile nucleotide through the major groove as for the family 1 and 2 UDGs. However, penetration of both motifs into the base stack creates a more extensive disruption of the dsDNA than seen for the other enzymes in the UDG family. A conserved Arg254 (Arg243 in hSMUG1; Figure 6) occupies the gap left behind from the flipped-out base, whereas a Pro from the unique α helix pushes into the base stack on the distal strand. At the SMUG1 protein bound to the 3´-end of the damage-containing strand, the base pairing remained intact and the active site was accessible to solvent. This fact was exploited when free uracil and hmU was soaked into the crystal, which revealed a rather remarkable mechanism for achieving pyrimidine specificity in SMUG1. The uracil N3-imino and O4 carbonyl moieties hydrogen bond to Asn174 (Asn163 in hSMUG1; Figure 5) side chain, and O2 accepts a hydrogen bond from Met95 main chain NH group and imidazole ring of His250 (His239 in hSMUG1; Figure 6). This hydrogen bonding pattern implies that cytosine is rejected by SMUG1 in a manner analogous to that for UNG (47).

1.4.2.2 SMUG1 is involved in telomerase RNA processing and RNA quality control

Telomerase is a specialized ribonucleoprotein (RNP) complex that extends telomeric repeats at the ends of chromosomes (48). The telomerase holoenzyme comprises three main subunits: the telomerase reverse transcriptase (hTERT), the telomerase RNA component (hTERC) and a complex of the major pseudouridine synthase in mammals dyskerin (DKC1) (DKC1, NHP2, NOP1, and GAR1) (49). hTERC biogenesis is a multistep process, initiated by transcription of the primary transcript by RNA polymerase II that can extend several hundred nucleotides downstream of the hTERC gene body (50). SMUG1 regulates the presence of base modifications (51) and interacts with hTERC, which is required for co-transcriptional processing of the nascent transcript into mature hTERC. It is the highly structured non-coding RNA that carries the complementary template of the telomeric repeat sequence and two H/ACA domains that bind to dyskerin (52). The hTERC/dyskerin RNP complex and hTERT associate in both nucleoli and Cajal bodies during S phase, suggesting that both these subnuclear structures are involved in the biogenesis and trafficking of the telomerase complex (53,54). In the nucleoli ribosomal RNA (rRNA) synthesis and processing, rather than DNA metabolism, takes place. Subsequent

end-processing steps lead to the formation of the 451 nucleotides long mature hTERC (50). Loss of SMUG1 leads to an imbalance between mature hTERC and its processing intermediates, resulting in accumulation of 3´-polyadenylated and 3´-extended intermediates that are degraded in an EXOSC10-independent RNA degradation pathway (51).

SMUG1 interacts and co-localizes with DKC1, and associates with the 47S rRNA precursor, which is a major substrate of DKC1. hSMUG1 amino acids 25–35 and 220–233 were indicated as potential DKC1-binding sequences, while the DKC1 peptides consisting of amino acids 16–29, 112–122, 247–260, 400–410 and 475–491 were indicated as potential binding sequences to hSMUG1. Molecular modeling indicates involvement of hSMUG1 Glu29 and Glu33, and DKC1 Arg110 and Arg111, and furthermore hSMUG1 Glu231, in the interaction surface. Eventually, site-directed mutagenesis demonstrated that hSMUG1 amino acids 29, 33 and 231 are required for binding to DKC1 (Table 1). It is important to note that interaction with DKC1 does not obstruct SMUG1 activity, nor does interaction with SMUG1 obstruct DKC1 activity. Loss of SMUG1 leads to rRNA processing defects and accumulation of hmU in rRNA. hSMUG1 excises hmU from a single deoxyribose moiety placed in single-stranded RNA *in vitro*, suggesting that the enzyme may excise hmU from RNA *in vivo*. hSMUG1 does not excise uracil or the abundant RNA base pseudouracil (ΨU) from RNA *in vitro* (51,55).

Table 1. Function of hSMUG1 amino acid residues

Residue	Function	Reference
Ala14	RNA	
Ala16	RNA	
Gly25	rRNA quality control: putatively binds DKC1	(55)
Ser26	rRNA quality control: putatively binds DKC1	(55)
Leu27	rRNA quality control: putatively binds DKC1	(55)
Ala28	rRNA quality control: putatively binds DKC1	(55)
Glu29	rRNA quality control: binds DKC1	(55)
Ser30	rRNA quality control: putatively binds DKC1	(55)
Phe31	rRNA quality control: putatively binds DKC1	(55)
Leu32	rRNA quality control: putatively binds DKC1	(55)
Glu33	rRNA quality control: binds DKC1	(55)
Glu34	rRNA quality control: putatively binds DKC1	(55)
Glu35	rRNA quality control: putatively binds DKC1	(55)
Asn85	*N*-glycosidic bond hydrolysis: coordination of catalytic H_2O	(41)
Gly87[1]	Substrate binding: binds H_2O^2, C^5-O, C^5-CO, discriminates C^5-CH_3	(41)
Phe89	Substrate binding: increases affinity for U:G	(41)
Gly90	Substrate binding: allows space for H_2O^2, C^5-O, C^5-CO	(41,56)
Met91[1]	Substrate binding: binds H_2O^2, C^5-O, C^5-CO, discriminates C^5-CH_3	(41)
Phe98	Substrate binding: stabilization of flipped-out U by π–π stacking	(41,57)
Asn163	Substrate binding: discriminate C^4-NH_2, bind N^3-H and O^4	(41)
Arg220	rRNA quality control: putatively binds DKC1	(55)
Ala221	rRNA quality control: putatively binds DKC1	(55)
Arg222	rRNA quality control: putatively binds DKC1	(55)
Arg223	rRNA quality control: putatively binds DKC1	(55)
Ala224	rRNA quality control: putatively binds DKC1	(55)
Leu225	rRNA quality control: putatively binds DKC1	(55)
Ala226	rRNA quality control: putatively binds DKC1	(55)
Gly227	rRNA quality control: putatively binds DKC1	(55)
Leu228	rRNA quality control: putatively binds DKC1	(55)
Met229	rRNA quality control: putatively binds DKC1	(55)
Pro230	rRNA quality control: putatively binds DKC1	(55)
Glu231	rRNA quality control: binds DKC1	(55)
Val232	rRNA quality control: putatively binds DKC1	(55)
Gln233	rRNA quality control: putatively binds DKC1	(55)
His239	*N*-glycosidic bond hydrolysis: binds O^2, stabilization of transition state	(41,57)
Pro240	Intercalating loop Excision-DNA incision	(41,56)
Ser241	Excision-DNA incision	(41)
Pro242	Excision-DNA incision	(41)

Arg243	Occupies empty space after base flipping, DNA-RNA discrimination	(41,57)
Asn244	Motif 2, intercalating loop	(41,56,58)
Pro245	Motif 2, intercalating loop	(41,58)
Gln246	Motif 2, intercalating loop	(41,58)
Asn248	Motif 2, intercalating loop	(41,56,58)
Lys249	Motif 2, intercalating loop	(41,58)

[1], main-chain NHs; [2], water-bridge to O^4 of uracil.

Aim of the project

hSMUG1 is the most important back-up enzyme for hUNG, the latter being the major UDG in human cells as well as having a crucial function in immunoglobulin gene diversification in activated B cells where cytosine in R-loop structures is deaminated. However, the (back-up) role for hSMUG1 in immune function is elusive. Thus, the aim of the present investigation was to determine hSMUG1 excision activity for uracil in R-loop DNA. This activity was compared to that in bubble U-DNA, another important structure formed transiently in cells during cellular processes as e.g. DNA replication.

Because hSMUG1 was found to exhibit uracil excision activity in both bubble and R-loop DNA, the next aim of the project was to produce purified hSMUG1 mutant protein to investigate whether certain amino acid replacements may interfere with enzyme function towards these U-DNA substrates. After purifying hSMUG1 S26R/E35D protein to apparent physical homogeneity, it was investigated for excision activity for uracil in bubble and R-loop DNA together with hSMUG1 P240G protein that was purified by another member of our research group.

2 Materials and methods

2.1 Production of recombinant hSMUG1 wild type and mutant proteins

2.1.1 Production of chemically competent *E. coli* strains BL21(DE3)pLysS and Rosetta(DE3)pLysS to prepare for transformation

The *E. coli* strain BL21(DE3)pLysS and Rosetta(DE3)pLysS are resistant to chloramphenicol (34 μg/ml). LB medium (3 ml) was inoculated with a single colony of the *E. coli*, and grown overnight at 37°C with vigorous shaking. On the following day, an aliquot of overnight culture (200 μl) was transferred to 25 ml LB medium followed by growth overnight using the same conditions until the culture reached an OD A_{600} of 0.3−0.5 (depending on the strain this takes 2−4 h). The culture was placed on ice for 10 min and split into 4 round-bottom tubes of 6 ml each, which were centrifuged for 10 min at 4000 rpm at 4°C. The pellet was mixed with 3 ml ice cold sterile 100 mM $CaCl_2$, left on ice for 30 min and centrifuged for 10 min at 4000 rpm a 4°C. The resulting pellet was mixed with 400 μl ice cold sterile 100 mM $CaCl_2$ and split into Eppendorf tubes with 200 μl cells per tube.

2.1.2 Transformation of *E. coli* strains BL21(DE3)pLysS and Rosetta(DE3)pLysS with plasmid pETM11-SMUG1

An amount of 1 μl of pETM11-SMUG1 (20 ng DNA for supercoiled plasmids) was added to 100−200 μl of competent cells and incubated for 30 min on ice, followed by incubation in a water bath for 45 s (BL21) or 30 s (Rosetta) at 42°C and placement on ice. Then, S.O.C. Medium (ThermoFisher Scientific), 900 μl for BL21 and 500 μl for Rosetta, was added to the tube followed by incubation for 1 h at 37°C with shaking (225 rpm). An appropriate volume (100−200 μl) of the putatively transformed cells was spread on LB plate(s) containing chloramphenicol (34 μg/ml) and kanamycin (50 μg/ml) and grown overnight at 37°C. Bacterial colonies for hSMUG1 protein production were stored on the plates in the fridge at 4°C.

2.1.3 Analysis for recombinant protein production

Autoinduction

For the un-induced sample, one colony of transformed cells was inoculated in 3 ml of MDG for autoinduction (ZY-5052) containing chloramphenicol (34 μg/ml) and kanamycin (50 μg/ml). Cells were grown for at least 4 h at 37°C with shaking (300 rpm). A major fraction of the culture (2 ml) was withdrawn for determination of OD_{600}, which needs to be in the range 0.4−0.6. When reaching the desired $OD_{600,}$ the volume of the culture ($V_{culture}$) to be used is given by the formula: $V_{culture}$ (μl) = OD_{600}/0.8 × 1000. Then, the culture was transferred to a 1.5-ml Eppendorf tube and centrifuged for 1 min at 13 000 rpm, followed by removal of the supernatant. The cell pellet was stored at −20°C. For the induced sample, shaking (300 rpm) was continued overnight at the lower temperature of 28°C. Subsequently, 200 μl of the culture was diluted 10-fold with 1× PBS (phosphate-buffered saline) to measure OD_{600}. When 0.8 is divided by the resulting OD_{600}, the volume of the culture ($V_{culture}$) to be used is given by the formula: $V_{culture}$ (μl) = OD_{600}/0.8 × 1000. For example, if 0.8/OD_{600} = 0.5, $V_{culture}$ = 500 μl is centrifuged and the cell pellet stored at −20°C.

Induction with isopropyl β-D-thiogalactoside

For un-induced and induced sample, 10 colonies of transformed bacteria were transferred from LB plate stored at 4°C to 25 ml of LB medium containing chloramphenicol (34 μg/ml) and kanamycin (50 μg/ml) in an Erlenmeyer flask and grown until OD_{600} reached 0.4−0.6. An aliquot of culture (1 ml) was removed and the $V_{culture}$ determined as above. The cells were harvested by centrifugation and the pellet stored at −20°C.

For the induced sample, the culture was split into 5 tubes 3 ml each, each added 3 μl of 1 mM isopropyl β-D-thiogalactoside (IPTG), which were incubated for, 1) 1 h at 37°C, 2) 2 h at 37°C, 3) 3 h at 37°C, 4) 4 h at 37°C and 5) overnight at 23°C, all with shaking (220−250 rpm). After each type of incubation, OD_{600} was measured and $V_{culture}$ determined, and the cells harvested as above.

Un-induced and IPTG-induced cells were mixed with in 100 μl of 1× Laemmli sodium dodecyl sulfate (SDS)-polyacrylamide gel electrophoresis (PAGE) sample buffer (Bio-Rad) and heated at 95°C for 10 min, followed by centrifugation at room temperature for 5 min at 13 000 rpm. 10

µl of all samples were analyzed at 12% TGX-SDS-PAGE gel (Bio-Rad) electrophoresed at 220 V for 35 min.

2.1.4 Gravity purification of wild type hSMUG and hSMUG S26R/E35D by large scale protein overproduction and affinity chromatography

Large scale protein overproduction

One colony of the Rosetta strain was transferred to 25 ml LB medium containing chloramphenicol (34 µg/ml) and kanamycin (50 µg/ml) followed by incubation overnight at 37°C with shaking (220 rpm). All of the overnight culture was transferred to 1000 ml LB medium containing kanamycin (50 µg/ml) and chloramphenicol (34 µg/ml), followed by measurement of OD_{600} and incubation at 37°C with shaking (220 rpm) until $OD_{600} \approx 0.6$. Then the culture (1024 ml) was added 1024 µl of 1 mM IPTG (final) and incubated for 2 h at 37°C with shaking (220 rpm), followed by harvesting of the cells by centrifugation (6000 rpm) for 20 min at room temperature. The cell pellet was stored at −20°C for later purification.

TALON affinity purification using gravity column

After addition of 20 ml of 20 mM Tris-HCl, pH 8.0, 10 mM imidazole, 150 mM NaCl, 0.2% (v/v) NP-40 (tergitol), 2 mM β-mercaptoethanol, 0.5 mM phenylmethylsulfonyl fluoride (PMSF) (lysis buffer), the cell pellet was solubilized and lysozyme (final concentration, 1 mg/ml) was added followed by incubation for 30 min at 4°C with gentle shaking. The sample was sonicated (30% amplitude) "10 s on, 10 s off" repeated 6 times with the beaker on ice. Then DNAase (final concentration, 40 µg/ml) was added, followed by incubation for 15 min at 4°C. The sample was transferred to SS-34 tubes and centrifuged (15 000 rpm) at 4°C for 30 min, followed by transfer of the supernatant (designated "crude extract") to a fresh tube. (20 µl of crude extract was taken to be analyzed by SDS-PAGE later. Crude extract was added to gravity column with 1 ml of equilibrated TALON beads (see Appendix), and the flow-through was collected. The beads were washed with 5 ml of 20 mM Tris-HCl, pH 8.0, 10 mM imidazole, 150 mM NaCl, 2 mM β-mercaptoethanol, 0.5 mM PMSF (wash 2), 5 ml of wash 3 (wash 2 containing 1 M NaCl) and 5 ml of wash 4 (wash 2 with 20−50 mM imidazole, without PMSF). Protein was eluted using 4 ml elution buffer (wash 2 with 330 mM imidazole, without PMSF) in four fractions. The fractions were pooled followed by addition of 50 µl of AcTEV (tobacco etch virus) protease (Themo Fisher Scientific, Product No. 12575015), and dialyzed against 2 l of lysis buffer (plus fresh 2 mM β-mercaptoethanol) using the Pre-wetted RC tubing MWCO

16 kDa membrane (Spectra/Por, No. 132562), which should putatively remove excised His-tag. The dialyzed protein was transferred to equilibrated TALON beads in a gravity column followed by incubation for 30 min at 4°C. The flow-through (i.e., protein without His-tag) was collected, followed by elution with 5 ml of wash 2 and 5 ml of wash 4 (to remove the rest of protein without His-tag). The AcTEV protease was removed from the beads with elution buffer (4 ml) in 4 different fractions. The protein concentration was determined by NanoDrop (ThermoFisher Scientific) using buffer A as blank solution.

2.1.5 Purification of wild type hSMUG1 and hSMUG1 A14T/A16T by small scale protein overproduction and affinity purification

Small scale protein overproduction

One colony of transformed Rosetta strain bacteria was added to 3 ml LB medium containing chloramphenicol (34 μg/ml) and kanamycin (50 μg/ml) and incubated overnight at 37°C with shaking (220 rpm). Overnight culture was transferred to 50 ml LB medium in an Erlenmeyer flask containing the same concentration of antibiotics and incubated until OD_{600} reached 0.6. Then gene expression was induced with 50 μl of 1 mM IPTG and the culture incubated overnight at 23°C. Bacteria were harvested by centrifugation at 3000 rpm for 20 min at room temperature, followed by addition of 2 ml lysis buffer. After addition of lysozyme (final concentration, 1 mg/ml), the sample was incubated with gentle shaking at 4°C for 30 min followed by sonication (10% amplitude) "10 s on, 10 s off" repeated 6 times with the beaker on ice. The sample was transferred to Eppendorf tubes and centrifuged (13 000 rpm) at 4°C for 10 min. Supernatant ("crude extract") was transferred to new Eppendorf tubes (20 μl was analyzed by SDS-PAGE).

Small scale TALON affinity purification

Crude extract was added to 0.5 ml of equilibrated TALON beads (see Appendix) and the suspension transferred to a gravity column, followed by incubation at 4°C for 30 min with gentle shaking. The flow-through was collected (20 μl for SDS-PAGE analysis), followed by elution with 5 ml of lysis buffer, and 5 ml each of wash 2−wash 4, where the eluted liquids were discarded. Then elution buffer (0.5 ml) was applied to the column 3−5 times where all eluted liquids was collected and analyzed by SDS-PAGE and Western Blot.

2.1.6 Expression of hSMUG1 A14T/A16T, hSMUG1 S26R|E35D and hSMUG1 wild type by autoinduction and batch affinity purification

Autoinduction

MDG solution (20 ml) and kanamycin (50 µg/ml) were mixed in a Falcon tube, and the mixture was distributed to 3 tubes with 5 ml each where two of them were inoculated with one transformed bacterial colony followed by incubation overnight at 37°C with shaking (220 rpm); one tube served as a control. On the following day, 500 µl of the overnight culture, 500 ml of ZYM-5052 and 500 µl of kanamycin (50 µg/ml) were mixed and incubated overnight at 28°C with shaking (220 rpm). Bacteria were harvested by centrifugation at 6000 rpm for 20 min at 4°C. The cell pellet was weighted, frozen using liquid nitrogen and stored at −80°C.

Batch purification with affinity TALON beads

Bacterial pellet was added to lysis buffer (7 ml per g). After addition of lysozyme (final concentration, 1 mg/ml) and one EDTA-free protease inhibitor cocktail tablet (Thermo Scientific; lot No. VC2936735), the sample was incubated with gentle shaking at 4°C for 30 min followed by addition of NP-40 [tergitol; final concentration, 0.5% (v/v)], MgCl2 (final concentration, 5 mM), DNAase (final concentration, 40 µg/ml) and RNAase (final concentration, 5 µg/ml) followed by incubation for 20 min at 4°C and sonication (30% amplitude) for 10 min "5 s on, 4 s off" with the beaker on ice with steering. The sample was centrifuged (20 000 rpm) for 45 min at 4°C. Supernatant ("crude extract") was placed on ice, where 20 µl was subjected to SDS-PAGE analysis.

Crude extract was mixed with 2 ml of equilibrated TALON beads (see Appendix) and the suspension transferred to a 50 ml Falcon tube, followed by incubation at 4°C for 30 min with gentle shaking and centrifugation for 5 min at 500 × g. [The supernatant was analyzed by SDS-PAGE (20 µl) and thereafter discarded]. Buffer A [50 mM Tris pH 7.5, 300 mM NaCl, 10 mM imidazole, 2 mM βME] (10 ml) containing 10 mM imidazole was added to the beads followed by incubation for 5 min at 4°C with gently shaking. After centrifugation for 5 min at 500 × g, the supernatant was discarded (the procedure was repeated twice). 2 ml of buffer A with 100 mM imidazole was added, followed by incubation for 10 min at 4°C with gentle shaking and thereafter centrifugation for 5 min at 500 × g. The eluted fraction of the protein was carefully transferred to a precooled 2 ml Eppendorf tube. This final procedure was repeated twice. Fractions

were analyzed by SDS-PAGE at 220 V for 40 min. The fractions of the purified protein were pooled followed by addition of 50 µl of AcTEV protease (Themo Fisher Scientific, Product No. 12575015), and dialyzed against 2 l of buffer A (plus 2 mM β-mercaptoethanol) using the Pre-wetted RC tubing MWCO 16 kDa membrane (Spectra/Por, No. 132562). The protein concentration was determined by NanoDrop (ThermoFisher Scientific) using buffer A as blank solution.

2.2 hSMUG1 wild type and mutant proteins from other sources

hSMUG1 was obtained from NEB (product No. M0336S); purified hSMUG1 wild type was provided by Trond Bærheim; hSMUG1 P240G protein was provided by Celine Lorentsen (59).

2.3 Western blot for verification of hSMUG1 protein

Performed SDS-PAGE for all samples used in expression test for hSMUG1.

Trans-Blot Turbo transfer pack (Bio-Rad) for the blotting were used with 3 min transfer time using the blotting machine (Bio-RAd). Membrane were transferred to the clean dish. Blocking solution 5% (w/v) BSA in PBST (0.1 % Tween 20) was applied for 1 h at room temperature with shaking. Primary antibody; primary rabbit anti-SMUG Ab 1:2000 in 10 ml of 5% (w/v) BSA in PBST was used. Membrane was washed 3 × 5 min PBST (0.1% Tween 20) with shaking at room temperature. Then, secondary Goat anti rabbit-HRP IgG 1:2000 (ThermoFisher Scientific, Product No. 31460) was added together with Precision Protein M Strep Tactin-HRP Conjugate for 1.5 h at room temperature with shaking. Then membrane was washed 3 × 5 min with PBST (0.1 %) with shaking in room temperature. Membrane were placed on the plastic cover and was applied with Clarity Western ECL substrate for 5 min. Excess substrate was removed and dried by dipping edges with paper. Figure was acquired using the Bio-RAd ChemDoc.

2.4 Base excision activity assay

hSMUG1 protein was incubated with substrate (1 pmol) in a reaction mixture of 5× HEPES buffer (225 mM HEPES, pH 7.5, 2 mM EDTA, 10% (v/v) glycerol) 10 mg/ml BSA, 1 mM DTT, and 1 M KCl. The reaction was terminated by the addition of (Stop solution) 20 mM EDTA, 0.5% (w/v) SDS, and 10 µg proteinase K, incubated for 10 min at 37°C. The DNA was ethanol precipitated by the addition of 16 µg transfer RNA (tRNA) and 0.1 M sodium acetate

at –20°C overnight. The DNA pellets were collected by centrifugation (13000 rpm, 4°C for 30 min) and washed in 70% ethanol (–20°C). Then, dried pellets were mixed with in 10 µl of 0.1 M NaOH and was heated at 90°C for 10 min. Before loading into the denaturing PAGE, the samples were mixed with formamide gel loading buffer [80% (v/v) formamide, 1 mM EDTA and 1% (w/v) blue dextran]. Samples (10 µl) were prepared for electrophoresis by the addition of 10 µl of the loading buffer. A volume of 5 µl was subjected to denaturing PAGE [20% (w/v) polyacrylamide gel with 3% (v/v) formamide] at 200 V for 1.5 h. Visualization and quantification were performed by fluorescence imaging analysis using ImageQuant Software (Molecular Dynamics Inc.). Figures was acquired using Typhoon Trio™ (GE Healthcare). The graphs were drawn using KaleidaGraph version 4.1.0 (Synergy Software).

2.5. Substrate hybridization

The only practical way of detecting specific nucleic acid sequences in a complex nucleic acid mixture is to use labeled probes in a hybridization reaction. In this case, Cy3-54Ucenterbubble18, 18RNAfor54comp and 18RNAfor54comp was used. DNA Substrate was hybridized by mixing, 1 µl Cy3-54Ucenterbubble18 (100 pmol/µl), 2 µl complementary strand (54bubble18comp, 100 pmol/µl), and 7 µl 1× STE buffer containing 10 mM Tris-HCl, pH 8.0, 50 mM NaCl and 1 mM EDTA. For R-loop, the mixture was the same as mentioned above but with the addition of 2 µl of 18RNAfor54comp and 5 µl of STE buffer. The mixture was incubated at 95°C, 3 min in the thermocycler (Bio-Rad) and was right after added with 90 µl of 1× TE buffer (10 mM Tris-HCl, pH 7.5 and 1 mM EDTA, pH 8.0). Hybridization was verified using the native PAGE with TBE by preparing a mixture of 9 µl of water and 1 µl of 10 pmol/µl substrate with 10 µl of non-denaturing loading buffer. 5 µl was subjected for SDS-PAGE at 150 V for 2 h. Gel was analyzed by Typhoon Trio (GE Healthcare).

3. Results

3.1 Production of recombinant hSMUG1 wild type and mutant proteins

To initiate hSMUG1 production, the *E. coli* strain BL21 Rosetta was used to overexpress a full-length version of the human SMUG1 gene inserted into the plasmid pETM11. As shown in Figures 7–9, gene expression was induced with 1 mM isopropyl β-D-thiogalactoside (IPTG) following incubation for, 1) 1 h at 37°C, 2) 2 h at 37°C, 3) 3 h at 37°C, 4) 4 h at 37°C and 5) overnight at 23°C. The results presented in Figures 7A, 8A and 9A show that the optimal incubation period was overnight at 23°C, which was consequently applied in further experiments. «Small scale protein overproduction» and «Large scale gravity purification» (see «Materials and Methods») was used (Figure 7B and 9B) in the purifications described below.

3.1.1 Wild type hSMUG1

The *E. coli* strain Rosetta(DE3)pLysS was transformed with the plasmid pETM11-SMUG1 where the *SMUG1* gene was induced with IPTG (Figure 7A). hSMUG1 was produced by «Small scale protein overproduction», where crude extract was subjected to a gravity column containing TALON beads attached with Co^{2+} resin (see "Materials and methods") able to bind the His-tagged hSMUG1 protein. After protein elution and removal of the His-tag by the AcTEV protease, the purified fractions were analyzed by SDS-PAGE, showing one single band with the expected MW of hSMUG1 protein, which indicates apparent physical homogeneity (Figure 7B). In addition, the identity of the protein was confirmed by Western blotting showing reaction with anti-SMUG1 antibody (Figure 7C and 9C). Because our aim was to analyze hSMUG1 activity for uracil in bubble-structured DNA, the purified fractions were tested using bubble U-DNA as substrate (see Figure 11B). Unfortunately, our purified hSMUG1 [designated hSMUG1(CAR)]did not show any activity for bubble U-DNA (Figure 7D, lanes 5 and 6), as compared to the commercially available hSMUG1 preparation provided by New England Biochemicals [hSMUG1(NEB)], which caused significant uracil excision (Figure 7, lanes 9 and 10). This contrasts with control incubations without enzyme showing no cleaved substrate (Figure 7D, lane 2). Thus, the presented purification were unsuccessful in producing an active uracil excising enzyme. This is a general challenge regarding the hSMUG1 protein. Interestingly, however, is the observation that hSMUG1(NEB), similar to the control incubation without enzyme (Figure 7D, lane 1), did not show any U-DNA incision activity for uracil in bubble U-

DNA (Figure 7D, lanes 7 and 8). This contrasts with the significant incision activity of hSMUG1 at uracil in dsDNA and ssDNA (42).

3.1.2 hSMUG1 A14T/A16T

Using a similar protocol as for hSMUG1(CAR), but this time with the plasmid pETM11-SMUG1 A14T/A16T expressing a mutated version of the *SMUG1* gene, pure hSMUG1 A14T/A16T mutant protein was attempted to be produced. The rationale was to investigate whether replacing Ala14 and Ala16, which is believed to participate in RNA binding or function, might influence hSMUG1 activity (Table 1). As before, protein production was optimal by incubating the bacteria overnight at 23°C (Figure 8A). Although *in vivo* overproduction of the hSMUG1 A14T/A16T protein was clearly detectable (Figure 8A) and crude cell extract was subjected to «Small scale protein overproduction», unfortunately, no purified protein bands were detectable in the SDS-PAGE gel (Figure 8B).

3.1.3 hSMUG1 S26R/E35D

Because Ser26 and Glu35 (Table 1) have been demonstrated to be involved in rRNA quality control by putatively binding DKC1 (55), it is important to investigate whether replacement of these amino acids also affects hSMUG1 activity. Consequently, the plasmid pETM11-SMUG1 S26R/E35D expressing such a double mutated version of the *SMUG1* gene was used to overproduce the corresponding hSMUG1 mutated protein by a similar protocol as before, where the *in vivo* protein production was optimal by incubating the bacteria overnight at 23°C (Figure 9A). However, this time crude extract was subjected to the «Large scale gravity purification» protocol. After protein elution from the TALON beads and removal of the His-tag by the AcTEV protease, the purified fractions were analyzed by SDS-PAGE, showing one single band with the expected MW of the hSMUG1 protein (Figure 9B), indicating apparent physical homogeneity. The identity of the hSMUG1 S26R/E35D protein was further confirmed by Western blotting showing reaction with anti-SMUG1 antibody (Figure 9C).

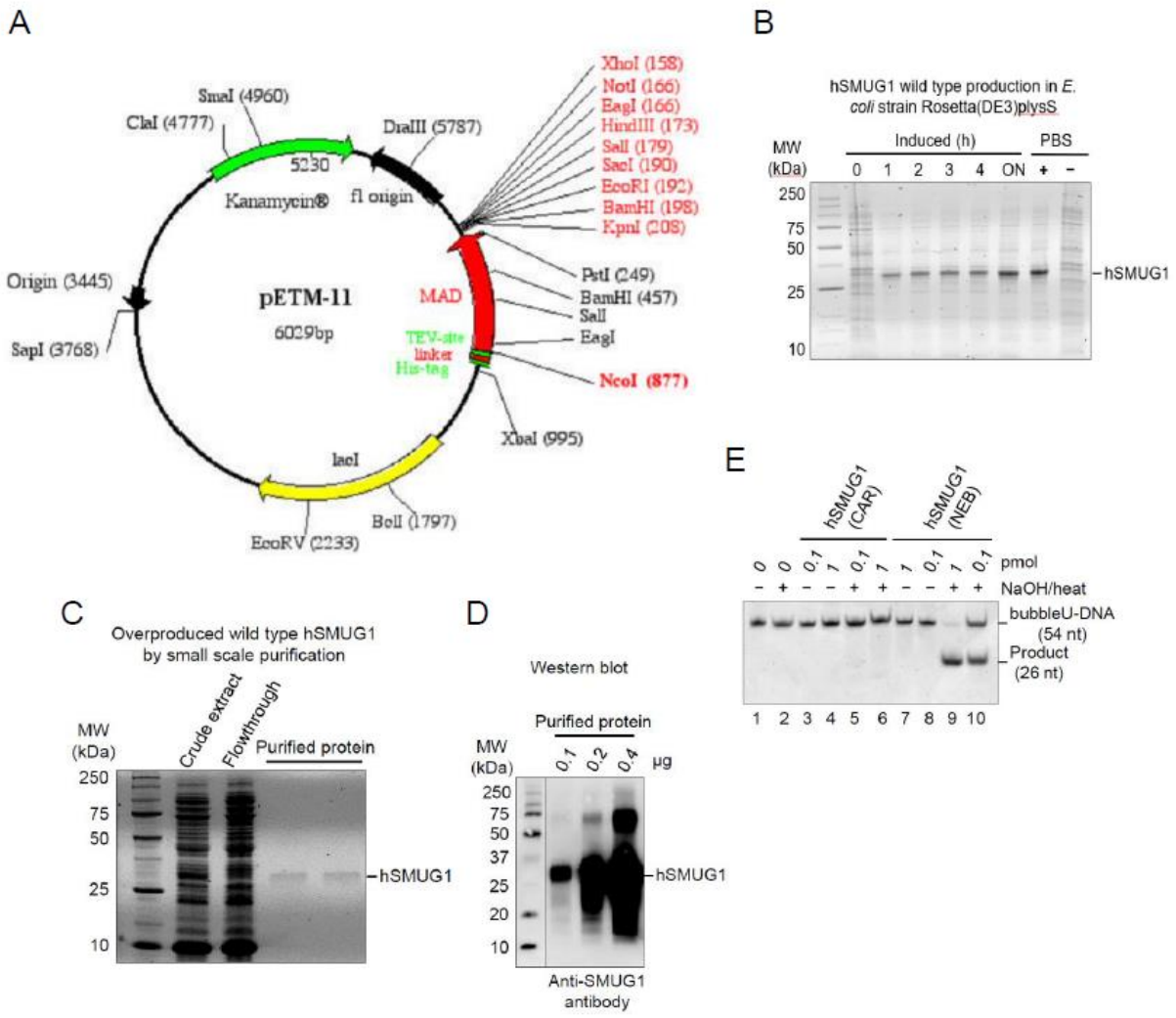

Figure 7. Production of recombinant hSMUG1 protein. (A) The pETM-11 vector. **(B)** Overproduction of wild type hSMUG1 protein in *E. coli* Rosetta(DE3)pLysS transformed with plasmid pETM11-SMUG1. **(C)** SDS-PAGE analysis of different fractions obtained during «Small scale protein overproduction» of hSMUG1, using gravity column containing TALON beads attached with Co^{2+} resin. Protein was eluted with 20 mM Tris-HCl, pH 8.0, 330 mM imidazole, 150 mM NaCl, 2 mM β-mercaptoethanol, 0.5 mM PMSF (elution buffer). Purified protein was collected in two fractions (last two lanes to the right; protein concentration of 0.085 mg/ml for the pooled fractions). **(D)** Western blot of the purified protein fractions using primary rabbit monoclonal anti-SMUG1 antibody and secondary (horseradish peroxidase conjugated) goat anti rabbit-HRP IgG, showing verification of the presence of hSMUG1 in different dilutions. **(E)** Test for enzyme activity of hSMUG1(NEB) and purified protein [hSMUG1(CAR)] with bubble U-DNA. Lanes 1 and 2, no enzyme; lanes 3 and 4, test for U-DNA incision activity of hSMUG1(CAR); lanes 5 and 6, test for uracil excision activity of hSMUG1(CAR); lanes 7 and 8, test for U-DNA incision activity of hSMUG1(NEB); lanes 9 and 10, uracil excision activity of hSMUG1(NEB). Since there was neither activity for U-DNA incision nor uracil excision exhibited by hSMUG1(CAR), our enzyme was clearly inactive. This contrasts with hSMUG1(NEB), which displayed excision activity, as opposed to U-DNA incision activity, for uracil in bubble DNA.

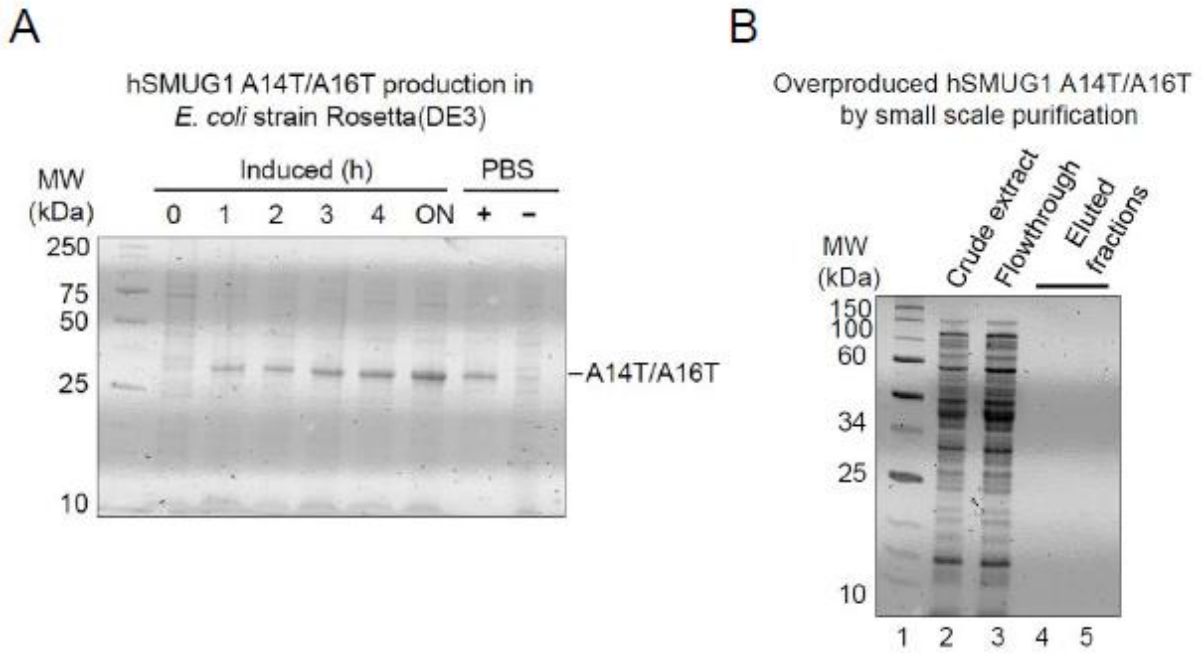

Figure 8. Production of recombinant hSMUG1 A14T/A16T protein. (A) Overproduction of hSMUG1 A14T/A16T protein in *E. coli* Rosetta(DE3)pLysS transformed with plasmid pETM11-SMUG1 A14T/A16T. **(B)** SDS-PAGE of different fractions obtained during «Small scale protein over-production» of hSMUG1 A14TA16T. Unfortunately, no bands of the expected MW of hSMUG1 was observed in the gel (lanes 4 and 5) indicating that the purification was unsuccessful. See Figure 7 and "Materials and methods" for experimental details.

3.2 hSMUG1 excises uracil in bubble and R-loop DNA

An oligodeoxyribonucleotide with the damaged base residue (in this case, uracil) inserted at a specific position is used in a common method to evaluate DNA glycosylase activity (Figure 11A). Enzymatic excision of uracil results in an alkali-labile AP site, which can be monitored by the extent that e.g. NaOH cleaves such sites by β/δ-elimination reaction, where cleaved DNA is separated from un-cleaved DNA by PAGE under denaturing conditions (Figure 11B). Such substrate was incubated with increasing amounts of hSMUG1, which was fluorescently labeled at the 5´ end of the damaged strand (Figure 11A).

3.2.1 Bubble and R-loop DNA substrates were efficiently prepared

The hybridization reaction is a sequence-specific interaction of two complementary single-stranded nucleic acids that results in the production of partial or complete double-stranded nucleic acid molecules. Bubble U-DNA was made by hybridizing a 5´ fluorescently labeled strand of 54 nucleotides (nt) with a partially complementary strand (also of 54 nt), where the 18-nt

central (i.e. the bubble) region of the former lacked proper complementarity to the latter. The R-loop U-DNA is identical to this bubble DNA, but contains an additional 18-nt RNA strand that is complementary to the "bubble region" of the unlabeled DNA strand (Figure 11A). Following the hybridization procedure (see Materials and Methods), the integrity and purity of the bubble and R-loop U-DNA substrates produced was verified by native PAGE. Consequently, the bubble U-DNA preparation showed no presence of un-hybridized labeled strand indicating that the two DNA oligonucleotides were successfully hybridized to produce the substrate (Figure 10). Likewise, the R-loop U-DNA preparation showed no presence of un-hybridized labeled strand or bubble U-DNA, indicating that the three oligonucleotides were successfully hybridized to produce the substrate (Figure 10). Therefore, in each case, the Cy3-labeled DNA strand was properly hybridized.

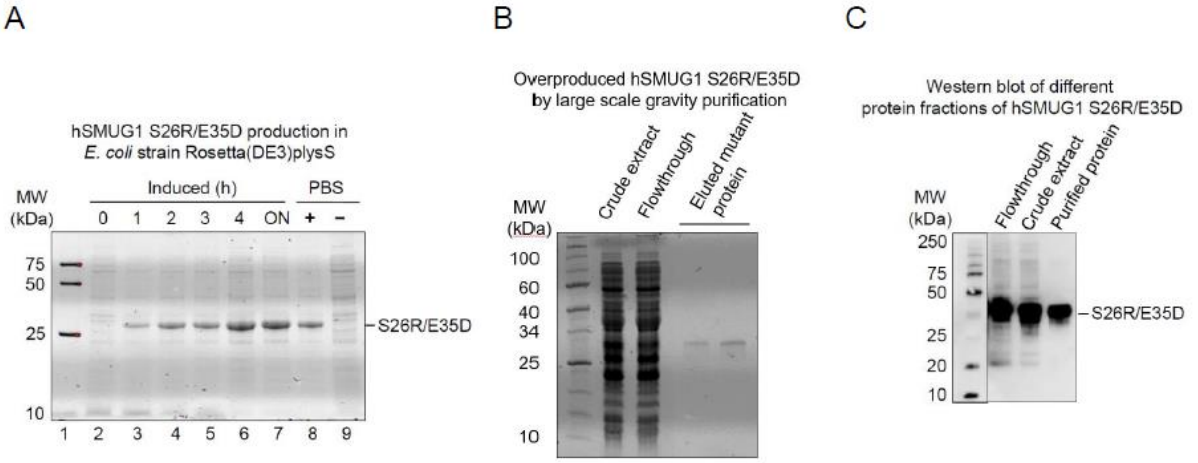

Figure 9. Production of recombinant hSMUG1 S26R/E35D protein. (A) Overproduction of hSMUG1 S26R/E35D protein in *E. coli* Rosetta(DE3)pLysS transformed with plasmid pETM11-SMUG1 S26R/E35D. **(B)** SDS-PAGE of different fractions obtained during «Large scale gravity purification» of hSMUG1 S26R/E35D using gravity column containing TALON beads attached with Co^{2+} resin. The eluted mutant protein fractions were pooled (final concentration, 0.12 mg/ml). **(C)** Western blot of the purified protein using anti-SMUG1 antibody verified the identity of hSMUG1 S26R/E35D. See Figure 7 and "Materials and methods" for experimental details.

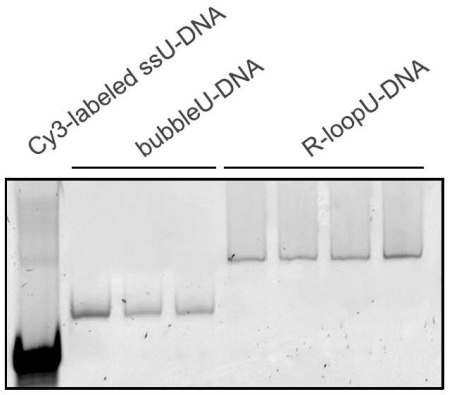

Figure 10. Verification of bubble and R-loop U-DNA integrity by native PAGE. The native PAGE gel was equilibrated and run with TBE buffer. DNA substrate (1 pmol) was loaded on the gel in a volume of 5 µl of non-denaturing loading buffer [10 mM Tris-HCl, pH 7.6, 60% (v/v) glycerol, 60 mM EDTA, 1% (w/v) blue dextran] and run at 150 V for 2 h.

3.2.2 hSMUG1 excises uracil from DNA bubble more efficient than from R-loop

The lack of knowledge on hSMUG1 activity for damaged bases in bubble and R-loop DNA prompted us to investigate hSMUG1 excision activity for uracil in these structures. In addition to the commercially available hSMUG1(NEB), another full-length enzyme was produced in our research group [hSMUG1(TB) (60)] and analyzed together with the former.

We observed that hSMUG1(NEB) exhibited significant activity for uracil in bubble and R-loop DNA (Figure 11C, upper and lower panels, respectively), increasing as a function of protein concentration (Figure 11D). Interestingly, the activity for bubble U-DNA was significantly higher than for R-loop U-DNA. The same was observed with hSMUG1(TB) (Figure 11E), which, however, demonstrated significantly lower activity (Figure 11F). This is probably due to protein inactivation during purification and handling, an issue which we routinely observed making preparation of active hSMUG1 challenging.

3.3 hSMUG1 S26R/E35D excises uracil from R-loop DNA similarly or slightly more efficient than from DNA bubble

Apparently physical homogeneous preparation of hSMUG1 S26R/E35D protein (Figure 9B) was exposed to uracil in bubble and R-loop DNA. As expected, this mutant protein, in which amino acid residues involved in RNA metabolism were replaced (55), demonstrated significant uracil-excising activity in both substrates (Figure 11A). However, quite interesting and unex-

pected, the protein dependent increase in hSMUG1 S26R/E35D activity exhibited altered preference for uracil in bubble and R-loop DNA. Thus, while wild type hSMUG1 excised uracil in DNA bubble more efficient than in R-loop (Figure 11D and F), hSMUG1 S26R/E35D protein excised uracil in R-loop DNA similarly or slightly more efficient than in DNA bubble (Figure 12B).

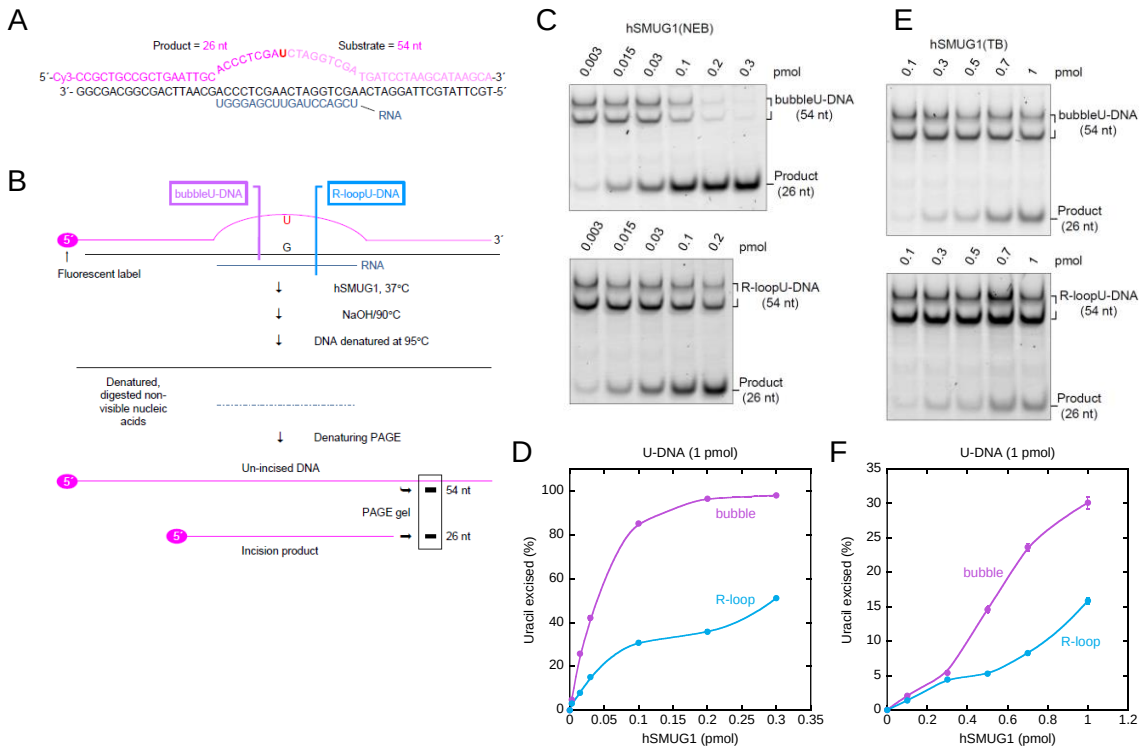

Figure 11. hSMUG1 excises uracil in DNA bubble and R-loop. (A) Bubble U-DNA substrate hybridized with RNA forms R-loop U-DNA substrate. **(B)** The base excision assay used. **(C–F)** Protein dependence of uracil excision from bubble (violet) and R-loop DNA (light blue). hSMUG1(NEB) (C and D) or hSMUG1(TB) (E and F) was incubated with either bubble U- DNA (C and E, upper panels) or R-loop U-DNA (C and E, lower panels) in 45 mM HEPES [4-(2-hydroxyethyl)-1-piperazineethane-sulfonic acid], pH 7.5, 0.4 mM EDTA, 1 mM DTT, 70 mM KCl, 2% (v/v) glycerol, 0.1 mg/ml BSA (reaction buffer) at 37°C for 20 min. Excision product was separated from un-excised DNA by PAGE at 200 V for 1.5 h using a 20% (w/v) gel with 3% (v/v) formamide. Each value in D and F represents the average (± SD) of 8–19 independent measurements. Abbreviation: nt, nucleotides.

3.4 hSMUG1 P240G excises uracil from R-loop DNA more efficient than from DNA bubbles

Because Pro240 is part of the His239–Lys249 intercalating loop in hSMUG1 (Table 1), which acts as a “wedge” and is inserted into the DNA double helix in the region of a damaged nucle-

otide (56), replacement of this amino acid might affect hSMUG1 activity including the substrates investigated in this report. Consequently, an apparently physical homogeneous preparation of hSMUG1 P240G protein produced in our research group (59) was exposed to uracil in bubble and R-loop DNA. As a result, this mutant protein demonstrated significant uracil-excising activity in both substrates (Figure 14A) increasing as a function of protein concentration (Figure 14B). Interestingly, hSMUG1 P240G exhibited altered preference for uracil in bubble and R-loop DNA. Thus, while wild type hSMUG1 excised uracil in DNA bubble more efficient than in R-loop (Figure 11D and F), this was completely reversed regarding the hSMUG1 P240G mutant protein (Figure 14B).

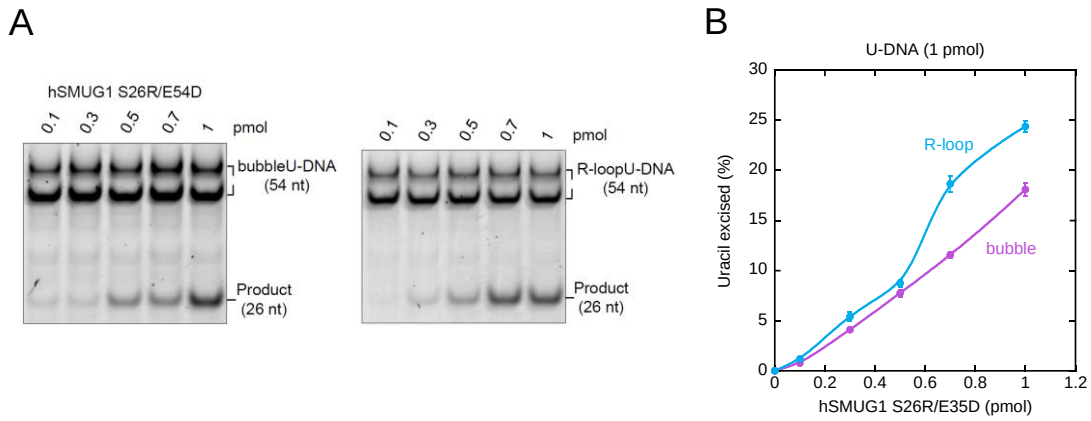

Figure 12. hSMUG1 S26R/E35D activity for excision of uracil in bubble and R-loop DNA (A) hSMUG1 S26R/E35D was incubated with bubble U-DNA (left panel) or R-loop U-DNA (right panel) as described in Figure 11. **(B)** Protein dependence of uracil excision from bubble (violet) and R-loop DNA (light blue). Each value represents the average (± SD) of 4–6 independent measurements. Abbreviation: nt, nucleotides.

3.5 Kinetic analysis of hSMUG1 wild type and mutant proteins for excision of uracil from bubble and R-loop DNA

The kinetic analysis is based on a model for hSMUG1 presented previously (42), considering that hSMUG1 obeys saturation kinetics regarding enzyme concentration at a certain substrate concentration. Specifically, we used $[S]_0$ = 50 nM in all our experiments, while $[E]_0$ was increased depending on the activity of the hSMUG1 preparation investigated. In each case, V_{max} (nM/min) and K_D (nM) were determined if the velocity (v) approaches saturating conditions. In several cases, the enzyme did not appear active enough to provide v values beyond the initial linear range, which prevents determination of V_{max} and K_D. Kinetic parameters were determined using both the average (± SD) and all measured values of v.

Based on the experiments with hSMUG1(NEB) exposed to bubble U-DNA, we made one "*v* versus $[E]_0$" graph from the average (± SD) values (Figure 14A), and another graph from all determined values (Figure 14B). Both graphs show that the enzyme excellently obeys saturation kinetics, giving a K_D of 2.5 ± 0.3 nM/V_{max} of 3.0 ± 0.1 nM/min (average values), and a K_D of 2.4 ± 0.1 nM/V_{max} of 2.99 ± 0.04 nM/min (all values) for uracil excision, resulting in a V_{max}/K_D of 1.2 min^{-1} (Table 2). Based on the experiments with hSMUG1(NEB) exposed to R-loop U-DNA, we made corresponding graphs from the average (± SD) (Figure 14A) and all determined values (Figure 14C). They also show that the enzyme excellently obeys saturation kinetics, giving a K_D of 6 ± 2 nM/V_{max} of 1.6 ± 0.2 nM/min (average values), and a K_D of 5.5 ± 0.6 nM/V_{max} of 1.58 ± 0.07 nM/min (all values) for uracil excision, resulting in a V_{max}/K_D of ~0.28 min^{-1} (Table 2). In conclusion, the V_{max}/K_D values show that hSMUG1 is about 4 times more efficient in excising uracil in bubble than in R-loop DNA, as reflected in both a higher V_{max} and a lower K_D (i.e., stronger binding to substrate) for the former compared to the latter (Table 2).

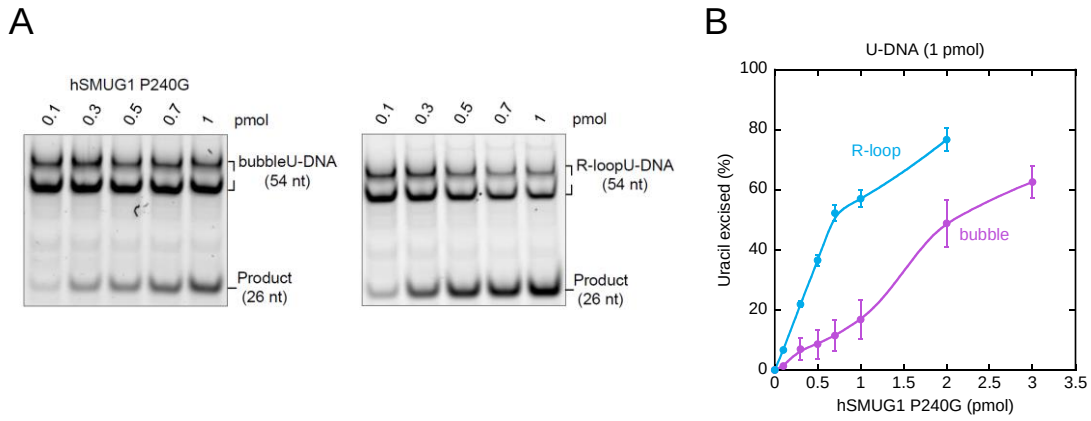

Figure 13. hSMUG1 P240G activity for excision of uracil in bubble and R-loop DNA. (A) hSMUG1 P240G was incubated with bubble U-DNA (left panel) or R-loop U-DNA (right panel) as described in Figure 11. **(B)** Protein dependence of uracil excision from bubble (violet) and R-loop DNA (light blue). Each value represents the average (± SD) of 8–16 independent measurements. Abbreviation: nt, nucleotides.

Unfortunately, the experiments with hSMUG1(TB) purified in our research group (60) resulted in linear "*v* versus $[E]_0$" graphs for both bubble (Figure 14D and E) and R-loop U-DNA (Figure 14D and F), excluding determination of K_D and V_{max}. The experiments with the hSMUG1 S26R/E35D protein (Figure 9B) also resulted in linear "*v* versus $[E]_0$" graphs for both bubble

(Figure 15A and B) and R-loop U-DNA (Figure 15A and C), excluding determination of K_D and V_{max}.

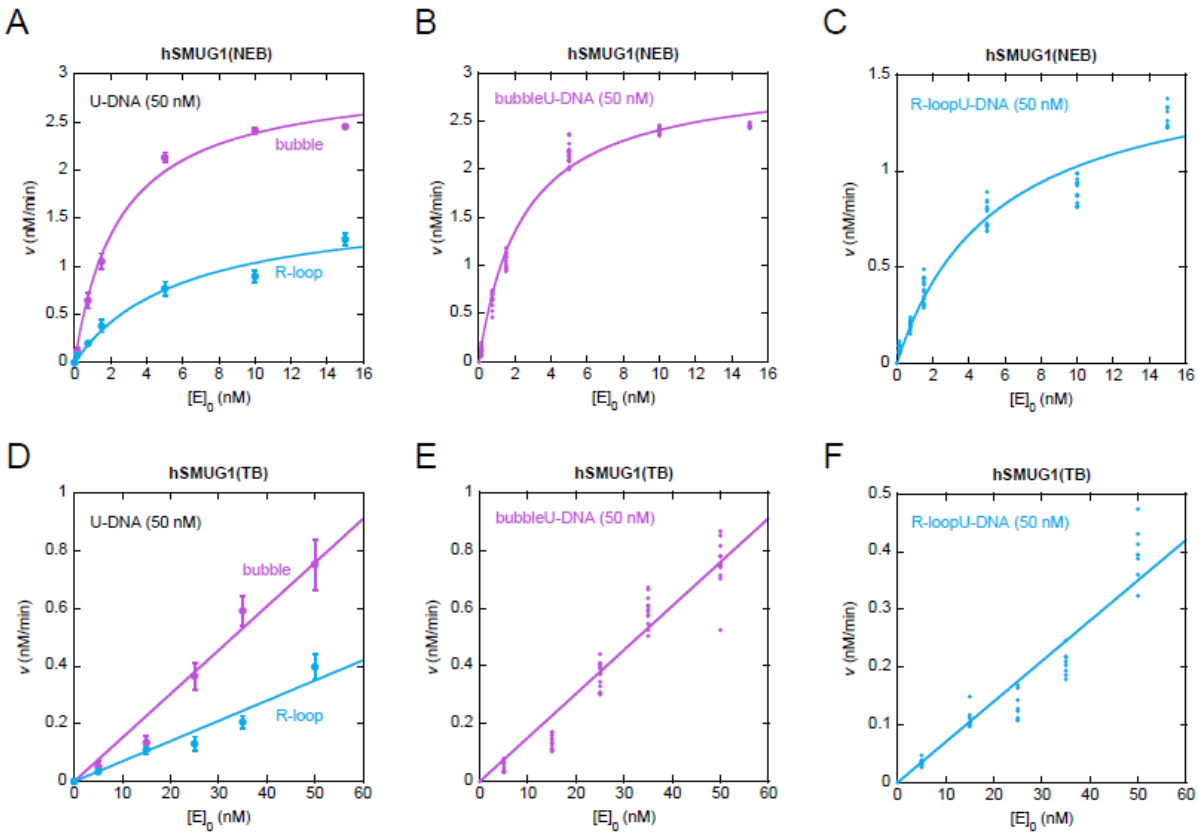

Figure 14. hSMUG1 kinetics for excision of uracil in bubble and R-loop DNA. (A–F) Uracil excision rate *v* as a function of enzyme concentration $[E]_0$ at an initial U-DNA concentration $[S]_0$ of 50 nM. The graphs for hSMUG1(NEB) obey saturation kinetics excellently for bubble DNA (A, R value of 0.99703; B, R value of 0.9929) as well as R-loop DNA (A, R value of 0.98798; C, R value of 0.97678), which resulted in the kinetic parameters presented in Table 2. This contrasts with the analysis of hSMUG1(TB) which only resulted in linear graphs excluding determination of K_D and V_{max} (D–F).

Fortunately, the experiments with the hSMUG1 P240G mutant protein purified in our research group (59) and exposed to R-loop U-DNA resulted in "*v* versus $[E]_0$" graphs from the average (± SD) (Figure 16A) and all determined values (Figure 16C) showing that the enzyme excellently obeys saturation kinetics, giving a K_D of 60 ± 10 nM/V_{max} of 3.1 ± 0.3 nM/min (average values), and a K_D of 62 ± 9 nM/V_{max} of 3.2 ± 0.3 nM/min (all values) for uracil excision (Table 2). However, the graphs for hSMUG1 P240G exposed to bubble U-DNA resulted in linear graphs only (Figure 16A and B), preventing determination of K_D and V_{max}.

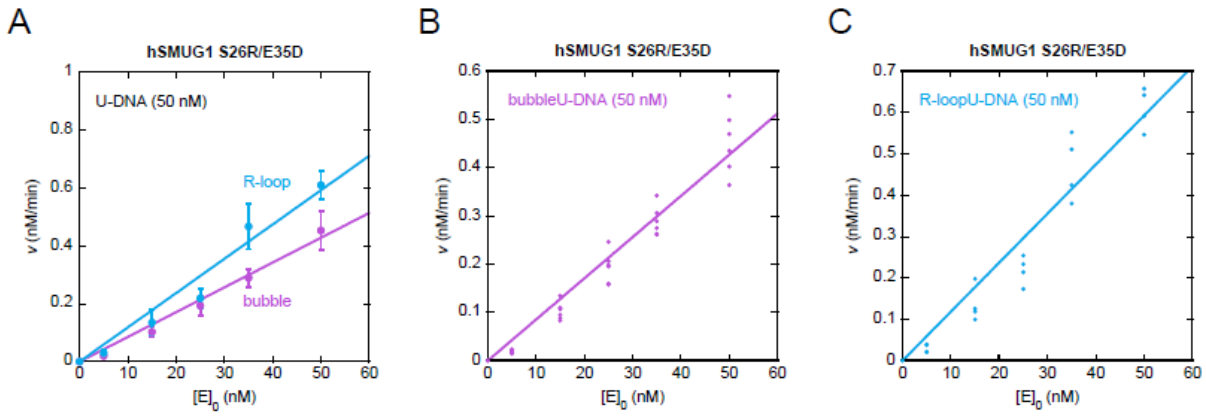

Figure 15. hSMUG1 S26R/E35D kinetics for excision of uracil in bubble and R-loop DNA. (A–C) Uracil excision rate *v* as a function of enzyme concentration $[E]_0$ at an initial U-DNA concentration $[S]_0$ of 50 nM. The graphs for hSMUG1 S26R/E35D resulted in linear graphs only, excluding determination of K_D and V_{max}. However, this mutant protein exhibits a marginally, although significant, higher activity for uracil in R-loop compared to bubble DNA.

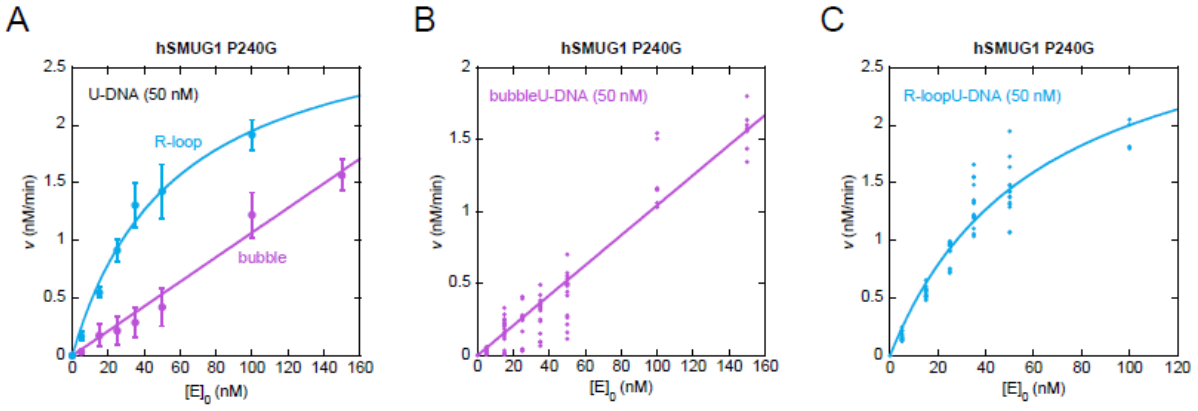

Figure 16. hSMUG1 P240G kinetics for excision of uracil in bubble and R-loop DNA. (A–C) Uracil excision rate *v* as a function of enzyme concentration $[E]_0$ at an initial U-DNA concentration $[S]_0$ of 50 nM. The graphs for hSMUG1 P240G using bubble DNA resulted in linear graphs only, excluding determination of K_D and V_{max}. The graphs for hSMUG1 P240G obey saturation kinetics excellently for R-loop DNA (A, R value of 0.99388; C, R value of 0.95531), which resulted in the kinetic parameters presented in Table 2.

Table 2. Kinetic parameters for hSMUG1(NEB) and hSMUG1 P240G in bubble and R-loop DNA

Parameter	Substrate (50 nM)			
	bubble U-DNA		R-loop U-DNA	
	Average[1]	All[2]	Average[1]	All[2]
hSMUG1(NEB)				
K_D (nM)	2.5 ± 0.3	2.4 ± 0.1	6 ± 2	5.5 ± 0.6
V_{max} (nM/min)	3.0 ± 0.1	2.99 ± 0.04	1.6 ± 0.2	1.58 ± 0.07
V_{max}/K_D (min^{-1})	1.2	1.2	0.27	0.29
hSMUG1 P240G				
K_D (nM)	nd	nd	60 ± 10	62 ± 9
V_{max} (nM/min)	nd	nd	3.1 ± 0.3	3.2 ± 0.3
V_{max}/K_D (min^{-1})			0.052	0.052

[1], determined from a graph showing the average values of *v* at each $[E]_0$; [2], determined from a graph showing all values of *v* determined for all $[E]_0$; nd, not determined (linear kinetics).

4 Discussion

During immunoglobulin gene diversification in activated B cells, targeted deamination by AID followed by hUNG engagement is important for CSR and SHM by providing DNA double strand breaks and mutagenesis (4), respectively. It has been reported that hSMUG1 may substitute for hUNG in CSR under certain conditions (27,45), although its role in immune function is largely unclear. The present results demonstrate that hSMUG1 excises uracil from a DNA bubble structure significantly more efficient than from a homologous R-loop structure (Figure 14A and D). This accords with the belief that the enzyme does not execute an important function in immunoglobulin gene diversification and maybe during transcription. It rather supports the role of hSMUG1 as a back-up UDG for hUNG (38), since transiently bubble structures arise during several processes in the genome. To our knowledge, this is the first report describing hSMUG1 activity for uracil in bubble and R-loop DNA. Importantly, another member of our research group analyzed hUNG using the same substrates (61), and comparing the hUNG results with that of hSMUG1 strongly support this conclusion. First, hUNG exhibits a similar level of uracil excision in bubble DNA at a five times lower concentration than hSMUG1 (Figure 17A), although the latter has a 4.4-times higher efficiency as indicated by V_{max}/K_D in bubble than R-loop DNA (Figure 17B and Table 3). Second, however, we observe the striking result that that hUNG only needs a two order of magnitude lower concentration to excise uracil in R-loop DNA similarly efficient as hSMUG1 (Figure 17A), where V_{max}/K_D shows a nearly three order of magnitude higher efficiency than hSMUG1 (Table 3). To largely exclude possible bias due to hSMUG1 inactivation, which lowers the V_{max} value, the K_D of hUNG is 20 times lower (reflecting 20 times higher affinity) for uracil in R-loop than in bubble DNA. This is very different from the K_D of hSMUG1, which is about twice higher for uracil in bubble than in R-loop DNA. In conclusion, the K_D of hUNG is 500 times lower for uracil in R-loop DNA than that of hSMUG1 (Table 3), suggesting that hSMUG1 hardly has any important role in immunoglobulin gene diversification or in DNA repair during transcription in general, although it may function as a back-up UDG in certain circumstances (27,45) (Figure 5).

Table 3. Kinetic parameters of hUNG and hSMUG1 for U-DNA (50 mM)

Parameter	Substrate (50 nM)	
	bubble U-DNA	R-loop U-DNA
hUNG(SM)		
K_D (nM)	0.25 ± 0.06	0.012 ± 0.003
V_{max} (nM/min)	3.4 ± 0.5	2.4 ± 0.1
V_{max}/K_D (min^{-1})	14	200
hSMUG1(NEB)		
K_D (nM)	2.5 ± 0.3	6 ± 2
V_{max} (nM/min)	3.0 ± 0.1	1.6 ± 0.2
V_{max}/K_D (min^{-1})	1.2	0.27

The parameters were calculated from the average values (±SD) using 0.0125–0.25 nM hUNG and 0.15–15 nM hSMUG1.

hSMUG1 is also believed to function in rRNA quality control which includes the telomerase RNA component (hTERC), by e.g. regulating the presence of base modifications. Thus, hSMUG1 binds dyskerin (DKC1), the major pseudouridine synthase in mammals, where the Ser26 and Glu35 residues is participating (55). However, these amino acids have not been suspected to be involved in the DNA glycosylase catalytic function (Table 1). Interestingly, the results show that the hSMUG1 S26R/E35D mutant protein excised uracil in R-loop DNA similarly or slightly more efficient than in DNA bubble, i.e., close to the opposite of wild type hSMUG1, suggesting that replacement of these amino acids alters enzyme function (Figures 13B and 16A). This feature was even more pronounced with the hSMUG1 P240G mutant protein (Figures 14B and 17A), even though Pro240 is part of the His239–Lys249 intercalating loop in hSMUG1, which acts as a "wedge" and is inserted into the DNA double helix in the region of a damaged nucleotide (56). However, the putative role of the intercalating loop in bubble and R-loop U-DNA is unknown. Thus, while wild type hSMUG1 excised uracil in DNA bubble significantly more efficient than in R-loop, this was completely reversed regarding the hSMUG1 P240G mutant protein, indicating a role of Pro240 in stabilizing the hSMUG1–bubble U-DNA complex, or inhibiting the hSMUG1–R-looop U-DNA complex.

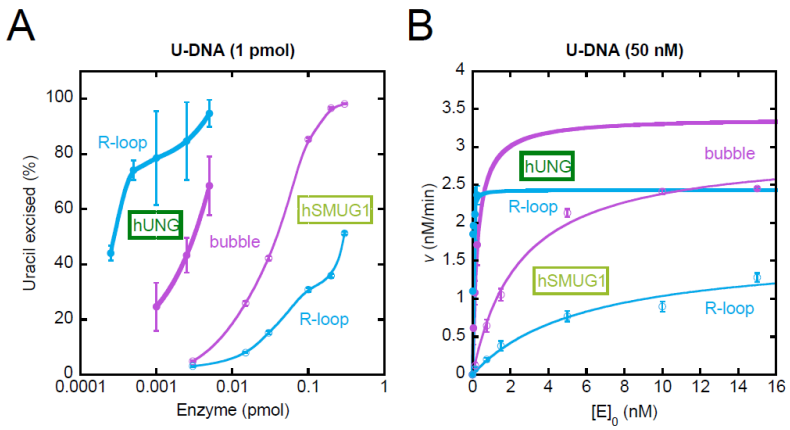

Figure 17. Uracil excision activity of hUNG and hSMUG1 in bubble and R-loop DNA. (A) Protein dependence of uracil excision from bubble (violet) and R-loop DNA (light blue). Each value represents the average (± SD) of 4–9 (hUNG) (61) and 9–19 (hSMUG1) independent measurements. (B) Uracil excision rate *v* as a function of enzyme concentration $[E]_0$ at an initial U-DNA concentration $[S]_0$ of 50 nM. The graphs for obey saturation kinetics where determined values of K_D and V_{max} are presented in Table 3.

Although the hSMUG1(TB), hSMUG1 S26R/E35D and hSMUG1 P240G proteins were produced by the same protocol, it is principally unreliable to compare their precise enzyme activity levels because of extensive hSMUG1 protein inactivation during production and storage. However, because their activities were determined at the same or similar time for all substrates using the same amount of enzyme, it should be safe to compare how effective each preparation is towards the different four substrates tested in our research group, where the data is presented for each substrate (Figure 18, A–D) as well as for each enzyme preparation (Figure 18, E–H), where the kinetic parameters for ssU-DNA and hmU-ssDNA is presented in Table 4. The results show that wild type hSMUG1 exhibits the highest catalytic efficiency for ssU-DNA (V_{max}/K_D 11–12 min^{-1}), followed by hmU-ssDNA (V_{max}/K_D ~3 min^{-1}) (Table 4) ≈ bubbleU-DNA (V_{max}/K_D, 1.2 min^{-1}) and then R-loopU-DNA (V_{max}/K_D ~0.27–0.29 min^{-1}) (Table 2). The mutated hSMUG1 proteins S26R/E35D and P240G exhibit no significant activity for hmU-ssDNA, while that for the uracil substrates is easily detectable. Thus, replacing S26 and E35, or P240, with another amino acid residue severely obstruct hSMUG1 activity for hmU as opposed to U in DNA. The velocity *v* for hSMUG1 S26R/E35D is highest for uracil in ssDNA followed by R-loop and bubble DNA (Figure 18G), while for hSMUG1 P240 *v* decreases for U in bubble DNA (Figure 18G) much more than in ssDNA (V_{max}/K_D, 0.1–0.2 min^{-1}, Table 4) with R-loop in between (V_{max}/K_D, 0.052 min^{-1}) (Table 2). The ten and 100–200 times higher K_D for uracil excision in R-loop (Table 2) and single-stranded DNA (Table 4) exhibited by wild type

hSMUG1 and hSMUG1 P240, respectively, shows that replacing Pro with Gly seems to obstruct binding to the substrate, which is especially pronounced for ssDNA. This may reflect more (unspecific) binding options for the enzyme in the more complex R-loop substrate compared to ssU-DNA. Because Pro240 is part of the His239–Lys249 intercalating loop in hSMUG1 (56) (Table 1) and is thus close to the catalytic function, it was not so surprising that replacing it with Gly obstructed the enzyme activity for hmU in ssDNA (Figure 18D). This contrasts with the interesting result that replacing Ser26 and Glu35 (Table 1), which is involved in rRNA quality control by putatively binding DKC1 (55), demonstrated devastating obstruction of activity for hmU in ssDNA (Figure 18D). Because crystal structure of hSMUG1 together with substrate or substrate analogs has not yet been obtained, computer-assisted molecular modeling of hmU-ssDNA bound to hSMUG1 with Ser26 and/or Glu35 replaced might contribute to a clarification.

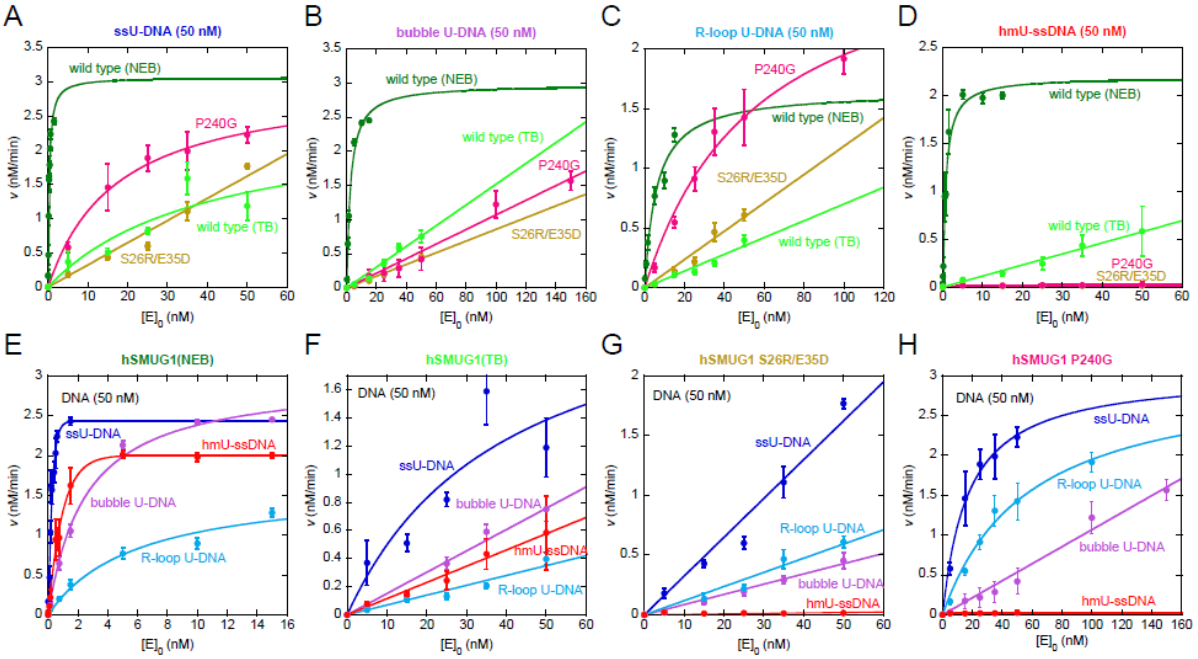

Figure 18. Comparison of hSMUG1 wild type, hSMUG1 S26R/E35D and hSMUG1 P240G base excision kinetics for ssU-DNA, bubble U-DNA, R-loop U-DNA and hmU-ssDNA. (A–D) Velocity (v) as a function of enzyme concentration $[E]_0$ for each substrate is compared. (E–H) v as a function of $[E]_0$ for each hSMUG1 preparation is compared. The original experiments using bubble and R-loop U-DNA (violet and light blue, respectively) is presented in this thesis, those using ssU-DNA (blue) in the thesis of Lorentsen (59), and those using hmU-ssDNA (red) in the thesis of Bærheim (60).

Table 4. Kinetic parameters for wild type hSMUG1(NEB, TB) and hSMUG1 P240G in ssU-DNA and hmU-ssDNA

Parameter	Substrate (50 nM)			
	ssU-DNA		hmU-ssDNA	
	Average	All	Average	All
NEB				
K_D (nM)	0.28 ± 0.07	0.25 ± 0.03	0.8 ± 0.1	0.77 ± 0.06
V_{max} (nM/min)	3.1 ± 0.3	3.0 ± 0.1	2.20 ± 0.08	2.20 ± 0.04
V_{max}/K_D (min^{-1})	11	12	2.8	2.9
TB[f]				
K_D (nM)	nd	nd	30 ± 20	30 ± 30
V_{max} (nM/min)	nd	nd	1.3 ± 0.3	1.3 ± 0.5
V_{max}/K_D (min^{-1})				
TB[c]				
K_D (nM)	40 ± 50	40 ± 20	nd	nd
V_{max} (nM/min)	2 ± 2	2.4 ± 0.6	nd	nd
P240G[f]				
K_D (nM)	40 ± 20	41 ± 9		
V_{max} (nM/min)	4.0 ± 0.9	4.2 ± 0.5	0	0
V_{max}/K_D (min^{-1})		0.1		
P240G[c]				
K_D (nM)	17 ± 3	18 ± 3		
V_{max} (nM/min)	3.0 ± 0.2	3.1 ± 0.2	0	0
V_{max}/K_D (min^{-1})	0.18	0.17		

[c], enzyme preparations compared/measured at similar time; [f], the most fresh enzyme preparation tested; nd, not determined (linear kinetics).

References

1. Lindahl, T. (1993) Instability and decay of the primary structure of DNA. *Nature*, **362**, 709–715.
2. Das, S.K. (2003) Harmful health effects of cigarette smoking. *Mol Cell Biochem*, **253**, 159–165.
3. Chatterjee, N. and Walker, G.C. (2017) Mechanisms of DNA damage, repair, and mutagenesis. *Environ Mol Mutagen*, **58**, 235–263.
4. Krokan, H.E., Sætrom, P., Aas, P.A., Pettersen, H.S., Kavli, B. and Slupphaug, G. (2014) Error-free *versus* mutagenic processing of genomic uracil–relevance to cancer. *DNA Repair (Amst)*, **19**, 38–47.
5. Lindahl, T. (1974) An *N*-glycosidase from *Escherichia coli* that releases free uracil from DNA containing deaminated cytosine residues. *Proc Natl Acad Sci USA*, **71**, 3649–3653.
6. Alexeeva, M. (2018) *DNA glycosylases in the repair of deaminated and dimethylated cytosine*. PhD Thesis, University of Stavanger, Stavanger.
7. Sousa, M.M., Krokan, H.E. and Slupphaug, G. (2007) DNA-uracil and human pathology. *Mol Aspects Med*, **28**, 276–306.
8. De Bont, R. and van Larebeke, N. (2004) Endogenous DNA damage in humans: a review of quantitative data. *Mutagenesis*, **19**, 169–185.
9. Muramatsu, M., Kinoshita, K., Fagarasan, S., Yamada, S., Shinkai, Y. and Honjo, T. (2000) Class switch recombination and hypermutation require activation-induced cytidine deaminase (AID), a potential RNA editing enzyme. *Cell*, **102**, 553–563.
10. Mates, J.M. and Sanchez-Jimenez, F. (1999) Antioxidant enzymes and their implications in pathophysiologic processes. *Front Biosci*, **4**, D339–345.
11. Cadet, J., Davies, K.J.A., Medeiros, M.H., Di Mascio, P. and Wagner, J.R. (2017) Formation and repair of oxidatively generated damage in cellular DNA. *Free Radic Biol Med*, **107**, 13–34.
12. Bjelland, S. and Seeberg, E. (2003) Mutagenicity, toxicity and repair of DNA base damage induced by oxidation. *Mutat Res*, **531**, 37–80.
13. Cadet, J., Douki, T. and Ravanat, J.L. (2010) Oxidatively generated base damage to cellular DNA. *Free Radic Biol Med*, **49**, 9–21.
14. Winterbourn, C.C. (2008) Reconciling the chemistry and biology of reactive oxygen species. *Nat Chem Biol*, **4**, 278–286.
15. Demple, B. and Harrison, L. (1994) Repair of oxidative damage to DNA: enzymology and biology. *Annu Rev Biochem*, **63**, 915–948.
16. Sedgwick, B. (2004) Repairing DNA-methylation damage. *Nat Rev Mol Cell Biol*, **5**, 148–157.
17. Hegde, M.L., Hazra, T.K. and Mitra, S. (2008) Early steps in the DNA base excision/single-strand interruption repair pathway in mammalian cells. *Cell Res*, **18**, 27–47.
18. Li, M. and Wilson, D.M., 3rd. (2014) Human apurinic/apyrimidinic endonuclease 1. *Antioxid Redox Signal*, **20**, 678–707.
19. Mol, C.D., Izumi, T., Mitra, S. and Tainer, J.A. (2000) DNA-bound structures and mutants reveal abasic DNA binding by APE1 and DNA repair coordination [corrected]. *Nature*, **403**, 451–456.
20. Wilson, D.M., 3rd. (2007) Processing of nonconventional DNA strand break ends. *Environ Mol Mutagen*, **48**, 772–782.
21. Hadi, M.Z., Ginalski, K., Nguyen, L.H. and Wilson, D.M., 3rd. (2002) Determinants in nuclease specificity of Ape1 and Ape2, human homologues of *Escherichia coli* exonuclease III. *J Mol Biol*, **316**, 853–866.
22. Friedberg, E.C., Walker, G.C., Siede, W., Wood, R.D., Schultz, R.A. and Ellenberger, T. (2006) *DNA Repair and Mutagenesis*. 2nd ed. ASM Press, Washington, DC.
23. Kim, Y.-J. and Wilson, D.M., 3rd (2012) Overview of base excision repair biochemistry. *Curr Mol Pharmacol*, **5**, 3–13.
24. Fortini, P. and Dogliotti, E. (2007) Base damage and single-strand break repair: mechanisms and functional significance of short- and long-patch repair subpathways. *DNA Repair (Amst)*, **6**, 398–409.

25. Tomkinson, A.E., Vijayakumar, S., Pascal, J.M. and Ellenberger, T. (2006) DNA ligases: structure, reaction mechanism, and function. *Chem Rev*, **106**, 687–699.
26. An, Q., Robins, P., Lindahl, T. and Barnes, D.E. (2005) C → T mutagenesis and γ-radiation sensitivity due to deficiency in the Smug1 and Ung DNA glycosylases. *EMBO J*, **24**, 2205–2213.
27. Di Noia, J.M., Rada, C. and Neuberger, M.S. (2006) SMUG1 is able to excise uracil from immunoglobulin genes: insight into mutation versus repair. *EMBO J*, **25**, 585–595.
28. Pettersen, H.S., Visnes, T., Vågbø, C.B., Svaasand, E.K., Doseth, B., Slupphaug, G., Kavli, B. and Krokan, H.E. (2011) UNG-initiated base excision repair is the major repair route for 5-fluorouracil in DNA, but 5-fluorouracil cytotoxicity depends mainly on RNA incorporation. *Nucleic Acids Res*, **39**, 8430–8444.
29. Otterlei, M., Warbrick, E., Nagelhus, T.A., Haug, T., Slupphaug, G., Akbari, M., Aas, P.A., Steinsbekk, K., Bakke, O. and Krokan, H.E. (1999) Post-replicative base excision repair in replication foci. *EMBO J*, **18**, 3834–3844.
30. Pearl, L.H. (2000) Structure and function in the uracil-DNA glycosylase superfamily. *Mutat Res*, **460**, 165–181.
31. Gallinari, P. and Jiricny, J. (1996) A new class of uracil-DNA glycosylases related to human thymine-DNA glycosylase. *Nature*, **383**, 735–738.
32. Haushalter, K.A., Todd Stukenberg, M.W., Kirschner, M.W. and Verdine, G.L. (1999) Identification of a new uracil-DNA glycosylase family by expression cloning using synthetic inhibitors. *Curr Biol*, **9**, 174–185.
33. Aravind, L. and Koonin, E.V. (2000) The α/β fold uracil DNA glycosylases: a common origin with diverse fates. *Genome Biol*, **1**, RESEARCH0007.
34. Cortazar, D., Kunz, C., Saito, Y., Steinacher, R. and Schär, P. (2007) The enigmatic thymine DNA glycosylase. *DNA Repair (Amst)*, **6**, 489-504.
35. Hardeland, U., Bentele, M., Jiricny, J. and Schär, P. (2000) Separating substrate recognition from base hydrolysis in human thymine DNA glycosylase by mutational analysis. *J Biol Chem*, **275**, 33449–33456.
36. Baba, D., Maita, N., Jee, J.G., Uchimura, Y., Saitoh, H., Sugasawa, K., Hanaoka, F., Tochio, H., Hiroaki, H. and Shirakawa, M. (2005) Crystal structure of thymine DNA glycosylase conjugated to SUMO-1. *Nature*, **435**, 979–982.
37. Nilsen, H., Haushalter, K.A., Robins, P., Barnes, D.E., Verdine, G.L. and Lindahl, T. (2001) Excision of deaminated cytosine from the vertebrate genome: role of the SMUG1 uracil-DNA glycosylase. *EMBO J*, **20**, 4278–4286.
38. Kavli, B., Sundheim, O., Akbari, M., Otterlei, M., Nilsen, H., Skorpen, F., Aas, P.A., Hagen, L., Krokan, H.E. and Slupphaug, G. (2002) hUNG2 is the major repair enzyme for removal of uracil from U:A matches, U:G mismatches, and U in single-stranded DNA, with hSMUG1 as a broad specificity backup. *J Biol Chem*, **277**, 39926–39936.
39. An, Q., Robins, P., Lindahl, T. and Barnes, D.E. (2007) 5-Fluorouracil incorporated into DNA is excised by the Smug1 DNA glycosylase to reduce drug cytotoxicity. *Cancer Res*, **67**, 940–945.
40. Boorstein, R.J., Cummings, A., Jr., Marenstein, D.R., Chan, M.K., Ma, Y., Neubert, T.A., Brown, S.M. and Teebor, G.W. (2001) Definitive identification of mammalian 5-hydroxymethyluracil DNA *N*-glycosylase activity as SMUG1. *J Biol Chem*, **276**, 41991–41997.
41. Matsubara, M., Tanaka, T., Terato, H., Ohmae, E., Izumi, S., Katayanagi, K. and Ide, H. (2004) Mutational analysis of the damage-recognition and catalytic mechanism of human SMUG1 DNA glycosylase. *Nucleic Acids Res*, **32**, 5291–5302.
42. Alexeeva, M., Moen, M.N., Grøsvik, K., Tesfahun, A.N., Xu, X.M., Muruzábal-Lecumberri, I., Olsen, K.M., Rasmussen, A., Ruoff, P., Kirpekar, F. *et al.* (2019) Excision of uracil from DNA by hSMUG1 includes strand incision and processing. *Nucleic Acids Res*, **47**, 779–793.
43. Alexeeva, M., Moen, M.N., Xu, X.M., Rasmussen, A., Leiros, I., Kirpekar, F., Klungland, A., Alsøe, L., Nilsen, H. and Bjelland, S. Intrinsic strand-incision activity of human UNG: implications for nick generation in immunoglobulin gene diversification. *Manuscript*.
44. Methot, S.P. and Di Noia, J.M. (2017) Molecular mechanisms of somatic hypermutation and class switch recombination. *Adv Immunol*, **133**, 37–87.

45. Dingler, F.A., Kemmerich, K., Neuberger, M.S. and Rada, C. (2014) Uracil excision by endogenous SMUG1 glycosylase promotes efficient Ig class switching and impacts on A:T substitutions during somatic mutation. *Eur J Immunol*, **44**, 1925–1935.
46. Masani, S., Han, L. and Yu, K. (2013) Apurinic/apyrimidinic endonuclease 1 is the essential nuclease during immunoglobulin class switch recombination. *Mol Cell Biol*, **33**, 1468–1473.
47. Wibley, J.E.A., Waters, T.R., Haushalter, K., Verdine, G.L. and Pearl, L.H. (2003) Structure and specificity of the vertebrate anti-mutator uracil-DNA glycosylase SMUG1. *Mol Cell*, **11**, 1647–1659.
48. de Lange, T. (2005) Shelterin: the protein complex that shapes and safeguards human telomeres. *Genes Dev*, **19**, 2100–2110.
49. Schmidt, J.C. and Cech, T.R. (2015) Human telomerase: biogenesis, trafficking, recruitment, and activation. *Genes Dev*, **29**, 1095–1105.
50. Nguyen, D., Grenier St-Sauveur, V., Bergeron, D., Dupuis-Sandoval, F., Scott, M.S. and Bachand, F. (2015) A polyadenylation-dependent 3′ end maturation pathway is required for the synthesis of the human telomerase RNA. *Cell Rep*, **13**, 2244–2257.
51. Kroustallaki, P., Lirussi, L., Carracedo, S., You, P., Esbensen, Q.Y., Gotz, A., Jobert, L., Alsoe, L., Saetrom, P., Gagos, S. *et al.* (2019) SMUG1 promotes telomere maintenance through telomerase RNA Processing. *Cell Rep*, **28**, 1690–1702 e1610.
52. Egan, E.D. and Collins, K. (2012) An enhanced H/ACA RNP assembly mechanism for human telomerase RNA. *Mol Cell Biol*, **32**, 2428–2439.
53. Lee, J.H., Lee, Y.S., Jeong, S.A., Khadka, P., Roth, J. and Chung, I.K. (2014) Catalytically active telomerase holoenzyme is assembled in the dense fibrillar component of the nucleolus during S phase. *Histochem Cell Biol*, **141**, 137–152.
54. MacNeil, D.E., Bensoussan, H.J. and Autexier, C. (2016) Telomerase regulation from beginning to the end. *Genes (Basel)*, **7**.
55. Jobert, L., Skjeldam, H.K., Dalhus, B., Galashevskaya, A., Vågbø, C.B., Bjørås, M. and Nilsen, H. (2013) The human base excision repair enzyme SMUG1 directly interacts with DKC1 and contributes to RNA quality control. *Mol Cell*, **49**, 339–345.
56. Alekseeva, I.V., Bakmana, A.S., Iakovleva, D.A., Kuznetsova, N.A. and Fedorova, O.S. (2021) Comparative analysis of the activity of the polymorphic variants of human uracil-DNA-glycosylases SMUG1 and MBD4. *Mol Biol*, **55**, 241–251.
57. Iakovlev, D.A., Alekseeva, I.V., Vorobjev, Y.N., Kuznetsov, N.A. and Fedorova, O.S. (2019) The role of active-site residues Phe98, His239, and Arg243 in DNA binding and in the catalysis of human uracil-DNA glycosylase SMUG1. *Molecules*, **24**.
58. Kuznetsova, A.A., Iakovlev, D.A., Misovets, I.V., Ishchenko, A.A., Saparbaev, M.K., Kuznetsov, N.A. and Fedorova, O.S. (2017) Pre-steady-state kinetic analysis of damage recognition by human single-strand selective monofunctional uracil-DNA glycosylase SMUG1. *Mol Biosyst*, **13**, 2638-2649.
59. Lorentsen, C. (2021) *Uracil-excising activity in single-stranded DNA of hSMUG1 S26R/E35D and P240G mutant proteins*. Master Thesis, University of Stavanger, Stavanger.
60. Bærheim, T. (2021) *5-Hydroxymethyluracil-excising activity of hSMUG1 in single-stranded DNA is lost in S26R/E35D and P240G mutant proteins*. Master thesis, University of Stavanger, Stavanger.
61. Mehanna, S. (2021) *hUNG activity for uracil in bubble and R-loop DNA*. Master Thesis, University of Stavanger, Stavanger.

APPENDICES

APPENDIX A

Protocols

Protocol 1

Equilibration of TALON beads for batch purification

Equilibration of beads include removal of storage buffer (20% ethanol), washing with Milli-Q water and then with buffer A (50 mM Tris-HCl, pH 7.5, 300 mM NaCl and 2 mM β-mercaptoethanol). The beads were collected by centrifugation at 500 × g for 5 min, where supernatant was discarded. 10× of beads volume of Milli-Q water were added followed by centrifugation again at 500 × g for 5 min. Buffer A (10 ml) was added followed by incubation for 10 min at 4°C and centrifugation for 5 min at 500 × g. Supernatant was discarded and the procedure was repeated twice. Buffer A (10 ml) with 10 mM imidazole was added followed by incubation for 5 min at 4°C and centrifugation for 5 min at 500 × g and removal of buffer.

Equilibration of TALON beads for large scale gravity purification

1 ml TALON beads were equilibrated using 4 ml Milli-Q water (Merck) and wash 2 (20 mM Tris-HCl, pH 8.0, 10 mM imidazole, 150 mM NaCl, 2 mM β-mercaptoethanol (add fresh) and 1 µl PMSF buffers (2 × 4 ml).

Equilibration of TALON beads for small scale gravity purification

Took 0.5 ml TALON beads, wash with 5 ml water and 2 times 5 ml wash 2 (20 mM Tris 8.0 10 mM imidazole, 150 mM NaCl, 2 mM β-mercaptoethanol, 0.5 mM PMSF).

Protocol 2: Base excision assay

Vials was kept on ice and in darkness during the assay.

Reaction Mixtures:

	Stock	**Reaction mix**	**Reaction 1× (µl)**	**Reaction 2× (µl)**
HEPES buffer + DTT	5×	1×	4	8
KCl	1 M	70 mM	1.4	2.8
BSA	10 mg/ml	5×	1	2
Labelled oligo	1 pmol/µl	1 pmol	1	2
Enzyme (protein)	Varying		1	2
H_2O (MilliQ)			11.6	23.2
Total volume			20	40

1. Take 199 µl of 5× HEPES buffer/Tris-HCl and add 1 µl of freshly made 1 M DTT prior to the experiment.
2. Mix the reaction and add enzyme at last
3. Spin down 4000 rpm for 1 min at RT.
4. In at 37°C for 20 min.
5. Put on ice. Spin down, terminate the reaction with 45 µl of stop solution and 1 µl of Protenase K (10 mg/ml), mix up and down by the pipet, incubate at 37°C for 10 min. Spin down and put on ice.
6. Cold down 96% ethanol/0.1 M NaAc in the freezer. Add 150 ml 96% ethanol/0.1 M NaAc to each tube and then + 1.6 µl tRNA (16 mg from Stock: 10 mg/ml) per sample. Invert the tubes several times.
7. Incubate the tubes at –70°C for 2 h, or overnight at –20°C in darkness.
8. Centrifuge the tubes at 13 000 rpm, 15 min two times with different position of the tubes at 4°C. Remove the supernatant.
9. Add 300 ml cold 70% ethanol (freezer).
10. Centrifuge at 13 000 rpm, 5 min at 4°C. Remove the supernatant.
11. Centrifuge at 13 000 rpm, 1 min at 4°C. Remove the rest of the supernatant with the pipette.
12. Dry the pellet for 1–20 min on ice at in the hood. Check that ethanol is completely evaporated.

13. Dissolve pellet in 10 ml 0.1 M NaOH (heat for 10 min at 90°C).
14. Mix with 10 µl of denaturing loading buffer prior the gel run (when gels are ready and, in the chamber), mix with up and down pipetting and load to the wells of gel.
15. Fill the gel chamber with running buffer and carefully remove the comb. Wash the gel wells carefully using the 1000 ml pipette to remove the residual gel particles. This part is very critical in making the DNA bands sharper and straight.
16. Load 5 µl of loading solution with sample DNA into the wells carefully and run the gels at 200 V for 2 h in darkness.

Protocol 3: Hybridization of bubble U-DNA and R-loop U-DNA

ICE AND DARKNESS DURING THE ASSAY!

1. Mix in PCR-tube:

bubbleU-DNA	R-loopU-DNA
1 µl Cy3-54Ucenterbubble18 (100 pmol/µl)	1 µl Cy3-54Ucenterbubble18 (100 pmol/µl)
2 µl complementary strand (54bubble18comp, 100 pmol/µl)	2 µl complementary strand (54bubble18comp, 100 pmol/µl)
	2 µl 18RNAfor54comp (100 pmol/µl)
7 µl 1× Salt-Tris-EDTA (STE) buffer.	5 µl 1× Salt-Tris-EDTA (STE) buffer.

2. Incubate at 95°C, 3 min (µg oligo) in the thermocycler.
3. Use the thermocycler with the program 1degree. It employs the cooling with the rate of 1°C per min for 2 h.
4. Dilute with 90 µl 1× TE buffer to make 1 pmol/µl. Store at –4°C, in the dark.
5. Verify the hybridization using the native PAGE with TBE.

Buffers:

Table 1. Activity assay mixture

Buffers	***Composition (for 5×)***	***Stock***	***Mix preparation***
HEPES buffer (5×) (hSMUG1)	225 mM HEPES, pH 7.5	1 M (lab stock)	22.5 ml
	10% glycerol	85% (Merck, Cat # 1.04094)	12 ml
	2 mM EDTA	0.5 M (lab stock)	400 µl
	Deionized H_2O		to 100 ml
Tris buffer (5×)	100 mM Tris, pH 7.5	1 M (lab stock)	10 ml
	300 mM NaOH	3 M (lab stock)	10 ml
	5 mM EDTA	0.5 M (lab stock)	1 ml
	Deionized H_2O		to 100 ml
Tris-EDTA-glycerol buffer (5×) (hSMUG1)	225 mM Tris-HCl, pH 7.5	1 M (lab stock)	5.625 ml
	10% glycerol	85% (Merck)	2.94 ml
	2 mM EDTA	500 mM EDTA	0.1 ml
	Deionized H_2O		to 25 ml

Stored at –20°C in aliquots.

Table 2. 96% ethanol with 0.1 M CH_3COONa (for DNA precipitation)

Composition	*Stock*	*Mix preparation*
0.1 M NaOAc	Sigma, Cat. # S2889, 82.03 g/mol	0.82 g
96% EtOH	99.5%	225 µl

Stored at room temperature.

Table 3. 1 M KCl

Composition	*Stock*	*Mix preparation*
1 M KCl	Sigma, Cat. # 5405, 74.55 g/mol	3.72 g
Deionized H_2O	96%	50 ml

Stored at –20°C in aliquots.

Table 4. Stop solution

Composition	*Stock*	*Mix preparation*
20 mM EDTA	0.5 M (lab stock)	2 ml
SDS, 0.5% (w/v)	99% (Sigma, Cat. # L3771, 288.38 g/mol)	252 mg
Deionized H_2O		to 50 ml

Stored at room temperature.

Table 5. Salt-TE (STE) buffer (for DNA oligomer hybridization)

Composition	*Stock*	*Mix preparation*
10 mM Tris, pH 8.0	1 M	200 µl
50 mM NaCl	Sigma, Cat. # S5886, 58.44 g/mol	58.44 mg
1 mM EDTA	0.5 M (lab stock)	40 µl
Deionized H_2O		to 20 ml

Filtrated and stored in aliquots at –20°C.

Table 6. Loading buffer (Note: no bromophenol blue)

Composition	*Stock*	*Mix preparation*
Formamide, 80%	99.5% (Sigma, Cat. # F9037)	40.20 ml
1 mM EDTA	0.5 M	100 µl
Blue dextran, 1% (w/v)	Sigma, Cat. # D5751	0.5 g
Deionized H_2O		to 50 ml

Stored at –20°C in aliquots.

Table 7. TE buffer (1×)

Composition	*Stock*	*Mix preparation*
10 mM Tris, pH 7.5	1 M	200 µl
1 mM EDTA, pH 8.0, sterile filtrated	0.5 M	1.6 ml
Deionized H_2O		to 20 ml

Stored in aliquots at –20°C.

Table 8. Taurine (20×), running buffer

Composition	***Stock***	***Mix preparation***
Tris base, 1.78 M	Sigma, Cat. # T6066, 121.14 g/mol	216 g
Taurine, 0.58 M	Sigma, Cat. # T0625, 125.15 g/mol	72 g
$Na_2EDTA \times 2H_2O$	Lab stock	4 g
Deionized H_2O		to 1000 ml

Table 9. TBE (10×), running buffer

Composition	***Stock***	***Mix preparation***
Tris base, 890 mM	Sigma, Cat. # T6066, 121.14 g/mol	108 g
Boric acid, 890 mM	MW 61.8	55 g
20 mM EDTA, pH 8	500 mM (lab stock)	40 ml
Deionized H_2O		to 1000 ml

Autoclaved before use.

Table 10. Denaturing 20% PAGE gel with urea 7 M (taurine buffer system)

Composition	***Stock***	***Big gel***	***Small gel***
Polyacrylamide, 20% (w/v)	40% (Saveen Werner AB, Cat. # BIAC21)	12.5 ml	4.166 ml
Taurine buffer (1×)	Taurine (20×) (lab stock)	1.25 ml	416.6 µl
Urea	99.5% (Sigma, Cat # F9037)	10.5 g	3.5 g
Deionized H_2O		3.75 ml	1.25 ml
Ammonium persulfate (APS)	BioRad, Cat. # 161-0700, 228.2 g/mol	125 µl (from 10% prepared stock)	41.66 µl
Tetramethylethylenediamine (Temed)	Invitrogen Cat. # 15524-010	25 µl	8.33 µl

Table 11. Denaturing 20% PAGE gel with urea 8 M (TBE buffer system)

Composition	***Stock***	***Small gel***
Polyacrylamide, 20% (w/v)	40% (Saveen Werner AB, Cat. # BIAC21)	3.5 ml
TBE (1×)	10× TBE (lab stock)	700 µl
Urea	99.5% (Sigma, Cat. # F9037)	3.363 g
Deionized H_2O		280 µl
Ammonium persulfate (APS)	(BioRad, Cat. # 161-0700, 228.2 g/mol)	35 µl
Tetramethylethylenediamine (Temed)	(Invitrogen Cat. # 15524-010)	3.5 µl

Table 12. 20% acrylamide native PAGE (Taurine buffer system)

Composition	***Stock***	***Small gel***
Polyacrylamide, 20% (w/v)	40% (Saveen Werner AB, Cat. # BIAC21)	3.25 ml
Taurine (1×)	Taurine (20×) (lab stock)	375 µl
Deionized H_2O		3.375 ml
Ammonium persulfate (APS)	(BioRad, Cat. # 161-0700, 228.2 g/mol)	75 µl
Tetramethylethylenediamine (Temed)	(Invitrogen Cat. # 15524-010)	7.5 µl

Table 13. Non-denaturing Loading buffer

Composition	***Stock***	***Small gel***
10 mM Tris, pH 7.6	1 M	50 µl
Taurine (1×)	Taurine (20×) (lab stock)	375 µl
60% glycerol	85% (Merck, Cat #: 1.04094)	3.45 ml (from 87% prepared stock)
60 mM EDTA	0.5 M (lab stock)	600 µl
1% (w/v) blue dextran		0.05 g
Deionized H_2O		To 5 ml (= 900 µl)

APPENDIX B

Kinetic parameters

hSMUG1 P240G bubble-DNA

hSMUG1 P240G bubbleU-DNA																				
$[S]_0$ = 1 pmol = 50 nM	Time = 20 min																			
$[E]_0$, nM	5																			
E, pmol	0.1																			
Performed by	Cyrell Ann Ruales (CAR)																			
Date	4/12/2021	4/12/2021	4/12/2021	4/12/2021	4/14/2021	4/14/2021	4/14/2021	4/14/2021	4/15/2021	4/15/2021	4/15/2021	4/15/2021	4/16/2021	4/16/2021	4/16/2021	4/16/2021	A	SD	M	
Substrate (S)	14428678.81	21906880.31	15740701.79	19367290.69	33854593.01	35845958.15	21591959.2	30100121.6	20385270.63	26865811.92	23429542.4	29484196.99	9593674.5	8519368.23	9937313.04	12036225.53				
Product (P)	226928.66	75634.32	247664.77	460485.5	533550.25	627212	185661.27	455229.09	424920.26	370012.04	265697.67	663697.53	33352.07	138343.28	78544.31	93895.14				
S + P	14655607.47	21982514.63	15988366.56	19827776.19	34388143.26	36473170.15	21777620.47	30555350.7	20810190.89	27235823.96	23695240	30147894.52	9627026.6	8657711.51	10015857.35	12130120.67				
Excision, %	1.54840842	0.344065824	1.549031098	2.322426356	1.551552947	1.719653097	0.852532398	1.48985065	2.04188545	1.358549095	1.12131242	2.201472244	0.3464421	1.597919726	0.784199567	0.774066001	1.35	0.60	1.52	
v, pmol/min	0.000774204	0.000172033	0.000774516	0.001161213	0.000775776	0.000859827	0.000426266	0.00074493	0.001020943	0.000679275	0.00056066	0.001100736	0.0001732	0.00079896	0.0003921	0.000387033				
v, nM/min	0.03871021	0.008601646	0.038725777	0.058060659	0.038788824	0.042991327	0.02131331	0.03724627	0.051047136	0.033963727	0.02803281	0.055036806	0.0086611	0.039947993	0.019604989	0.01935165	0.03	0.02	0.04	
$[E]_0$, nM	15																			
E, pmol	0.3																			
Performed by	CAR																			
Date	4/12/2021	4/12/2021	4/12/2021	4/12/2021	4/14/2021	4/14/2021	4/14/2021	4/14/2021	4/15/2021	4/15/2021	4/15/2021	4/15/2021	4/16/2021	4/16/2021	4/16/2021	4/16/2021	A	SD	M	
Substrate (S)	15042771.7	17450668.39	11858508.98	19262252.19	36472224.55	36364822.27	23734831.38	23251161.6	11024642.09	20534091.43	22807637	20664579.02	5644951.9	9041790.51	23343171.95	18857747.34				
Product (P)	1458167.97	1891125.48	1124390.28	2941061.07	2356578.85	1759249.99	1364646.26	1871332.13	1239299.24	1843517.97	2288757.68	2655615.3	17947.23	623445.79	176040.35	260679.59				
S + P	16500939.67	19341793.87	12982899.26	22203313.26	38828803.4	38124072.26	25099477.64	25122493.7	12263941.33	22377609.4	25096394.7	23320194.32	5662899.2	9665236.3	23519212.3	19118426.93				
Excision, %	8.836878379	9.777404788	8.660548445	13.24604592	6.069151361	4.614538494	5.436950838	7.44883112	10.10522806	8.238225706	9.11986646	11.3876208	0.3169265	6.450393665	0.748495943	1.363499157	6.99	3.77	7.84	
v, pmol/min	0.004418439	0.004888702	0.004330274	0.006623023	0.003034576	0.002307269	0.002718475	0.00372442	0.005052614	0.004119113	0.00455993	0.00569381	0.0001585	0.003225197	0.000374248	0.00068175				
v, nM/min	0.220921959	0.24443512	0.216513711	0.331151148	0.151728784	0.115363462	0.135923771	0.18622078	0.252630701	0.205955643	0.22799666	0.28469052	0.0079232	0.161259842	0.018712399	0.034087479	0.17	0.09	0.20	
$[E]_0$, nM	25																			
E, pmol	0.5																			
Performed by	CAR																			
Date	4/12/2021	4/12/2021	4/12/2021	4/12/2021	4/14/2021	4/14/2021	4/14/2021	4/14/2021	4/15/2021	4/15/2021	4/15/2021	4/15/2021	4/16/2021	4/16/2021	4/16/2021	4/16/2021	A	SD	M	
Substrate (S)	12321338.06	17856712.42	15085976.54	16914945.1	30490487.03	31667148.81	24015701.17	17213698.5	18207126.26	21844550.43	25630542.1	25197678.48	5331802	8493747.33	9197392.06	9476332.46				
Product (P)	1547573.56	2080007.48	1826271.47	1850217.58	3310577.46	2255148.53	2735419.79	2044344.65	2165465.02	2477326.47	5011882.43	4726844.35	93516.46	105381.14	155340.27	139634.79				
S + P	13868911.62	19936719.9	16912248.01	18765162.68	33801064.49	33922297.34	26751120.96	19258043.1	20372591.28	24321876.9	30642424.5	29924522.83	5425318.4	8599128.47	9352732.33	9615967.25				
Excision, %	11.15857972	10.43304761	10.79851401	9.859853664	9.79429941	6.64798291	10.22543988	10.6155368	10.62930577	10.18558921	16.3560244	15.7958888	1.7237045	1.225486285	1.660907899	1.452113827	8.66	4.81	10.21	
v, pmol/min	0.00557929	0.005216524	0.005399257	0.004929927	0.00489715	0.003323991	0.00511272	0.00530777	0.005314653	0.005092795	0.00817801	0.007897944	0.0008619	0.000612743	0.000830454	0.000726057				
v, nM/min	0.278964493	0.26082619	0.26996285	0.246496342	0.244857485	0.166199573	0.255635997	0.26538842	0.265732644	0.25463973	0.40890061	0.39489722	0.0430926	0.030637157	0.041522697	0.036302846	0.22	0.12	0.26	
$[E]_0$, nM	35																			
E, pmol	0.7																			
Performed by	CAR																			
Date	4/12/2021	4/12/2021	4/12/2021	4/12/2021	4/14/2021	4/14/2021	4/14/2021	4/14/2021	4/15/2021	4/15/2021	4/15/2021	4/15/2021	4/16/2021	4/16/2021	4/16/2021	4/16/2021	A	SD	M	
Substrate (S)	16096533.71	18166910.16	13176024.74	17963268.38	32553022.56	34556877.71	22118812.08	28359966.5	21639881.81	21527062.79	25887988.4	23659744.7	3989656	6584820.83	12827872.68	10431224.18				
Product (P)	2411397.8	3664073.26	1886817.08	3048078.07	5127474.92	3633401.45	2464233.49	4688574.82	3489374.48	3605488.75	6324837.01	4275258.06	106582.69	262325.09	482752.46	673912.84				
S + P	18507931.51	21830983.42	15062841.82	21011346.45	37680497.48	38190279.16	24583045.57	33048541.3	25129256.29	25132551.54	32212825.4	27935002.76	4096238.6	6847145.92	13310625.14	11105137.02				
Excision, %	13.02899678	16.78382137	12.52630216	14.50681934	13.60776864	9.513943155	10.02411798	14.1869342	13.88570533	14.3458922	19.6345304	15.30430513	2.6019649	3.831159626	3.62682034	6.068478388	11.47	5.05	13.32	
v, pmol/min	0.006514498	0.008391911	0.006263151	0.00725341	0.006803884	0.004756972	0.005012059	0.00709347	0.006942853	0.007172946	0.00981727	0.007652153	0.001301	0.00191558	0.00181341	0.003034239				
v, nM/min	0.325724919	0.419595534	0.313157554	0.362670483	0.340194216	0.237848579	0.250602949	0.35467336	0.347142633	0.358647305	0.49086326	0.382607628	0.0650491	0.095778991	0.090670509	0.15171196	0.29	0.13	0.33	
$[E]_0$, nM	50																			
E, pmol	1																			
Performed by	CAR																			
Date	4/12/2021	4/12/2021	4/12/2021	4/12/2021	4/14/2021	4/14/2021	4/14/2021	4/14/2021	4/15/2021	4/15/2021	4/15/2021	4/15/2021	4/16/2021	4/16/2021	4/16/2021	4/16/2021	A	SD	M	
Substrate (S)	16840573.11	18758735.58	13511783.62	20075331.23	31203908.41	35728624.89	22780319.78	29430472.1	18612728.21	14932483.25	21674625.6	22519494.95	5237449.9	12225926.48	10727975.06	10572464.84				
Product (P)	4039551.27	5317841.95	3390624.25	975632.96	7586873.42	7673710.14	6757748.42	5882518.28	5070068.24	3697793.76	8446337.49	5593550.71	494420.13	1534495.45	729772.48	1245598.36				
S + P	20880124.38	24076577.53	16902407.87	21050964.19	38790781.83	43402335.03	29538068.2	35312990.4	23682796.45	18630277.01	30120963	28113045.66	5731870.1	13760421.93	11457747.54	11818063.2				
Excision, %	19.34639467	22.08720049	20.06000728	4.634623627	19.5584442	17.68040852	22.87809878	16.6582275	21.40823298	19.84830262	28.0413926	19.89663723	8.6258084	11.15151452	6.369249082	10.53978422	16.80	6.59	19.45	
v, pmol/min	0.009673197	0.0110436	0.010030004	0.002317312	0.009779222	0.008840204	0.011439049	0.00832911	0.010704116	0.009924151	0.0140207	0.009948319	0.0043129	0.005575757	0.003184625	0.005269892				
v, nM/min	0.483659867	0.552180012	0.501500182	0.115865591	0.488961105	0.442010213	0.571952469	0.41645569	0.535205824	0.496207566	0.70103481	0.497415931	0.2156452	0.278787863	0.159231227	0.263494605	0.42	0.16	0.49	
$[E]_0$, nM	100																			
E, pmol	2																			
Performed by	CAR																			
Date	23/04/21	23/04/21	23/04/21	23/04/21	24/04/21	24/04/21	24/04/21	24/04/21									A	SD	M	
Substrate (S)	7948156.65	11114442.36	9649548.33	24819750.95	19677431.44	15345725.2	11051547.36	11783344												
Product (P)	12039306.96	9677730.49	15612012.36	17404992.41	16816644.05	13121825.86	8129446.92	10046150.4												
S + P	19987463.61	20792172.85	25261560.69	42224743.36	36494075.49	28467551.06	19180994.28	21829494.4												
Excision, %	60.23429083	46.54506559	61.80145618	41.21988916	46.08047697	46.09397497	42.38282334	46.0209944									48.79737142	7.80059549	46.08722597	
v, pmol/min	0.030117145	0.023272533	0.030900728	0.020609945	0.023040238	0.023046987	0.021191412	0.0230105												
v, nM/min	1.505857271	1.16362664	1.545036404	1.030497229	1.152011924	1.152349374	1.059570583	1.15052486									1.219934286	0.19501489	1.152180649	
$[E]_0$, nM	150																			
E, pmol	3																			
Performed by	CAR																			
Date	23/04/21	23/04/21	23/04/21	23/04/21	24/04/21	24/04/21	24/04/21	24/04/21									A	SD	M	
Substrate (S)	10876721.96	10895179.82	10420067.37	7696130.11	8137145.44	8038699.61	12232427.49	9050092.84												
Product (P)	17958415.28	12689953.34	18561157.02	19870479.8	13926827.87	13523499.7	16520926.14	17150137.8												
S + P	28835137.24	23585133.16	28981224.39	27566609.91	22063973.31	21562199.31	28753353.63	26200230.7												
Excision, %	62.27962479	53.80488316	64.04545498	72.08169545	63.12021717	62.71855438	57.45738863	65.457965									62.62072295	5.40296572	62.91938578	
v, pmol/min	0.031139812	0.026902442	0.032022727	0.036040848	0.031560109	0.031359277	0.026728694	0.03272898												
v, nM/min	1.55699062	1.345122079	1.601136375	1.802042386	1.578005429	1.56796386	1.436434716	1.63644913									1.565518074	0.13507414	1.572984644	

CAR	nM	nM/min	SD	pmol	% excision	SD	Number of parallels
	0	0	0	0	0	0	
	5	0.033755	0.015079	0.1	1.35021	0.603175	16
	15	0.17472	0.094162	0.3	6.988788	3.766482	16
	25	0.216504	0.120362	0.5	8.660142	4.814488	16
	35	0.286684	0.126166	0.7	11.46735	5.046631	16
	50	0.419976	0.164774	1	16.79902	6.590953	16
	100	1.219934286	0.195014887	2	48.79737142	7.800595486	8
	150	1.565518074	0.135074143	3	62.62072295	5.402965725	8

All values

0	0	15	0.220921959	25	0.26082619	35	0.313157554	50	0.115865591	100	1.15201192	
5	0.03871021	15	0.24443512	25	0.26996285	35	0.362670483	50	0.488961105	100	1.15234937	
5	0.008601646	15	0.216513711	25	0.246496342	35	0.340194216	50	0.442010213	100	1.05957058	
5	0.038725777	15	0.331151148	25	0.244857485	35	0.237848579	50	0.571952469	100	1.15052486	
5	0.058060659	15	0.151728784	25	0.166199573	35	0.250602949	50	0.416455688	150	1.55699062	
5	0.038788824	15	0.115363462	25	0.255635997	35	0.354673356	50	0.535205824	150	1.34512208	
5	0.042991327	15	0.135923771	25	0.265388419	35	0.347142633	50	0.496207566	150	1.60113638	
5	0.02131331	15	0.186220778	25	0.265732644	35	0.358647305	50	0.701034814	150	1.80204239	
5	0.037246266	15	0.252630701	25	0.25463973	35	0.49086326	50	0.497415931	150	1.57800543	
5	0.051047136	15	0.205955643	25	0.40890061	35	0.382607628	50	0.21564521	150	1.56796386	
5	0.033963727	15	0.227996661	25	0.39489722	35	0.06504912	50	0.276787863	150	1.43643472	
5	0.028032811	15	0.28469052	25	0.04309261	35	0.095778991	50	0.159231227	150	1.63644913	
5	0.055036806	15	0.00792316	25	0.030637157	35	0.090670509	50	0.263494605			
5	0.00866105	15	0.161259842	25	0.041522697	35	0.15171196	100	1.505857271			
5	0.039947993	15	0.018712399	25	0.036302846	50	0.483659867	100	1.16362664			
5	0.019604989	15	0.034087479	35	0.325724919	50	0.552180012	100	1.545036404			
5	0.01935165	25	0.278964493	35	0.419595534	50	0.501500182	100	1.030497229			

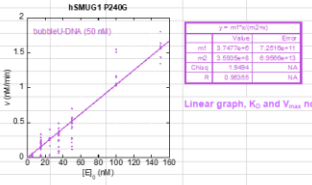

y = mI*x/(mI+x)		
	Value	Error
mI	3.7473e+6	7.2818e+11
mS	3.5935e+6	6.9969e+13
Chisq	1.9484	NA
R	0.96355	NA

Linear graph, K_D and V_{max} not determined

hSMUG1 P240G R-loopU-DNA

hSMUG1 P240G R-loopU-DNA																		
$[S]_0$ = 1 pmol = 50 nM	Time = 20 min																	
$[E]_0$, nM	5																	
E, pmol	0.1																	
Performed by	Cyrell Ann Ruales (CAR)															A	SD	M
Date	**29/04/2021**	**29/04/2021**	**29/04/2021**	**29/04/2021**	**5/5/2021**	**5/5/2021**	**5/5/2021**	**5/5/2021**	**5/5/2021**	**5/5/2021**	**5/5/2021**	**5/5/2021**	**5/5/2021**	**5/6/2021**	**5/6/2021**			
Substrate (S)	14507973.88	111895132.5	13471438.88	12480032.41	14658283.29	22340256.66	64129637.71	78767143.58	23806494	27521762.4	40933707.1	47191901	14850325.41	20595440.54				
Product (P)	1366058.37	5977711.58	922749.43	930073.69	872210.64	1203479.56	4205515.72	4561827.71	1975054.65	3016952.88	2624575.34	4520871.67	848437.36	1529401.27				
S + P	15874032.25	117872844.1	14394188.31	13410106.1	15530493.93	23588057.22	68335153.43	83328971.29	25781548.7	30538715.3	43556282.5	51712772.7	15698762.77	22124841.81				
Excision, %	8.605616698	5.071322091	6.410569392	6.935617683	5.616116551	5.102071564	6.154249327	5.474479811	7.66072929	9.8791087	6.02543349	8.74227282	5.404485515	6.912597537	6.71	1.50	6.28	
v, pmol/min	0.004302808	0.002535661	0.003205285	0.003467809	0.002808058	0.002551036	0.003077125	0.00273724	0.00383036	0.00493955	0.00301272	0.00437114	0.002702243	0.003456299				
v, nM/min	0.215140417	0.126783052	0.160264235	0.173390442	0.140402914	0.127551789	0.153856233	0.136861995	0.19151823	0.24697772	0.15063584	0.21855682	0.135112138	0.172814938	0.17	0.04	0.16	
$[E]_0$, nM	15																	
E, pmol	0.3																	
Performed by	CAR															A	SD	M
Date	**29/04/2021**	**29/04/2021**	**29/04/2021**	**29/04/2021**	**5/5/2021**	**5/5/2021**	**5/5/2021**	**5/5/2021**	**5/5/2021**	**5/5/2021**	**5/5/2021**	**5/5/2021**	**5/6/2021**	**5/6/2021**				
Substrate (S)	13170036.7	112861439.1	13326633.72	14088745.88	16676475.85	26302524.01	48431911.87	75179813.28	16282634.4	21787561.3	19933750.9	40744639	11662714.13	21120595.34				
Product (P)	3700336.29	35545987.21	3462711.84	4109982.33	3979148.74	6493436.51	17201973.08	19673796.15	4435238	6509861.12	5867901.93	12322851.6	3069385.52	5442860.55				
S + P	16870372.99	148407426.3	16789345.56	18198728.21	20655624.59	32795960.52	65633884.95	94853609.43	20762193.4	28297422.4	25801652.9	53067490.6	14732099.65	26563455.89				
Excision, %	21.93393289	23.95162298	20.62445989	22.58389863	19.26423828	19.79950094	26.20898198	20.74122036	21.3620879	23.0051381	22.742349	23.2210935	20.83467797	20.49003177	21.91	1.85	21.65	
v, pmol/min	0.010966966	0.011975811	0.01031223	0.011291949	0.009632119	0.00989975	0.013104491	0.01037061	0.01068104	0.01150257	0.01137117	0.01161055	0.010417339	0.010245016				
v, nM/min	0.548348322	0.598790574	0.515611497	0.564597466	0.481605957	0.494987523	0.65522455	0.518530509	0.5340522	0.57512845	0.56855872	0.58052734	0.520866949	0.512250794	0.55	0.05	0.54	
$[E]_0$, nM	25																	
E, pmol	0.5																	
Performed by	CAR															A	SD	M
Date	**29/04/2021**	**29/04/2021**	**29/04/2021**	**29/04/2021**	**5/5/2021**	**5/5/2021**	**5/5/2021**	**5/5/2021**	**5/5/2021**	**5/5/2021**	**5/5/2021**	**5/5/2021**	**5/6/2021**	**5/6/2021**				
Substrate (S)	9540285.7	7978368.29	9208934.49	13829146.74	17266949.33	15408130.07	54350363.22	54832841.92	19313156	17036250.5	28019602.1	34114657.7	11035512.2	12320798.05				
Product (P)	3990402.14	5110953.71	5993209.33	5994564.3	10852166.61	10188991.05	31508973.88	34106084.67	7776258.59	10785898.7	15899334.4	21448093	6813590.15	7933158.34				
S + P	13530687.84	13089322	15202143.82	19823711.04	28119115.94	25597121.12	85859337.1	88938926.59	27089414.5	27822149.2	43918936.4	55562750.7	17849102.35	20253956.39				
Excision, %	29.49149509	39.04674138	39.42344844	30.23936481	38.59355548	39.80522264	36.69836612	38.34775837	28.7058939	38.7673097	36.2015469	38.601568	38.17329307	39.16843794	36.52	3.95	38.47	
v, pmol/min	0.014745748	0.019523371	0.019711724	0.015119682	0.019296778	0.019902611	0.018349183	0.019173879	0.01435295	0.01938365	0.01810077	0.01930078	0.019086647	0.019584219				
v, nM/min	0.737287377	0.976168535	0.985586211	0.75598412	0.964838887	0.995130566	0.917459153	0.958693959	0.71764735	0.96918274	0.90503867	0.9650392	0.954332327	0.979210949	0.91	0.10	0.96	
$[E]_0$, nM	35																	
E, pmol	0.7																	
Performed by	CAR															A	SD	M
Date	**29/04/2021**	**29/04/2021**	**29/04/2021**	**29/04/2021**	**5/5/2021**	**5/5/2021**	**5/5/2021**	**5/5/2021**	**5/5/2021**	**5/5/2021**	**5/5/2021**	**5/5/2021**	**5/6/2021**	**5/6/2021**				
Substrate (S)	7560151.72	5661034.46	10258289.59	7254246.61	13674825.77	16977859.71	41880039.7	41884563.65	15162156.7	19703380.9	11481398	19936187.4	10187817.86	13905179.89				
Product (P)	7261517.51	8257022.96	8087781.24	8152006.33	12755791.13	12032520.65	49188183.95	38299286.08	11134902.6	18620259.8	13095908	39282526.7	16587315.13	22776832.45				
S + P	14821669.23	13918057.42	18346070.83	15406252.94	26430616.9	29010380.36	91068223.65	80183849.73	26297059.3	38323640.7	24577306	59218714.1	26775132.99	36682012.34				
Excision, %	48.99257565	59.32597281	44.08454167	52.91362125	48.26142038	41.47660424	54.01245569	47.76433934	42.3427673	48.5868761	53.2845545	66.33465	61.95044908	62.09264704	52.24	7.77	50.95	
v, pmol/min	0.024496288	0.029662986	0.022042271	0.026456811	0.0241307	0.020738302	0.027006228	0.02388217	0.02117138	0.02429344	0.02664228	0.03316733	0.030975225	0.031046324				
v, nM/min	1.224814391	1.48314932	1.102113542	1.322840531	1.206535509	1.036915106	1.350311392	1.194108483	1.05856918	1.2146719	1.33211386	1.65836625	1.548761227	1.552316176	1.31	0.19	1.27	
$[E]_0$, nM	50																	
E, pmol	1																	
Performed by	CAR															A	SD	M
Date	**29/04/2021**	**29/04/2021**	**29/04/2021**	**29/04/2021**	**5/5/2021**	**5/5/2021**	**5/5/2021**	**5/5/2021**	**5/5/2021**	**5/5/2021**	**5/5/2021**	**5/5/2021**	**5/6/2021**	**5/6/2021**				
Substrate (S)	7519577.59	3038628.99	3072298.97	13805853.13	14375377.64	32303037.4	35352780.42	41657314.36	20364192.3	15212394.6	11650582.8	22298424	8077035.7	8175004.8				
Product (P)	8016558.81	10741161.98	5840330.34	10285119.55	32170344.25	42623563.09	50921667.7	50890028.87	29717712.4	18735542.2	15482011.6	16813448	8958317.73	9271921.08				
S + P	15536136.4	13779790.97	8912629.31	24090972.68	46545721.89	74926600.49	86274448.12	92547343.23	50081904.7	33947936.9	27132594.4	39111872.1	17035353.43	17446925.88				
Excision, %	51.59943633	77.94865687	65.52870244	42.69283639	69.11557699	56.88709058	59.02288431	54.98810349	59.3382231	55.1890452	57.0605648	42.9880932	52.58662679	53.14358039	57.01	9.36	56.04	
v, pmol/min	0.025799718	0.038974328	0.032764351	0.021346418	0.034557788	0.028443545	0.029511442	0.027494052	0.02966911	0.02759452	0.02853028	0.02149405	0.026293313	0.02657179				
v, nM/min	1.289985908	1.948716422	1.638217561	1.06732091	1.727889425	1.422177265	1.475572108	1.374702587	1.48345558	1.37972613	1.42651412	1.07470233	1.31466567	1.32858951	1.43	0.23	1.40	
$[E]_0$, nM	100																	
E, pmol	2																	
Performed by	CAR					A	SD	M										
Date	**29/04/2021**	**29/04/2021**	**29/04/2021**	**29/04/2021**														
Substrate (S)	1234865.77	3075003.28	5400518.41	4055282.77														
Product (P)	5010301.13	13998599.67	14300404.26	10348767.22														
S + P	6245166.9	17073602.95	19700922.67	14404049.99														
Excision, %	80.22685719	81.98972244	72.58748486	71.84623232		76.6625742	5.192498558	76.40717102										
v, pmol/min	0.040113429	0.040994861	0.036293742	0.035923116														
v, nM/min	2.00567143	2.049743061	1.814687121	1.796155808		1.916564355	0.129812464	1.910179276										

CAR	**nM**	**nM/min**	**SD**	**pmol**	**% excision**	**SD**	**Number of parallels**
	0	0	0	0	0	0	
	5	0.167847626	0.03755	0.1	6.713905034	150.199	14
	15	0.54779149	0.046337	0.3	21.91165958	1.8535	14
	25	0.912971432	0.098649	0.5	36.51885727	3.945963	14
	35	1.306113348	0.194268	0.7	52.24453393	7.770719	14
	50	1.42515968	0.234092	1	57.00638721	9.363674	14
	100	1.916564355	0.129812464	2	76.6625742	5.192498558	4

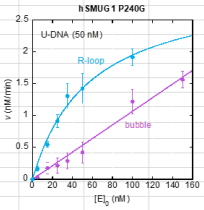

y = m1*x/(m2+x)		
	Value	Error
m1	3.0622	0.3278
m2	57.083	11.702
Chisq	0.03911	NA
R	0.99388	NA

K_D = 60 ± 10 nM

V_{max} = 3.1 ± 0.3 nM/min

y = m1*x/(m2+x)		
	Value	Error
m1	2.1493e+5	4.9693e+9
m2	2.0136e+7	4.6579e+11
Chisq	0.046152	NA
R	0.99974	NA

Linear graph, K_D and V_{max} not determined

0	0	15	0.65522455	25	0.979210949	50	1.475572108		
5	0.215140417	15	0.518530509	35	1.224814391	50	1.374702587		
5	0.126783052	15	0.534052196	35	1.48314932	50	1.483455578		
5	0.160264235	15	0.575128453	35	1.102113542	50	1.37972613		
5	0.173390442	15	0.56855872	35	1.322840531	50	1.42651412		
5	0.140402914	15	0.58052734	35	1.206535509	50	1.07470233		
5	0.127551789	15	0.520866949	35	1.036915106	50	1.31466567		
5	0.153856233	15	0.512250794	35	1.350311392	50	1.32858951		
5	0.136861995	25	0.737287377	35	1.194108483	100	2.00567143		
5	0.191518232	25	0.976168535	35	1.058569183	100	2.049743061		
5	0.246977717	25	0.985586211	35	1.214671902	100	1.814687121		
5	0.15063584	25	0.75598412	35	1.33211386	100	1.796155808		
5	0.21855682	25	0.964838887	35	1.65836625				
5	0.135112138	25	0.995130566	35	1.548761227				
5	0.172814938	25	0.917459153	35	1.552316176				
15	0.548348322	25	0.958693959	50	1.289985908				
15	0.598790574	25	0.717647347	50	1.948716422				
15	0.515611497	25	0.969182741	50	1.638217561				
15	0.564597466	25	0.90503867	50	1.06732091				
15	0.481605957	25	0.9650392	50	1.727889425				
15	0.494987523	25	0.954332327	50	1.422177265				

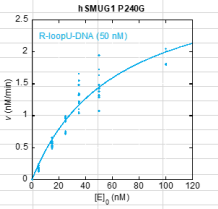

y = m1*x/(m2+x)		
	Value	Error
m1	3.2466	0.2762
m2	62.311	8.8319
Chisq	1.9017	NA
R	0.99531	NA

K_D = 62 ± 9 nM

V_{max} = 3.2 ± 0.3 nM/min

hSMUG1(TB) bubble-DNA

hSMUG1(TB) bubbleU-DNA															
$[S]_0$ = 1 pmol = 50 nM	Time = 20 min														
$[E]_0$, nM	5														
E, pmol	0.1														
Performed by	Cyrell Ann Ruales (CAR)												A	SD	M
Date	5/8/2021	5/8/2021	5/8/2021	5/8/2021	5/9/2021	5/9/2021	5/9/2021	5/9/2021	5/11/2021	5/11/2021	5/11/2021	5/11/2021			
Substrate (S)	34022446.53	48793002.14	11407788.82	16782345	11227011.5	10327928.93	8506986.9	14436259.6	16416480.5	20369900.9	21645152.16	30994380.8			
Product (P)	676271.11	973695.71	322744.41	415555.17	148761.61	327440.46	277037.55	393883.42	216635.23	325023.91	305230.89	433055.61			
S + P	34698717.64	49766697.85	11730533.23	17197900	11375773.1	10655369.39	8784024.45	14830143.02	16633115.7	20694924.8	21950383.05	31427436.4			
Excision, %	1.948980124	1.956520629	2.751319174	2.4163135	1.30770549	3.073008997	3.153879541	2.655965081	1.30243325	1.57054888	1.390549264	1.37795398	2.08	0.71	1.95
v, pmol/min	0.00097449	0.00097826	0.00137566	0.0012082	0.00065385	0.001536504	0.00157694	0.001327983	0.00065122	0.00078527	0.000695275	0.00068898			
v, nM/min	0.048724503	0.048913016	0.068782979	0.0604078	0.03269264	0.076825225	0.078846989	0.066399127	0.03256083	0.03926372	0.034763732	0.03444885	0.05	0.02	0.05
$[E]_0$, nM	15														
E, pmol	0.3														
Performed by	CAR												A	SD	M
Date	5/8/2021	5/8/2021	5/8/2021	5/8/2021	5/9/2021	5/9/2021	5/9/2021	5/9/2021	5/11/2021	5/11/2021	5/11/2021	5/11/2021			
Substrate (S)	30008984.38	33950625.3	15705951.47	19926427	11232370.5	17152958.65	13352329.36	11666380.39	21635862.3	19474026.8	29878910.61	33822508.1			
Product (P)	1686021.88	2451014.65	1067466.03	1202588.7	538345.37	804458.57	592554.26	622214.16	942519.25	1096628.24	2199365.01	2136082.32			
S + P	31695006.26	36401639.95	16773417.5	21129016	11770715.9	17957417.22	13944883.62	12288594.55	22578381.6	20570655	32078275.62	35958590.4			
Excision, %	5.319519	6.733253374	6.364034223	5.6916454	4.57359922	4.479812214	4.249259271	5.063346809	4.17443229	5.33103219	6.856244507	5.94039504	5.40	0.94	5.33
v, pmol/min	0.002659759	0.003366627	0.003182017	0.0028458	0.0022868	0.002239906	0.00212463	0.002531673	0.00208722	0.00266552	0.003428122	0.0029702			
v, nM/min	0.132987975	0.168331334	0.159100856	0.1422911	0.11433998	0.111995305	0.106231482	0.12658367	0.10436081	0.1332758	0.171406113	0.14850988	0.13	0.02	0.13
$[E]_0$, nM	25														
E, pmol	0.5														
Performed by	CAR												A	SD	M
Date	5/8/2021	5/8/2021	5/8/2021	5/8/2021	5/9/2021	5/9/2021	5/9/2021	5/9/2021	5/11/2021	5/11/2021	5/11/2021	5/11/2021			
Substrate (S)	21576079.3	33140648.24	15276807.03	23339782	7972912.97	17480242.44	11192189.19	17425751.57	27669217.8	23008280.1	43470884.03	23704445.8			
Product (P)	4621914.55	6436438.41	2156164.15	3744449.4	1098329.43	3435505.6	2123070.51	2645954.36	5118129.69	3154324.43	7574794.22	4199008.14			
S + P	26197993.85	39577086.65	17432971.18	27084231	9071242.4	20915748.04	13315259.7	20071705.93	32787347.5	26162604.5	51045678.25	27903454			
Excision, %	17.64224611	16.26304247	12.36831133	13.825201	12.107817	16.42544935	15.94464215	13.1825086	15.6100755	12.0566147	14.83924689	15.0483454	14.61	1.88	14.94
v, pmol/min	0.008821123	0.008131521	0.006184156	0.0069126	0.00605391	0.008212725	0.007972321	0.006591254	0.00780504	0.00602831	0.007419623	0.00752417			
v, nM/min	0.441056153	0.406576062	0.309207783	0.34563	0.30269543	0.410636234	0.398616054	0.329562715	0.39025189	0.30141537	0.370981172	0.37620864	0.37	0.05	0.37
$[E]_0$, nM	35														
E, pmol	0.7														
Performed by	CAR												A	SD	M
Date	5/8/2021	5/8/2021	5/8/2021	5/8/2021	5/9/2021	5/9/2021	5/9/2021	5/9/2021	5/11/2021	5/11/2021	5/11/2021	5/11/2021			
Substrate (S)	29719948.12	37085494.59	14036526.61	22439400	8770018.41	13791500.86	6875262.36	14231391.71	18661183.7	26636204.9	26372219.86	34247919.3			
Product (P)	9588299.15	12622736.27	5158745.38	5658609	2629633.31	4253194.07	2204518.7	5162208.16	5837345.04	7920685.46	7017851.16	9573368.12			
S + P	39308247.27	49708230.86	19195271.99	28098009	11399651.7	18044694.93	9079781.06	19393599.87	24498528.7	34556890.4	33390071.02	43821287.4			
Excision, %	24.39258887	25.39365423	26.87508352	20.138825	23.0676636	23.5703296	24.27942574	26.61810182	23.827329	22.9207124	21.01777848	21.8463872	23.66	2.06	23.70
v, pmol/min	0.012196294	0.012696827	0.013437542	0.0100694	0.01153383	0.011785165	0.012139713	0.013309051	0.01191366	0.01146036	0.010508889	0.01092319			
v, nM/min	0.609814722	0.634841356	0.671877088	0.5034706	0.57669159	0.58925824	0.606985644	0.665452546	0.59568323	0.57301781	0.525444462	0.54615968	0.59	0.05	0.59
$[E]_0$, nM	50														
E, pmol	1														
Performed by	CAR												A	SD	M
Date	5/8/2021	5/8/2021	5/8/2021	5/8/2021	5/9/2021	5/9/2021	5/9/2021	5/9/2021	5/11/2021	5/11/2021	5/11/2021	5/11/2021			
Substrate (S)	26081065.55	29924706.19	18193133.78	21501177	7614775.87	13605916.79	11126830.79	11840917.05	23554881.2	28150348.7	48842314.66	30658596.4			
Product (P)	11822407.86	15457273.46	7847927.47	9747608.6	2020514.75	5436851.37	5388874.95	5133689.72	9936905.39	11997972.9	25904983.35	11997414.3			
S + P	37903473.41	45381979.65	26041061.25	31248785	9635290.62	19042768.16	16515705.74	16974606.77	33491786.6	40148321.6	74747298.01	42656010.7			
Excision, %	31.19082975	34.06037722	30.1367421	31.19356	20.9699409	28.55074076	32.62879004	30.2433499	29.6696785	29.8841207	34.65674886	28.1259643	30.11	3.51	30.19
v, pmol/min	0.015595415	0.017030189	0.015068371	0.0155968	0.01048497	0.01427537	0.016314395	0.015121675	0.01483484	0.01494206	0.017328374	0.01406298			
v, nM/min	0.779770744	0.851509431	0.753418553	0.779839	0.52424852	0.713768519	0.815719751	0.756083748	0.74174196	0.74710302	0.866418721	0.70314911	0.75	0.09	0.75

CAR	nM	nM/min	SD	pmol	% excision	SD	Number of parallels
	0	0	0	0	0	0	
	5	0.051885787	0.017671	0.1	2.07543149	0.706834	12
	15	0.134951195	0.023458	0.3	5.39804779	0.93833	12
	25	0.365236459	0.046897	0.5	14.6094584	1.875889	12
	35	0.591558083	0.051465	0.7	23.6623233	2.058588	12
	50	0.752730923	0.087625	1	30.1092369	3.505019	12

All values						
0	0	15	0.104360807	35	0.58925824	
5	0.048724503	15	0.133275805	35	0.60698564	
5	0.048913016	15	0.171406113	35	0.66545255	
5	0.068782979	15	0.14850988	35	0.59568323	
5	0.06040784	25	0.441056153	35	0.57301781	
5	0.03269264	25	0.406576062	35	0.52544446	
5	0.076825225	25	0.309207783	35	0.54615968	
5	0.078846989	25	0.34563002	50	0.77977074	
5	0.066399127	25	0.30269543	50	0.85150943	
5	0.032560831	25	0.410636234	50	0.75341855	
5	0.039263722	25	0.398616054	50	0.779839	
5	0.034763732	25	0.329562715	50	0.52424852	
5	0.03444885	25	0.390251887	50	0.71376852	
15	0.132987975	25	0.301415368	50	0.81571975	
15	0.168331334	25	0.370981172	50	0.75608375	
15	0.159100856	25	0.37620864	50	0.74174196	
15	0.14229113	35	0.609814722	50	0.74710302	
15	0.11433998	35	0.634841356	50	0.86641872	
15	0.111995305	35	0.671877088	50	0.70314911	
15	0.106231482	35	0.50347063			
15	0.12658367	35	0.57669159			

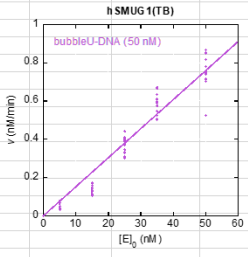

y = m1*x/(m2+x)		
	Value	Error
m1	3.2207e+13	7.9521e-15
m2	2.1206e+15	1.2072e-16
Chisq	0.30393	NA
R	0.9657	NA

Linear graph, K_D and V_{max} not determined

hSMUG1(TB) R-loopU-DNA

hSMUG1(TB) R-loopU-DNA												
$[S]_0$ = 1 pmol = 50 nM	Time = 20 min											
$[E]_0$, nM	5											
E, pmol	0.1											
Performed b	Cyrell Ann Ruales (CAR)									A	SD	M
Date	5/27/2021	5/27/2021	5/27/2021	5/27/2021	5/27/2021	5/27/2021	5/27/2021	5/27/2021	5/27/2021			
Substrate (S	9525343.43	17730644.39	13390302.58	15452609.81	15680693.65	18615004.16	1087029.97	13748944				
Product (P)	142489.84	252696.84	208043.51	162781.84	207111.87	221899.66	20671.87	172058.86				
S + P	9667833.27	17983341.23	13598346.09	15615391.65	15887805.52	18836903.82	1107701.84	13921002.86				
Excision, %	1.473854958	1.405171802	1.529917746	1.042444811	1.303590164	1.178004953	1.866194426	1.235965984		1.37939	0.25344	1.35438
v, pmol/min	0.000736927	0.000702586	0.000764959	0.000521222	0.000651795	0.000589002	0.000933097	0.000617983				
v, nM/min	0.036846374	0.035129295	0.038247944	0.02606112	0.032589754	0.029450124	0.046654861	0.03089915		0.03448	0.00634	0.03386
$[E]_0$, nM	15											
E, pmol	0.3											
Performed b	CAR									A	SD	M
Date	5/27/2021	5/27/2021	5/27/2021	5/27/2021	5/27/2021	5/27/2021	5/27/2021	5/27/2021				
Substrate (S	11632953.75	18173818.59	11614015.28	15169477.28	18424497.01	19644675.76	11601563.89	12165270.19				
Product (P)	506273.24	1147811.64	468694.89	745680.8	757106.48	834315.22	505863.58	569977.93				
S + P	12139226.99	19321630.23	12082710.17	15915158.08	19181603.49	20478990.98	12107427.47	12735248.12				
Excision, %	4.170555839	5.940552771	3.879054313	4.685349629	3.947044784	4.074005506	4.178126041	4.475593445		4.41879	0.67	4.17434
v, pmol/min	0.002085278	0.002970276	0.001939527	0.002342675	0.001973522	0.002037003	0.002089063	0.002237797				
v, nM/min	0.104263896	0.148513819	0.096976358	0.117133741	0.09867612	0.101850138	0.104453151	0.111889836		0.11047	0.01675	0.10436
$[E]_0$, nM	25											
E, pmol	0.5											
Performed b	CAR									A	SD	M
Date	5/27/2021	5/27/2021	5/27/2021	5/27/2021	5/27/2021	5/27/2021	5/27/2021	5/27/2021				
Substrate (S	10893079.87	17952491.22	12413188.59	14638820.72	19115465.98	15716624.79	20464327.6	14384895.72				
Product (P)	762423.7	966117.22	559996.28	685505.42	996314.4	708287.29	1240557.42	1039857.79				
S + P	11655503.57	18918608.44	12973184.87	15324326.14	20111780.38	16424912.08	21704885.02	15424753.51				
Excision, %	6.541319261	5.106703398	4.316567486	4.473315262	4.953884645	4.312274468	5.715567804	6.741487242		5.27014	0.96862	5.03029
v, pmol/min	0.00327066	0.002553352	0.002158284	0.002236658	0.002476942	0.002156137	0.002857784	0.003370744				
v, nM/min	0.163532982	0.127667585	0.107914187	0.111832882	0.123847116	0.107806862	0.142889195	0.168537181		0.13175	0.02422	0.12576
$[E]_0$, nM	35											
E, pmol	0.7											
Performed b	CAR									A	SD	M
Date	5/27/2021	5/27/2021	5/27/2021	5/27/2021	5/27/2021	5/27/2021	5/27/2021	5/27/2021				
Substrate (S	15178446.54	12595879.64	11830875.71	15137788.45	27001800.99	18129370.75	7864332.1	18903293.12				
Product (P)	1389818.86	1198382.67	1046013.04	1167080.87	2269905.24	1459132.35	751957.56	2062528.78				
S + P	16568265.4	13794262.31	12876888.75	16304869.32	29271706.23	19588503.1	8616289.66	20965821.9				
Excision, %	8.388439142	8.687544452	8.123181463	7.157867059	7.754605154	7.448922169	8.727162035	9.837576556		8.26566	0.8496	8.25581
v, pmol/min	0.00419422	0.004343772	0.004061591	0.003578934	0.003877303	0.003724461	0.004363581	0.004918788				
v, nM/min	0.209710979	0.217188611	0.203079537	0.178946676	0.193865129	0.186223054	0.218179051	0.245939414		0.20664	0.02124	0.2064
$[E]_0$, nM	50											
E, pmol	1											
Performed b	CAR									A	SD	M
Date	5/27/2021	5/27/2021	5/27/2021	5/27/2021	5/27/2021	5/27/2021	5/27/2021	5/27/2021				
Substrate (S	15769785.44	15682781.71	8810050.25	18106875.73	17656036.85	18907554.21	14511802.46	20657242.76				
Product (P)	2341887.26	2937535.25	2059022.85	3772614.35	2972402.32	3470998.55	2870592.02	3871744.71				
S + P	18111672.7	18620316.96	10869073.1	21879490.08	20628439.17	22378552.76	17382394.48	24528987.47				
Excision, %	12.93026491	15.77596803	18.9438679	17.24269778	14.4092449	15.5103799	16.51436471	15.78436417		15.8889	1.79947	15.7802
v, pmol/min	0.006465132	0.007887984	0.009471934	0.008621349	0.007204622	0.00775519	0.008257182	0.007892182				
v, nM/min	0.323256623	0.394399201	0.473596697	0.431067444	0.360231123	0.387759498	0.412859118	0.394609104		0.39722	0.04499	0.3945

CAR	nM	nM/min	SD	pmol	% excision	SD	Number of parallels
	0	0	0	0	0	0	0
	5	0.034485	0.006336	0.1	1.379393	0.253442	8
	15	0.11047	0.01675	0.3	4.418785	0.670002	8
	25	0.131753	0.024216	0.5	5.27014	0.968624	8
	35	0.206642	0.02124	0.7	8.265662	0.849597	8
	50	0.397222	0.044987	1	15.88889	1.799471	8

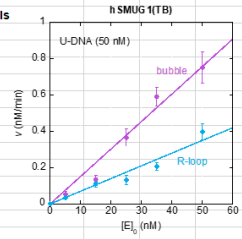

y = m1*x/(m2+x)		
	Value	Error
m1	-4.2666e+17	2.1434e+24
m2	-2.8666e+19	1.4143e+26
Chisq	0.013052	NA
R	0.98606	NA

Linear graph, K_D and V_{max} not determined

y = m1*x/(m2+x)		
	Value	Error
m1	1.2481e+7	1.4242e-9
m2	1.7821e+9	9.9694e-12
Chisq	0.0056017	NA
R	0.97215	NA

Linear graph, K_D and V_{max} not determined

All values

0	0	25	0.123847116
5	0.036846374	25	0.107806862
5	0.035129295	25	0.142889195
5	0.038247944	25	0.168537181
5	0.02606112	35	0.209710979
5	0.032589754	35	0.217188611
5	0.029450124	35	0.203079537
5	0.046654861	35	0.178946676
5	0.03089915	35	0.193865129
15	0.104263896	35	0.186223054
15	0.148513819	35	0.218179051
15	0.096976358	35	0.245939414
15	0.117133741	50	0.323256623
15	0.09867612	50	0.394399201
15	0.101850138	50	0.473596697
15	0.104453151	50	0.431067444
15	0.111889836	50	0.360231123
25	0.163532982	50	0.387759498
25	0.127667585	50	0.412859118
25	0.107914187	50	0.394609104
25	0.111832882		

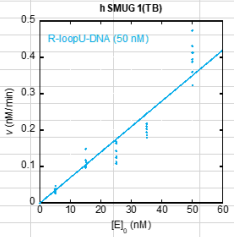

y = m1*x/(m2+x)		
	Value	Error
m1	1.2482e+7	4.5107e-9
m2	1.7822e+9	3.1575e-11
Chisq	0.068488	NA
R	0.94696	NA

Linear graph, K_D and V_{max} not determined

hSMUG1(NEB) bubbleU-DNA

hSMUG1(NEB) bubbleU-DNA

$[S]_0$ = 1 pmol = 50 nM | Time = 20 min

$[E]_0$, nM: 0.15
E, pmol: 0.003
Performed by: Cyrell Ann Ruales (CAR)

Date	2/18/2021	2/18/2021	2/22/2021	2/22/2021	2/22/2021	5/21/2021	5/21/2021	5/21/2021	5/21/2021	5/25/2021	5/25/2021	5/25/2021	5/25/2021	5/25/2021	5/25/2021	5/25/2021	5/25/2021	A	SD	M
Substrate (S)	3376645.67	49805371.45	55937078.52	54610564	53380320.22	11065503.8	16479045.2	9405596.14	16463222	4179829.3	8602458.77	5508570.6	7539316.01	9308559.16	10125768.15	9125390	12738212.88			
Product (P)	174415.1	1139406.76	2975355.5	2963292.2	2516919.6	535372.86	497180.2	390479.31	522122.89	259986.64	323684.07	252878.79	430962.2	692739.87	545967.46	782375.16	911436.73			
S + P	3551060.77	50944778.21	58912434.02	57573856	55897239.82	11600876.7	16976225.4	9796075.45	16985344	4439816	8926142.84	5761449.4	7970278.21	10001299.03	10671735.61	9907765.2	13649649.61			
Excision, %	4.91163377	2.236552597	5.050471177	5.1469406	4.502761868	4.61493451	2.9286852	3.98607904	3.0739611	5.8557977	3.62624793	4.3891523	5.407116146	6.926498927	5.116013739	7.8965856	6.677363566	4.8439292	1.47405	4.91163
v, pmol/min	0.00245582	0.001118276	0.002525236	0.0025735	0.002251381	0.00230747	0.00146434	0.00199304	0.001537	0.0029279	0.001813124	0.0021946	0.002703558	0.003463249	0.002558007	0.0039483	0.003338682			
v, nM/min	0.12279084	0.055913815	0.126261779	0.1286735	0.112569047	0.11537336	0.07321713	0.09965198	0.076849	0.1463949	0.090656198	0.1097288	0.135177904	0.173162473	0.127900343	0.1974146	0.166934089	0.1210982	0.03685	0.12279

$[E]_0$, nM: 0.75
E, pmol: 0.015
Performed by: CAR

Date	5/21/2021	5/21/2021	5/21/2021	5/21/2021	5/25/2021	5/25/2021	5/25/2021	5/25/2021	5/25/2021	5/25/2021	5/25/2021	5/25/2021	A	SD	M
Substrate (S)	12976646	16911486.79	12224375.59	11626459	5140146.99	3165031.23	5259697.51	3472874.15	3502487.3	6651139.8	7272727.98	3701735.6			
Product (P)	3475094.97	3845605.79	3759495.47	4047220.1	2107778.3	1204912.98	1887765.67	1389439.74	1359519.6	2273737.6	3070946.52	1308939.6			
S + P	16451740.9	20757092.58	15983871.06	15673679	7247925.29	4369944.21	7147463.18	4862313.89	4862006.9	8924877.4	10343674.5	5010675.2			
Excision, %	21.1229619	18.52670732	23.52055679	25.821763	29.08112619	27.5727314	26.4116879	28.5756899	27.962107	25.476401	29.68912566	26.123018	25.82365634	3.329771178	26.267353
v, pmol/min	0.01056148	0.009263354	0.011760278	0.0129109	0.014540563	0.01378637	0.01320584	0.01428784	0.0139811	0.0127382	0.014844563	0.0130615			
v, nM/min	0.52807405	0.463167683	0.58801392	0.6455441	0.727028155	0.68931829	0.6602922	0.71439225	0.6990527	0.63691	0.742228141	0.6530754	0.645591408	0.083244279	0.6566838

$[E]_0$, nM: 1.5
E, pmol: 0.03
Performed by: CAR

Date	5/21/2021	5/21/2021	5/21/2021	5/21/2021	5/25/2021	5/25/2021	5/25/2021	5/25/2021	5/25/2021	5/25/2021	5/25/2021	5/25/2021	A	SD	M
Substrate (S)	9206092.27	9703600.28	13388814.36	10791977	2670979.18	2307140.85	3586787.47	3074549.99	1552495.2	5333105.4	3026695.86	2309564.8			
Product (P)	7704073.61	7391503	8691466.54	6883076.8	1641615.96	1394274.71	2591676.86	2529118.34	1201948.8	4786966.5	2063884.07	1831103.2			
S + P	16910165.9	17095103.28	22080280.9	17675054	4312595.14	3701415.56	6178464.33	5603668.33	2754443.9	10120072	5090579.93	4140668			
Excision, %	45.5588293	43.23754516	39.36302522	38.942325	38.06561726	37.6686888	41.9469422	45.1332626	43.636712	47.301704	40.54320133	44.222409	42.13502194	3.193588203	42.592244
v, pmol/min	0.02277941	0.021618773	0.019681513	0.0194712	0.019032809	0.01883434	0.02097347	0.02256663	0.0218184	0.0236509	0.020271601	0.0221112			
v, nM/min	1.13897073	1.080938629	0.984075631	0.9735581	0.951640432	0.94171722	1.04867355	1.12833156	1.0909178	1.1825426	1.013580033	1.1055602	1.053375548	0.079839705	1.0648061

$[E]_0$, nM: 5
E, pmol: 0.1

Performed by								CAR														
Date	3/10/2021	3/10/2021	3/10/2021	3/10/2021	3/10/2021	3/10/2021	3/16/2021	5/21/2021	5/21/2021	5/21/2021	5/21/2021	5/25/2021	5/25/2021	5/25/2021	5/25/2021	5/25/2021	5/25/2021	5/25/2021	5/25/2021	A	SD	M
Substrate (S)	9741211.35	2727716.47	5712707.9	2335914.3	2551104.09	6549483.61	68915.29	3189446.89	4042116.2	2304437.4	5595489.65	177404.88	331244.62	195667	811858.95	495265.21	2861678.37	533592.19	82570.89			
Product (P)	48442602.5	26633151.71	42435036.03	38119853	46491105.31	48526083	277061.53	16398230	20715262	14471489	23684396.48	1254229.9	1770222.62	1346370.8	4845345.51	2546972.8	19385001.02	3045766.27	601033.6			
S + P	58183813.8	29360868.18	48147743.93	40455767	49042209.4	55075566.6	345976.82	19587676.9	24757378	16775926	29279886.13	1431634.8	2101467.24	1542037.8	5657204.46	3042238	22246679.39	3579358.46	683604.49			
Excision, %	83.2578673	90.70968728	88.13504552	94.226004	94.79814608	88.1081866	80.0809517	83.7170742	83.673084	86.263427	80.88964682	87.608231	84.23745973	87.31114114	85.64911423	83.720366	87.13660444	85.09251879	87.921248	85.2683	2.10898	85.3708
v, pmol/min	0.04162893	0.045354844	0.044067523	0.047113	0.047399073	0.04405409	0.04004048	0.04185854	0.0418365	0.0431317	0.040444823	0.0438041	0.04211873	0.043655571	0.042824557	0.0418602	0.043568302	0.042546259	0.0439606			
v, nM/min	2.08144668	2.267742182	2.203376138	2.3556501	2.369953652	2.20270467	2.00202379	2.09292686	2.0918271	2.1565857	2.022241171	2.1902058	2.105936493	2.182778529	2.141227856	2.0930091	2.178415111	2.12731297	2.1980312	2.13171	0.05272	2.13427

$[E]_0$, nM: 10
E, pmol: 0.2
Performed by: CAR

Date	3/10/2021	3/10/2021	3/10/2021	3/10/2021	3/10/2021	3/10/2021	5/21/2021	5/21/2021	5/21/2021	5/21/2021	5/25/2021	5/25/2021	5/25/2021	5/25/2021	5/25/2021	5/25/2021	5/25/2021	5/25/2021	A	SD	M
Substrate (S)	1817488.75	414840.49	199041.91	354920.19	753492.97	2868862.54	1276115.2	417920.28	1184384	1438288.7	691937.96	415897.23	249673.46	379349.99	298482.62	92167.67	383026.69	366453.24			
Product (P)	47003110.8	13006923.11	11588746.53	11030298	39475229.44	70739834.3	21440013.3	19274140.8	24601289	23160091	11727323.07	12157634	12842489.22	11128310.62	10901012.31	2204038.6	11687382.49	15332256.51			
S + P	48820599.6	13421763.6	11787788.44	11385218	40228722.41	73608696.9	22716128.5	19692061.1	25785673	24598379	12419261.03	12573532	13092162.68	11507660.61	11199494.93	2296206.3	12070409.18	15698709.75			
Excision, %	96.2772093	96.90919538	98.31145672	96.882623	98.12697763	96.1025495	94.3823385	97.877722	95.406814	94.152913	94.42850941	96.69228	98.0929548	96.70350037	97.33485642	95.986089	96.82672986	97.66571109	96.5645	1.30148	96.7651
v, pmol/min	0.0481386	0.048454598	0.049155728	0.0484413	0.049063489	0.04805127	0.04719117	0.04893886	0.0477034	0.0470765	0.047214255	0.0483461	0.049046477	0.04835175	0.048667428	0.047993	0.048413365	0.048832856			
v, nM/min	2.40693023	2.422729884	2.457786418	2.4220656	2.453174441	2.40256374	2.35955846	2.44694305	2.3851703	2.3538228	2.360712735	2.417307	2.45232387	2.417587509	2.433371411	2.3996522	2.420668247	2.441642777	2.41411	0.03254	2.41913

$[E]_0$, nM: 15
E, pmol: 0.3
Performed by: CAR

Date	5/21/2021	5/21/2021	5/21/2021	5/21/2021	5/25/2021	5/25/2021	5/25/2021	5/25/2021	5/25/2021	5/25/2021	5/25/2021	5/25/2021	A	SD	M
Substrate (S)	663424.68	1239151.92	456066.38	776550.57	333073.38	188396.2	222088.19	118020.67	60991.12	224639.56	261794.09	249633.88			
Product (P)	25927874	42188796.73	23202488.02	30163665	14925226.92	9973141.37	11142687.8	14525797.4	14406984	13072241	14461744.81	12402827			
S + P	26591298.6	43427948.65	23658554.4	30940215	15258300.3	10161537.6	11364776	14643818.1	14467975	13296880	14723538.9	12652461			
Excision, %	97.5051061	97.14664874	98.0722982	97.490158	97.81710038	98.1459873	98.0458199	99.1940581	99.578441	98.310584	98.22193501	98.026994	98.11062411	0.79861351	98.04582
v, pmol/min	0.04875255	0.048573324	0.049036149	0.0487451	0.04890855	0.04907299	0.04902291	0.04959703	0.0497892	0.0491553	0.049110968	0.0490135			
v, nM/min	2.43762765	2.428666218	2.451807455	2.4372539	2.445427509	2.45364968	2.4511455	2.47985145	2.489461	2.4577646	2.455548375	2.4506748	2.452765603	0.019965338	2.4511455

CAR	nM	nM/min	SD	pmol	% excision	SD	Number of parallels
	0	0	0	0	0	0	
	0.15	0.121098229	0.036851	0.003	4.843929168	1.474049	17
	0.75	0.645591408	0.083244279	0.015	25.82365634	3.32977118	12
	1.5	1.053375548	0.079839705	0.03	42.13502194	3.1935882	12
	5	2.131708	0.052724	0.1	85.26833	2.108979	19
	10	2.414112	0.032537	0.2	96.56447	1.301475	18
	15	2.452765603	0.019965338	0.3	98.11062411	0.79861351	12

All values

0	0	0.75	0.528074047	1.5	1.048673554	5	2.10593649	10	2.417307	15	2.450674838
0.15	0.12279084	0.75	0.463167683	1.5	1.128331564	5	2.18277853	10	2.4523239		
0.15	0.05591382	0.75	0.58801392	1.5	1.09091781	5	2.14122786	10	2.4175875		
0.15	0.12626178	0.75	0.645544063	1.5	1.182542612	5	2.09300915	10	2.4333714		
0.15	0.12867352	0.75	0.727028155	1.5	1.013580033	5	2.17841511	10	2.3996522		
0.15	0.11256905	0.75	0.689318285	1.5	1.105560235	5	2.12731297	10	2.4206682		
0.15	0.11537336	0.75	0.660292198	5	2.081446681	5	2.1980312	10	2.4416428		
0.15	0.07321713	0.75	0.714392248	5	2.267742182	10	2.40693023	15	2.4376277		
0.15	0.09965198	0.75	0.699052685	5	2.203376138	10	2.42272988	15	2.4286662		
0.15	0.07684903	0.75	0.636910033	5	2.355650104	10	2.45778642	15	2.4518075		
0.15	0.14639494	0.75	0.742228141	5	2.369953652	10	2.42206557	15	2.4372539		
0.15	0.0906562	0.75	0.653075442	5	2.202704665	10	2.45317444	15	2.4454275		
0.15	0.10972881	1.5	1.138970733	5	2.002023792	10	2.40256374	15	2.4536497		
0.15	0.1351779	1.5	1.080938629	5	2.092926855	10	2.35955846	15	2.4511455		
0.15	0.17316247	1.5	0.984075631	5	2.091827107	10	2.44694305	15	2.4798515		
0.15	0.12790034	1.5	0.973558129	5	2.156585667	10	2.38517035	15	2.489461		
0.15	0.19741464	1.5	0.951640432	5	2.022241171	10	2.35382282	15	2.4577646		
0.15	0.16693409	1.5	0.941717221	5	2.190205773	10	2.36071274	15	2.4555484		

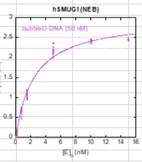

y = m1*x/(m2+x)		
	Value	Error
m1	2.9934	0.040952
m2	2.4237	0.11472
Chisq	1.1362	NA
R	0.9929	NA

K_D = 2.4 ± 0.1 nM
V_{max} = 2.99 ± 0.04 nM/min

hSMUG1(NEB) R-loopU-DNA

hSMUG1(NEB) R-loopU-DNA																	
$[S]_0$ = 1 pmol = 50 nM	Time = 20 min																
$[E]_0$, nM	0.15																
E, pmol	0.003																
Performed by	CAR														A	SD	M
Date	5/12/2021	5/12/2021	5/12/2021	5/12/2021	5/14/2021	5/14/2021	5/14/2021	5/14/2021	5/14/2021	5/14/2021	5/14/2021	5/14/2021	5/14/2021	5/14/2021			
Substrate (S)	12299742.02	17295056.92	9941876.34	12751265.98	6547507.79	9278491.48	4679145.93	10252997.94	9497603.79	12536737.48	9075039.11	13086410.43					
Product (P)	286086.16	365294.51	206730.98	275835.55	263791.71	445760.41	176234.61	370240.12	226004.99	476740.53	253854.98	509487.49					
S + P	12585828.18	17660351.43	10148607.32	13027101.53	6855629.5	9768581.89	4855380.54	10623238.06	9723608.78	13013478.01	9328894.09	13595897.92					
Excision, %	2.273081723	2.068444173	2.037037925	2.117397714	3.847811642	4.56320493	3.629676573	3.485190842	2.32429127	3.663436705	2.721169064	3.747361837			3.04	0.87	3.10
v, pmol/min	0.001136541	0.001034222	0.001018519	0.001058699	0.001923906	0.0022816	0.001814838	0.001742595	0.001162146	0.001831718	0.001360585	0.001873681					
v, nM/min	0.056827043	0.051711104	0.050925948	0.052934943	0.096195291	0.11408012	0.090741914	0.087129771	0.058107282	0.091585918	0.068029227	0.093684046			0.08	0.02	0.08
$[E]_0$, nM	0.75																
E, pmol	0.015																
Performed by	CAR														A	SD	M
Date	5/12/2021	5/12/2021	5/12/2021	5/12/2021	5/14/2021	5/14/2021	5/14/2021	5/14/2021	5/14/2021	5/14/2021	5/14/2021	5/14/2021					
Substrate (S)	15959189.81	9995204.1	10778767.32	13094494.94	6652014.84	8754228.92	6411453.39	10382852.49	8203397.14	10558962.96	12107188.67	8115249.61					
Product (P)	1052693.05	903349.37	965724.6	1143161.18	568059.57	648454.44	584244.76	1021622.64	664492.4	998853.87	1276297.7	643611.88					
S + P	17011882.86	10898553.47	11744491.92	14237656.12	7220074.41	9402683.36	6995698.15	11404475.13	8867889.54	11557816.83	13383486.37	8758861.49					
Excision, %	6.187986707	8.288708887	8.222787385	8.029138858	7.867779994	6.89648279	8.35148612	8.958085562	7.493241735	8.642236546	9.536361937	7.348122593			7.99	0.91	8.13
v, pmol/min	0.003093993	0.004144354	0.004111394	0.004014569	0.00393389	0.00344824	0.004175743	0.004479043	0.003746621	0.004321118	0.004768181	0.003674061					
v, nM/min	0.154699668	0.207217722	0.205569685	0.200728471	0.1966945	0.17241207	0.208787153	0.223952139	0.187331043	0.216055914	0.238409048	0.183703065			0.20	0.02	0.20
$[E]_0$, nM	1.5																
E, pmol	0.03																
Performed by	CAR														A	SD	M
Date	5/12/2021	5/12/2021	5/12/2021	5/12/2021	5/14/2021	5/14/2021	5/14/2021	5/14/2021	5/14/2021	5/14/2021	5/14/2021	5/14/2021					
Substrate (S)	11011103.85	14504588.41	13746067.8	9701417.54	8649100.11	7174383.76	7304002.97	9985627.91	7708105.03	13831769.95	7365385.13	11757266.04					
Product (P)	1783649.28	1987154.85	1965363.67	1493008.16	1132223.1	1294014.18	1429300.52	2129072.43	1872796.13	2818343.51	1287228.68	2560697.12					
S + P	12794753.13	16491743.26	15711431.47	11194425.7	9781323.21	8468397.94	8733303.49	12114700.34	9580901.16	16650113.46	8652613.81	14317963.16					
Excision, %	13.94047436	12.04939235	12.5091318	13.33706793	11.5753572	15.2805075	16.36609241	17.57428884	19.54718141	16.9268727	14.87676104	17.88450697			15.16	2.55	15.08
v, pmol/min	0.006970237	0.006024696	0.006254566	0.006668534	0.005787679	0.00764025	0.008183046	0.008787144	0.009773591	0.008463436	0.007438381	0.008942253					
v, nM/min	0.348511859	0.301234809	0.312728295	0.333426698	0.28938393	0.38201269	0.40915231	0.439357221	0.488679535	0.423171818	0.371919026	0.447112674			0.38	0.06	0.38
$[E]_0$, nM	5																
E, pmol	0.1																
Performed by	CAR														A	SD	M
Date	5/12/2021	5/12/2021	5/12/2021	5/12/2021	5/14/2021	5/14/2021	5/14/2021	5/14/2021	5/14/2021	5/14/2021	5/14/2021	5/14/2021					
Substrate (S)	12522268.42	9263105.05	9514755.75	11173479.27	6113561.36	7323135.78	5958139.29	7850721.76	10149944.61	7289649.63	9939136.06	6049376.84					
Product (P)	4756497.33	3525619.52	3817051.75	4575425.82	2901382.71	2944954.25	3054008.74	3780857.66	4010191.98	3383622.9	5006559.15	3349348.6					
S + P	17278765.75	12788724.57	13331807.5	15748905.09	9014944.07	10268090	9012148.03	11631579.42	14160136.59	10673272.53	14945695.21	9398725.44					
Excision, %	27.52799244	27.56818712	28.6311646	29.05234233	32.18414543	28.6806431	33.88768948	32.50510978	28.32029165	31.70183175	33.49833567	35.63620005			30.77	2.79	30.38
v, pmol/min	0.013763996	0.013784094	0.014315582	0.014526171	0.016092073	0.01434032	0.016943845	0.016252555	0.014160146	0.015850916	0.016749168	0.0178181					
v, nM/min	0.688199811	0.689204678	0.715779115	0.726308558	0.804603636	0.71701608	0.847192237	0.812627745	0.708007291	0.792545794	0.837458392	0.890905001			0.77	0.07	0.76
$[E]_0$, nM	10																
E, pmol	0.2																
Performed by	CAR														A	SD	M
Date	5/12/2021	5/12/2021	5/12/2021	5/12/2021	5/14/2021	5/14/2021	5/14/2021	5/14/2021	5/14/2021	5/14/2021	5/14/2021	5/14/2021					
Substrate (S)	9957023.18	10881119.16	8812556.53	8907684.46	5177172.11	4584767.47	6698467.36	4230980.06	4886061.89	5742681.44	5872712.3	6168447.64					
Product (P)	4774612.88	5445559.55	4693444.74	4347253.42	2507116.28	2688793.88	4374352.59	2624217.49	2903822.94	3481037.17	3174602	4019235.74					
S + P	14731636.06	16326678.71	13506001.27	13254937.88	7684288.39	7273561.35	11072819.95	6855197.55	7789884.83	9223718.61	9047314.3	10187683.38					
Excision, %	32.41060844	33.35374969	34.75080926	32.79723722	32.6265251	36.9666763	39.50531671	38.28069827	37.27684046	37.74006252	35.0888882	39.45191061			35.85	2.67	36.03
v, pmol/min	0.016205304	0.016676875	0.017375405	0.016398619	0.016313263	0.01848334	0.019752658	0.019140349	0.01863842	0.018870031	0.017544444	0.019725955					
v, nM/min	0.810265211	0.833843742	0.868770232	0.819930931	0.815663127	0.92416691	0.987632918	0.957017457	0.931921011	0.943501563	0.877222205	0.986297765			0.90	0.07	0.90
$[E]_0$, nM	15																
E, pmol	0.3																
Performed by	Cyrell Ann Ruales (CAR)											A	SD	M			
Date	5/20/2021	5/20/2021	5/20/2021	5/20/2021	5/20/2021	5/20/2021	5/20/2021	5/20/2021	5/20/2021								
Substrate (S)	5387601.41	5638245.26	6583810.3	8723722.86	8466875.3	9181379.54	9333833.61	10987861.37	12813979.71								
Product (P)	6599179.95	6409523.31	6324379.4	8394651.07	8315994.55	8848731.96	10627261.7	12068537.26	13035359.04								
S + P	11986781.36	12047768.57	12908189.7	17118373.93	16782869.85	18030111.5	19961095.31	23056398.63	25849338.75								
Excision, %	55.05381096	53.20091661	48.99509185	49.03883455	49.55049181	49.0775221	53.23987254	52.34354876	50.42821082			51.21425556	2.282437981	50.42821082			
v, pmol/min	0.027526905	0.026600458	0.024497546	0.024519417	0.024775246	0.02453876	0.026619936	0.026171774	0.025214105								
v, nM/min	1.376345274	1.330022915	1.224877296	1.225970864	1.238762295	1.22693805	1.330996813	1.308588719	1.26070527			1.280356389	0.05706095	1.26070527			

CAR	nM	nM/min	SD	pmol	% excision	SD	Number of parallels
	0	0	0	0	0	0	
	0.15	0.07599605	0.021861	0.003	3.03984203	0.874423	12
	0.75	0.19963004	0.022796	0.015	7.98520159	0.911838	12
	1.5	0.37889091	0.063752	0.03	15.1556362	2.550099	12
	5	0.76915403	0.069648	0.1	30.7661611	2.785937	12
	10	0.89635276	0.066852	0.2	35.8541102	2.674062	12
	15	1.280356389	0.05706095	0.3	51.21425556	2.28243798	9

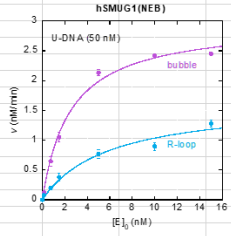

y = m1*x/(m2+x)		
	Value	Error
m1	2.9774	0.12127
m2	2.4959	0.34117
Chisq	0.040394	NA
R	0.99703	NA

K_D = 2.5 ± 0.3 nM

V_{max} = 3.0 ± 0.1 nM/min

y = m1*x/(m2+x)		
	Value	Error
m1	1.6471	0.22647
m2	5.8969	1.9972
Chisq	0.032765	NA
R	0.96798	NA

K_D = 6 ± 2 nM

V_{max} = 1.6 ± 0.2 nM/min

y = m1*x/(m2+x)		
	Value	Error
m1	1.5827	0.071839
m2	5.4716	0.60771
Chisq	0.54213	NA
R	0.97678	NA

K_D = 5.5 ± 0.6 nM

V_{max} = 1.58 ± 0.07 nM/min

All values

0	0	0.75	0.223952139	5	0.726308558	10	0.986297765
0.15	0.056827043	0.75	0.187331043	5	0.804603636	15	1.376345274
0.15	0.051711104	0.75	0.216055914	5	0.71701608	15	1.330022915
0.15	0.05092595	0.75	0.238409048	5	0.847192237	15	1.2248773
0.15	0.052934943	0.75	0.183703065	5	0.812627745	15	1.225970864
0.15	0.096195291	1.5	0.348511859	5	0.708007291	15	1.238762295
0.15	0.11408012	1.5	0.301234809	5	0.792545794	15	1.22693805
0.15	0.090741914	1.5	0.31272829	5	0.837458392	15	1.330996813
0.15	0.087129771	1.5	0.333426698	5	0.890905001	15	1.308588719
0.15	0.058107282	1.5	0.28938393	10	0.810265211	15	1.26070527
0.15	0.091585918	1.5	0.38201269	10	0.833843742		
0.15	0.068029227	1.5	0.40915231	10	0.86877023		
0.15	0.093684046	1.5	0.439357221	10	0.819930931		
0.75	0.154699668	1.5	0.488679535	10	0.815663127		
0.75	0.207217722	1.5	0.423171818	10	0.92416691		
0.75	0.20556968	1.5	0.371919026	10	0.987632918		
0.75	0.200728471	1.5	0.447112674	10	0.957017457		
0.75	0.1966945	5	0.688199811	10	0.931921011		
0.75	0.17241207	5	0.689204678	10	0.943501563		
0.75	0.208787153	5	0.71577912	10	0.877222205		

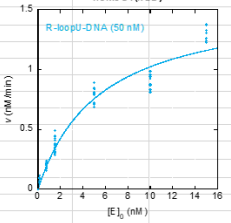

hSMUG1 S26R/E35D bubbleU-DNA

hSMUG1 S26R/E35D bubbleU-DNA									
$[S]_o$ = 1 pmol = 50 nM	Time = 20 min								
$[E]_o$, nM	5								
E, pmol	0.1								
Performed by	Cyrell Ann Ruales (CAR)						A	SD	M
Date	**6/8/2021**	**6/8/2021**	**6/8/2021**	**6/8/2021**	**6/8/2021**	**6/8/2021**			
Substrate (S)	11938515.88	26151484.08	17576732.49	22569021.44	17276166.94	24601644.59			
Product (P)	112103.25	181455.46	146874.97	207328.38	122934.5	146848.92			
S + P	12050619.13	26332939.54	17723607.46	22776349.82	17399101.44	24748493.51			
Excision, %	0.93026963	0.689081672	0.828696812	0.910279222	0.706556603	0.593365087	0.77637	0.13442	0.76763
v, pmol/min	0.000465135	0.000344541	0.000414348	0.00045514	0.000353278	0.000296683			
v, nM/min	0.023256741	0.017227042	0.02071742	0.022756981	0.017663915	0.014834127	0.01941	0.00336	0.01919
$[E]_o$, nM	15								
E, pmol	0.3								
Performed by	CAR						A	SD	M
Date	**6/8/2021**	**6/8/2021**	**6/8/2021**	**6/8/2021**	**6/8/2021**	**6/8/2021**			
Substrate (S)	14569215.24	25938075.25	21167248.36	22538182.62	16184063.03	21920401.13			
Product (P)	530716.67	1161679.38	974624.95	779309.29	919483.52	866203.68			
S + P	15099931.91	27099754.63	22141873.31	23317491.91	17103546.55	22786604.81			
Excision, %	3.514695782	4.286678591	4.401727606	3.342166014	5.375981626	3.801372285	4.12044	0.74264	4.04403
v, pmol/min	0.001757348	0.002143339	0.002200864	0.001671083	0.002687991	0.001900686			
v, nM/min	0.087867395	0.107166965	0.11004319	0.08355415	0.134399541	0.095034307	0.10301	0.01857	0.1011
$[E]_o$, nM	25								
E, pmol	0.5								
Performed by	CAR						A	SD	M
Date	**6/8/2021**	**6/8/2021**	**6/8/2021**	**6/8/2021**	**6/8/2021**	**6/8/2021**			
Substrate (S)	16960317.63	21949814.5	22008673.1	18430998.84	16110041.57	21093407.31			
Product (P)	1157073.13	1893280.34	1483438.77	1562304.85	1760503.43	1896800.91			
S + P	18117390.76	23843094.84	23492111.87	19993303.69	17870545	22990208.22			
Excision, %	6.386532947	7.940581341	6.314625004	7.814140545	9.851425516	8.250472949	7.75963	1.31344	7.87736
v, pmol/min	0.003193266	0.003970291	0.003157313	0.00390707	0.004925713	0.004125236			
v, nM/min	0.159663324	0.198514534	0.157865625	0.195353514	0.246285638	0.206261824	0.19399	0.03284	0.19693
$[E]_o$, nM	35								
E, pmol	0.7								
Performed by	CAR						A	SD	M
Date	**6/8/2021**	**6/8/2021**	**6/8/2021**	**6/8/2021**	**6/8/2021**	**6/8/2021**			
Substrate (S)	35607183.29	21085149.91	24004674.24	19762556.69	17007234.29	25101700.21			
Product (P)	4399338.18	2460826.05	3807471.55	2758057.52	2225400.55	2952411.89			
S + P	40006521.47	23545975.96	27812145.79	22520614.21	19232634.84	28054112.1			
Excision, %	10.99655261	10.45115333	13.6899597	12.24681305	11.57096034	10.52398978	11.5799	1.23503	11.2838
v, pmol/min	0.005498276	0.005225577	0.00684498	0.006123407	0.00578548	0.005261995			
v, nM/min	0.274913815	0.261278833	0.342248992	0.306170326	0.289274009	0.263099744	0.2895	0.03088	0.28209
$[E]_o$, nM	50								
E, pmol	1								
Performed by	CAR						A	SD	M
Date	**6/8/2021**	**6/8/2021**	**6/8/2021**	**6/8/2021**	**6/8/2021**	**6/8/2021**			
Substrate (S)	26887662.36	17600229.04	20291773.41	20427542.98	16158922.21	25776101.03			
Product (P)	4585179.9	4947804.44	4273451.06	5086921.65	3740730.54	4946570			
S + P	31472842.26	22548033.48	24565224.47	25514464.63	19899652.75	30722671.03			
Excision, %	14.56868707	21.94339672	17.39634443	19.93740305	18.79796892	16.10071597	18.1241	2.6681	18.0972
v, pmol/min	0.007284344	0.010971698	0.008698172	0.009968702	0.009398984	0.008050358			
v, nM/min	0.364217177	0.548584918	0.434908611	0.498435076	0.469949223	0.402517899	0.4531	0.0667	0.45243

CAR	nM	nM/min	SD	pmol	% excision	SD	Number of parallels
	0	0	0	0	0	0	0
	5	0.019409	0.00336	0.1	0.776375	0.134416	6
	15	0.103011	0.018566	0.3	4.120437	0.742642	6
	25	0.193991	0.032836	0.5	7.75963	1.313445	6
	35	0.289498	0.030876	0.7	11.5799	1.235032	6
	50	0.453102	0.066703	1	18.12409	2.668103	6

All values

0.00000	0.00000
5.00000	0.023256741
5.00000	0.017227042
5.00000	0.02071742
5.00000	0.022756981
5.00000	0.017663915
5.00000	0.014834127
15.00000	0.087867395
15.00000	0.107166965
15.00000	0.11004319
15.00000	0.08355415
15.00000	0.134399541
15.00000	0.095034307
25.00000	0.159663324
25.00000	0.198514534
25.00000	0.157865625
25.00000	0.195353514
25.00000	0.246285638
25.00000	0.206261824
35.00000	0.274913815
35.00000	0.261278833
35.00000	0.342248992
35.00000	0.306170326
35.00000	0.289274009
35.00000	0.263099744
50.00000	0.364217177
50.00000	0.548584918
50.00000	0.434908611
50.00000	0.498435076
50.00000	0.469949223
50.00000	0.402517899

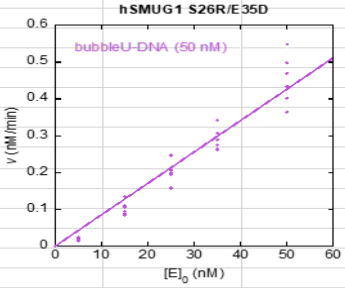

y = m1*x/(m2+x)		
	Value	Error
m1	-3.408e+16	4.3916e+22
m2	-3.9918e+18	5.1465e+24
Chisq	0.048117	NA
R	0.96775	NA

Linear graph, K_D and V_{max} not determined

hSMUG1 S26R/E35D R-loopU-DNA

hSMUG1 S26R/E35D R-loopU-DNA							
$[S]_0$ = 1 pmol = 50 nM	Time = 20 min						
$[E]_0$, nM	5						
E, pmol	0.1						
Performed b	Cyrell Ann Ruales (CAR)				A	SD	M
Date	6/11/2021	6/11/2021	6/11/2021	6/11/2021			
Substrate (S	13064037.75	18445176.29	10247825.52	15539201.64			
Product (P)	113581.56	284940.57	165524.69	132329.23			
S + P	13177619.31	18730116.86	10413350.21	15671530.87			
Excision, %	0.861927768	1.521296274	1.589543102	0.844392492	1.20428991	0.40647	1.19161
v, pmol/min	0.000430964	0.000760648	0.000794772	0.000422196			
v, nM/min	0.021548194	0.038032407	0.039738578	0.021109812	0.03010725	0.01016	0.02979
$[E]_0$, nM	15						
E, pmol	0.3						
Performed b	CAR				A	SD	M
Date	6/11/2021	6/11/2021	6/11/2021	6/11/2021			
Substrate (S	12455290.67	15437485.82	13808235.87	10194888.47			
Product (P)	518306.95	773232.99	733781.01	875158.76			
S + P	12973597.62	16210718.81	14542016.88	11070047.23			
Excision, %	3.995090376	4.769887129	5.045936998	7.905646126	5.42914016	1.70988	4.90791
v, pmol/min	0.001997545	0.002384944	0.002522968	0.003952823			
v, nM/min	0.099877259	0.119247178	0.126148425	0.197641153	0.1357285	0.04275	0.1227
$[E]_0$, nM	25						
E, pmol	0.5						
Performed b	CAR				A	SD	M
Date	6/11/2021	6/11/2021	6/11/2021	6/11/2021			
Substrate (S	17023309.53	13419994.62	12919467.3	11417761.76			
Product (P)	1271860.61	1256184.36	1464093.85	1176234.2			
S + P	18295170.14	14676178.98	14383561.15	12593995.96			
Excision, %	6.951892769	8.559342058	10.17893854	9.339642507	8.75745397	1.37342	8.94949
v, pmol/min	0.003475946	0.004279671	0.005089469	0.004669821			
v, nM/min	0.173797319	0.213983551	0.254473464	0.233491063	0.21893635	0.03434	0.22374
$[E]_0$, nM	35						
E, pmol	0.7						
Performed b	CAR				A	SD	M
Date	6/11/2021	6/11/2021	6/11/2021	6/11/2021			
Substrate (S	13569974.74	15204405.83	15484299.87	10277900.34			
Product (P)	3848399.91	3905804.33	2777407.19	2101052.95			
S + P	17418374.65	19110210.16	18261707.06	12378953.29			
Excision, %	22.09390938	20.43831176	15.20891328	16.97278357	18.6784795	3.14693	18.7055
v, pmol/min	0.011046955	0.010219156	0.007604457	0.008486392			
v, nM/min	0.552347734	0.510957794	0.380222832	0.424319589	0.46696199	0.07867	0.46764
$[E]_0$, nM	50						
E, pmol	1						
Performed b	CAR				A	SD	M
Date	6/11/2021	6/11/2021	6/11/2021	6/11/2021			
Substrate (S	13893916.28	13139086.13	10395321.3	12223262.51			
Product (P)	4962868.83	4075085.51	3593909.93	3420750.58			
S + P	18856785.11	17214171.64	13989231.23	15644013.09			
Excision, %	26.3187431	23.67285278	25.69054633	21.8661961	24.3870846	2.02446	24.6817
v, pmol/min	0.013159372	0.011836426	0.012845273	0.010933098			
v, nM/min	0.657968577	0.59182132	0.642263658	0.546654902	0.60967711	0.05061	0.61704

CAR	nM	nM/min	SD	pmol	% excision	SD	Number of parallels
	0	0	0	0	0	0	0
	5	0.03010725	0.010162	0.1	1.20428991	0.406469	4
	15	0.1357285	0.042747	0.3	5.42914016	1.709877	4
	25	0.21893635	0.034336	0.5	8.75745397	1.373422	4
	35	0.46696199	0.078673	0.7	18.6784795	3.146928	4
	50	0.60967711	0.050612	1	24.3870846	2.024461	4

All values	
0.00000	0.00000
5.00000	0.021548194
5.00000	0.038032407
5.00000	0.039738578
5.00000	0.021109812
15.00000	0.099877259
15.00000	0.119247178
15.00000	0.126148425
15.00000	0.197641153
25.00000	0.173797319
25.00000	0.213983551
25.00000	0.254473464
25.00000	0.233491063
35.00000	0.552347734
35.00000	0.510957794
35.00000	0.380222832
35.00000	0.424319589
50.00000	0.657968577
50.00000	0.59182132
50.00000	0.642263658
50.00000	0.546654902

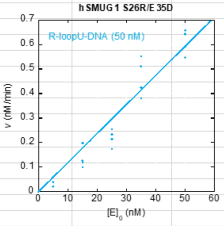

y = m1*x/(m2+x)	Value	Error
m1	-8.4713e+16	2.41e+23
m2	-7.1446e+18	2.033e+25
Chisq	0.082038	NA
R	0.95961	NA

Linear graph, K_D and V_{max} not determined

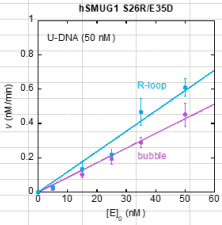

y = m1*x/(m2+x)	Value	Error
m1	-9.8046e+20	4.4151e-23
m2	-9.2773e+22	5.2272e-25
Chisq	0.011614	NA
R	0.99952	NA

Linear graph, K_D and V_{max} not determined

y = m1*x/(m2+x)	Value	Error
m1	5.121e+12	2.7317e-15
m2	5.9843e+14	2.3365e-17
Chisq	0.0023238	NA
R	0.99227	NA

Linear graph, K_D and V_{max} not determined